ISSN 1949-8470 (online)

World Journal of *Radiology*

World J Radiol 2015 July 28; 7(7): 143-183

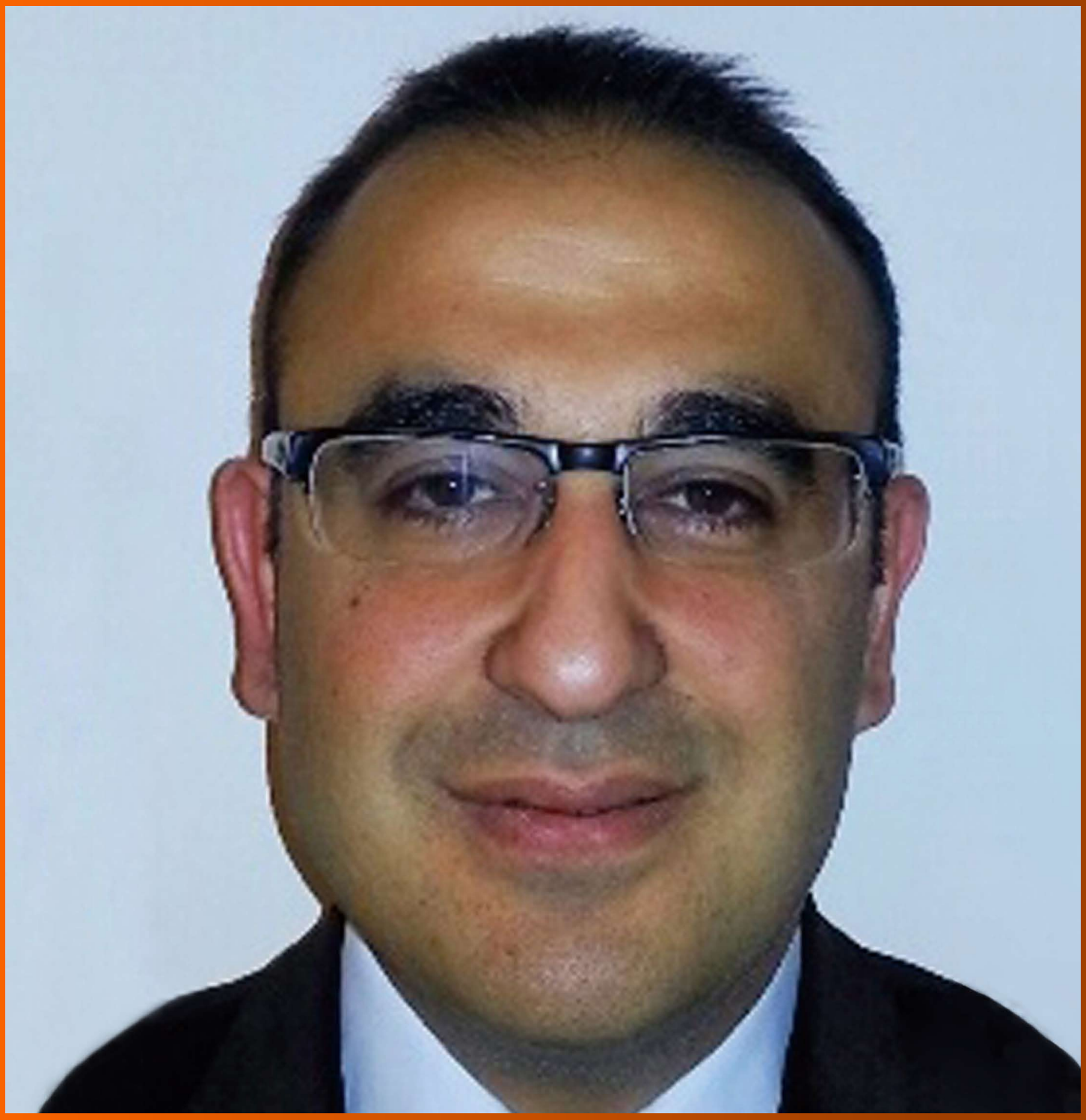

Published by Baishideng Publishing Group Inc

WJR World Journal of Radiology

A peer-reviewed, online, open-access journal of Radiology

Editorial Board

2014-2017

The *World Journal of Radiology* Editorial Board consists of 365 members, representing a team of worldwide experts in radiology. They are from 36 countries, including Afghanistan (1), Argentina (2), Australia (5), Austria (7), Belgium (2), Brazil (8), Canada (6), Chile (1), China (43), Croatia (1), Denmark (4), Egypt (6), France (5), Germany (22), Greece (10), India (12), Iran (6), Ireland (2), Israel (3), Italy (47), Japan (13), Netherlands (1), New Zealand (1), Pakistan (1), Poland (2), Portugal (1), Serbia (1), Singapore (3), Slovakia (1), South Korea (18), Spain (4), Sweden (2), Switzerland (4), Thailand (1), Turkey (26), United Kingdom (11), and United States (82).

Yue-Qi Zhu, *Shanghai*

Croatia

Goran Kusec, Osijek

Denmark

Poul E Andersen, *Odense*
Lars J Petersen, *Aalborg*
Thomas Z Ramsoy, *Frederiksberg*
Morten Ziebell, *Copenhagen*

Egypt

Mohamed F Bazeed, *Mansoura*
Mohamed Abou El-Ghar, *Mansoura*
Reem HA Mohamed, *Cairo*
Mohamed R Nouh, *Alexandria*
Ahmed AKA Razek, *Mansoura*
Ashraf A Zytoon, *Shebin El-Koom*

France

Sabine F Bensamoun, *Compiègne*
Romaric Loffroy, *Dijon*
Stephanie Nougaret, *Montpellier*
Hassane Oudadesse, *Rennes*
Vincent Vinh-Hung, *Fort-de-France*

Germany

Henryk Barthel, *Leipzig*
Peter Bannas, *Hamburg*
Martin Beeres, *Frankfurt*
Ilja F Ciernik, *Dessau*
A Dimitrakopoulou-Strauss, *Heidelberg*
Peter A Fasching, *Erlanegn*
Andreas G Schreyer, *Regensburg*
Philipp Heusch, *Duesseldorf*
Sonja M Kirchhoff, *Munich*
Sebastian Ley, *Munich*
Adel Maataoui, *Frankfurt am Main*
Stephan M Meckel, *Freiburg*
Hans W Muller, *Duesseldorf*
Kay Raum, *Berlin*
Dirk Rades, *Luebeck*
Marc-Ulrich Regier, *Hamburg*
Alexey Surov, *Halle*
Martin Walter, *Magdeburg*
Axel Wetter, *Essen*
Christoph Zilkens, *Düsseldorf*

Greece

Panagiotis Antoniou, *Thessaloniki*
Nikos Efthimiou, *Athens*
Dimitris Karnabatidis, *Patras*
George Latsios, *Athens*
Stylianos Megremis, *Iraklion*
Alexander D Rapidis, *Athens*
Kiki Theodorou, *Larissa*
Ioannis A Tsalafoutas, *Athens*
Evanthia E Tripoliti, *Ioannina*
Athina C Tsili, *Ioannina*

India

Ritesh Agarwal, *Chandigarh*
Chandan J Das, *New Delhi*
Prathamesh V Joshi, *Mumbai*
Naveen Kalra, *Chandigarh*
Chandrasekharan Kesavadas, *Trivandrum*
Jyoti Kumar, *New Delhi*
Atin Kumar, *New Delhi*
Kaushala P Mishra, *Allahabad*
Daya N Sharma, *New Delhi*
Binit Sureka, *New Delhi*
Sanjay Sharma, *New Delhi*
Raja R Yadav, *Allahabad*

Iran

Majid Assadi, *Bushehr*
SeyedReza Najafizadeh, *Tehran*
Mohammad Ali Oghabian, *Tehran*
Amir Reza Radmard, *Tehran*
Ramin Sadeghi, *Mashhad*
Hadi Rokni Yazdi, *Tehran*

Ireland

Tadhg Gleeson, *Wexford*
Frederik JAI Vernimmen, *Cork*

Israel

Dafna Ben Bashat, *Tel Aviv*
Amit Gefen, *Tel Aviv*
Tamar Sella, *Jerusalem*

Italy

Adriano Alippi, *Rome*
Dante Amelio, *Trento*
Michele Anzidei, *Rome*
Filippo F Angileri, *Messinas*
Stefano Arcangeli, *Rome*
Roberto Azzoni, *San Donato milanese*
Tommaso V Bartolotta, *Palermo*
Tommaso Bartalena, *Imola*
Livia Bernardin, *San Bonifacio*
Federico Boschi, *Verona*
Sergio Casciaro, *Lecce*
Emanuele Casciani, *Rome*
Musa M Can, *Napoli*
Alberto Cuocolo, *Napoli*
Michele Ferrara, *Coppito*
Mauro Feola, *Fossano*
Giampiero Francica, *Castel Volturno*
Luigi De Gennaro, *Rome*
Giulio Giovannetti, *Pisa*
Francesca Iacobellis, *Napoli*
Formato Invernizzi, *Monza Brianza*
Francesco Lassandro, *Naples*
Lorenzo Livi, *Florence*
Pier P Mainenti, *Napoli*
Laura Marzetti, *Chieti*
Giuseppe Malinverni, *Crescentino*
Enrica Milanesi, *Turin*
Giovanni Morana, *Treviso*
Lorenzo Monti, *Milan*
Silvia D Morbelli, *Genoa*
Barbara Palumbo, *Perugia*
Cecilia Parazzini, *Milan*
Stefano Pergolizzi, *Messina*
Antonio Pinto, *Naples*
Camillo Porcaro, *Rome*
Carlo C Quattrocchi, *Rome*
Alberto Rebonato, *Perugia*
Giuseppe Rizzo, *Rome*
Roberto De Rosa, *Naples*
Domenico Rubello, *Rovigo*
Andrea Salvati, *Bari*
Sergio Sartori, *Ferrara*
Luca M Sconfienza, *Milano*
Giovanni Storto, *Rionero*
Nicola Sverzellati, *Parma*
Alberto S Tagliafico, *Genova*
Nicola Troisi, *Florence*

Japan

Yasuhiko Hori, *Chiba*
Hidetoshi Ikeda, *Koriyama*
Masahito Kawabori, *Sapporo*
Tamotsu Kamishima, *Sapporo*
Hiro Kiyosue, *Yufu*
Yasunori Minami, *Osaka-sayama*
Yasuhiro Morimoto, *Kitakyushu*
Satoru Murata, *Tokyo*
Shigeki Nagamachi, *Miyazaki*
Hiroshi Onishi, *Yamanashi*
Morio Sato, *Wakayama Shi*
Yoshito Tsushima, *Maebashi*
Masahiro Yanagawa, *Suita*

Netherlands

Willem Jan van Rooij, *Tilburg*

New Zealand

W Howell Round, *Hamilton*

Pakistan

Wazir Muhammad, *Abbottabad*

Poland

Maciej S Baglaj, *Wroclaw*

Piotr Czauderna, *Gdansk*

Portugal

Joao Manuel RS Tavares, *Porto*

Serbia

Olivera Ciraj-Bjelac, *Belgrade*

Singapore

Gopinathan Anil, *Singapore*
Terence KB Teo, *Singapore*
Cher Heng Tan, *Singapore*

Slovakia

Stefan Sivak, *Martin*

South Korea

Ki Seok Choo, *Busan*
Seung Hong Choi, *Seoul*
Dae-Seob Choi, *Jinju*
Hong-Seok Jang, *Seoul*
Yong Jeong, *Daejeon*
Chan Kyo Kim, *Seoul*
Se Hyung Kim, *Seoul*
Joong-Seok Kim, *Seoul*
Sang Eun Kim, *Seongnam*
Sung Joon Kwon, *Seoul*
Jeong Min Lee, *Seoul*
In Sook Lee, *Busan*
Noh Park, *Goyang*
Chang Min Park, *Seoul*
Sung Bin Park, *Seoul*
Deuk Jae Sung, *Seoul*
Choongsoo Shin, *Seoul*
Kwon-Ha Yoon, *Iksan*

Spain

Miguel A De Gregorio, *Zaragoza*
Antonio Luna, *Jaén*
Enrique Marco de Lucas, *Santander*
Fernando Ruiz Santiago, *Granada*

Sweden

Dmitry Grishenkov, *Stockholm*
Tie-Qiang Li, *Stockholm*

Switzerland

Nicolau Beckmann, *Basel*
Christian Boy, *Bern*
Giorgio Treglia, *Bellinzona*

Stephan Ulmer, *Kiel*

Thailand

Sirianong Namwongprom, *Chiang Mai*

Turkey

Kubilay Aydin, *Istanbul*
Ramazan Akdemir, *Sakarya*
Serhat Avcu, *Ankara*
Ayse Aralasmak, *Istanbul*
Oktay Algin, *Ankara*
Nevbahar Akcar, *Meselik*
Bilal Battal, *Ankara*
Zulkif Bozgeyik, *Elazig*
Nazan Ciledag, Aakara
Fuldem Y Donmez, *Ankara*
Gulgun Engin, *Istanbul*
Ahmet Y Goktay, *Izmir*
Oguzhan G Gumustas, *Bursa*
Kaan Gunduz, *Ankara*
Pelin Ozcan Kara, *Mersin*
Kivanc Kamburoglu, *Ankara*
Ozgur Kilickesmez, *Istanbul*
Furuzan Numan, *Istanbul*
Cem Onal, *Adana*
Ozgur Oztekin, *Izmir*
Seda Ozbek (Boruban), *Konya*
Selda Sarikaya, *Zonguldak*
Figen Taser, *Kutahya*
Baran Tokar, *Eskisehir*
Ender Uysal, *Istanbul*
Ensar Yekeler, *Istanbul*

United Kingdom

Indran Davagnanam, *London*
M DC Valdés Hernández, *Edinburgh*
Alan Jackson, *Manchester*
Suneil Jain, *Belfast*
Long R Jiao, *London*
Miltiadis Krokidis, *Cambridge*
Pradesh Kumar, *Liverpool*
Peter D Kuzmich, *Derby*
Georgios Plataniotis, *Brighton*
Vanessa Sluming, *Liverpool*

United States

Garima Agrawal, *Saint Louis*
James R Brasic, *Baltimore*
Rajendra D Badgaiyan, *Buffalo*
Ulas Bagci, *Bethesda*
Anat Biegon, *Stony Brook*
Ramon Casanova, *Winston Salem*
Wenli Cai, *Boston*
Zheng Chang, *Durham*
Corey J Chakarun, *Long Beach*
Kai Chen, *Los Angeles*
Hyun-Soon Chong, *Chicago*
Marco Cura, *Dallas*
Ravi R Desai, *Bensalem*
Delia DeBuc, *Miami*
Carlo N De Cecco, *Charleston*
Timm-Michael L Dickfeld, *Baltimore*
Subba R Digumarthy, *Boston*
Huy M Do, *Stanford*
Todd A Faasse, *Grand Rapids*
Salomao Faintuch, *Boston*
Girish M Fatterpekar, *New York*
Dhakshinamoorthy Ganeshan, *Houston*
Robert J Griffin, *Little Rock*
Andrew J Gunn, *Boston*
Sandeep S Hedgire, *Boston*
Timothy J Hoffman, *Columbia*
Mai-Lan Ho, *San Francisco*
Juebin Huang, *Jackson*
Abid Irshad, *Charleston*
Matilde Inglese, *New York*
El-Sayed H Ibrahim, *Jacksonville*
Paul R Julsrud, *Rochester*
Pamela T Johnson, *Baltimore*
Ming-Hung Kao, *Tempe*
Sunil Krishnan, *Houston*
Richard A Komoroski, *Cincinnati*
Sandi A Kwee, *Honolulu*
King Kim, *Ft. Lauderdale*
Guozheng Liu, *Worcester*
Yiyan Liu, *Newark*
Venkatesh Mani, *New York*
Lian-Sheng Ma, *Pleasanton*
Rachna Madan, *Boston*
Zeyad A Metwalli, *Houston*
Yilong Ma, *Manhasset*
Hui Mao, *Atlanta*
Feroze B Mohamed, *Philadelphia*
Gul Moonis, *Boston*
John L Nosher, *New Brunswick*
Rahmi Oklu, *Boston*
Aytekin Oto, *Chicago*
Bishnuhari Paudyal, *Philadelphia*
Rajul Pandya, *Youngstown*
Chong-Xian Pan, *Sacramento*
Jay J Pillai, *Baltimore*
Neal Prakash, *Duarte*
Reza Rahbar, *Boston*
Ali S Raja, *Boston*
Gustavo J Rodriguez, *El Paso*
David J Sahn, *Portlsand*
Steven Schild, *Scottsdale*
Ali R Sepahdari, *Los Angeles*
Li Shen, *Indianapolis*
JP Sheehan, *Charlottesville*
Atul B Shinagare, *Boston*
Sarabjeet Singh, *Boston*
Charles J Smith, *Columbia*
Kenji Suzuki, *Chicago*
Monvadi Srichai-Parsia, *Washington*
Sree H Tirumani, *Boston*
Hebert A Vargas, *New York*
Sachit Verma, *Philadelphia*
Yoichi Watanabe, *Minneapolis*
Li Wang, *Chapel Hill*
Carol C Wu, *Boston*
Shoujun Xu, *Houston*
Min Yao, *Cleveland*
Xiaofeng Yang, *Atlanta*
Qingbao Yu, *Albuquerque*
Aifeng Zhang, *Chicago*
Chao Zhou, *Bethlehem*
Hongming Zhuang, *Philadelphia*

WJR World Journal of Radiology

Contents

Monthly Volume 7 Number 7 July 28, 2015

NAME OF JOURNAL
World Journal of Radiology

ISSN
ISSN 1949-8470 (online)

LAUNCH DATE
December 31, 2009

FREQUENCY
Monthly

EDITORIAL OFFICE
Jin-Lei Wang, Director
Xiu-Xia Song, Vice Director
World Journal of Radiology
Room 903, Building D, Ocean International Center,
No. 62 Dongsihuan Zhonglu, Chaoyang District,
Beijing 100025, China
Telephone: +86-10-59080039
Fax: +86-10-85381893
E-mail: editorialoffice@wjgnet.com
Help Desk: http://www.wjgnet.com/esps/helpdesk.aspx
http://www.wjgnet.com

PUBLISHER
Baishideng Publishing Group Inc
8226 Regency Drive,
Pleasanton, CA 94588, USA
Telephone: +1-925-223-8242
Fax: +1-925-223-8243
E-mail: bpgoffice@wjgnet.com
Help Desk: http://www.wjgnet.com/esps/helpdesk.aspx
http://www.wjgnet.com

PUBLICATION DATE
July 28, 2015

INSTRUCTIONS TO AUTHORS
Full instructions are available online at http://www.wjgnet.com/1949-8470/g_info_20100316162358.htm.

ONLINE SUBMISSION
http://www.wjgnet.com/esps/

World Journal of Radiology

Submit a Manuscript: http://www.wjgnet.com/esps/
Help Desk: http://www.wjgnet.com/esps/helpdesk.aspx
DOI: 10.4329/wjr.v7.i7.143

World J Radiol 2015 July 28; 7(7): 143-148
ISSN 1949-8470 (online)

EDITORIAL

Endovascular management of visceral artery aneurysms: When to watch, when to intervene?

Romaric Loffroy, Sylvain Favelier, Pierre Pottecher, Pierre-Yves Genson, Louis Estivalet, Sophie Gehin, Jean-Pierre Cercueil, Denis Krausé

Romaric Loffroy, Sylvain Favelier, Pierre Pottecher, Pierre-Yves Genson, Louis Estivalet, Sophie Gehin, Jean-Pierre Cercueil, Denis Krausé, Department of Vascular, Oncologic and Interventional Radiology, University of Dijon School of Medicine, Bocage Teaching Hospital, 21079 Dijon Cedex, France

Author contributions: Loffroy R, Favelier S and Pottecher P wrote the paper; Genson PY, Estivalet L, Gehin S, Cercueil JP and Krausé D revised the article for important intellectual content; all authors read and approved the final manuscript.

Conflict-of-interest statement: The authors have no conflict of interest to declare.

Correspondence to: Romaric Loffroy, MD, PhD, Professor, Department of Vascular, Oncologic and Interventional Radiology, Le2i UMR CNRS 6306, University of Dijon School of Medicine, Bocage Teaching Hospital, 14 Rue Paul Gaffarel, BP 77908, 21079 Dijon Cedex, France. romaric.loffroy@chu-dijon.fr
Telephone: +33-380-293677
Fax: +33-380-295455

Received: January 12, 2015
Peer-review started: January 15, 2015
First decision: April 10, 2015
Revised: April 17, 2015
Accepted: May 5, 2015
Article in press: May 6, 2015
Published online: July 28, 2015

Abstract

Visceral artery aneurysms (VAA) include splanchnic and renal artery aneurysms. They represent a rare clinical entity, although their detection is rising due to an increased use of cross-sectional imaging. Rupture is the most devastating complication, and is associated with a high morbidity and mortality. In addition, increased percutaneous endovascular interventions have raised the incidence of iatrogenic visceral artery pseudoaneurysms (VAPAs). For this reason, elective repair is preferable in the appropriately chosen patient. Controversy still exists regarding their treatment. Over the past decade, there has been steady increase in the utilization of minimally invasive, non-operative interventions, for vascular aneurysmal disease. All VAAs and VAPAs can technically be fixed by endovascular techniques but that does not mean they should. These catheter-based techniques constitute an excellent approach in the elective setting. However, in the emergent setting it may carry a higher morbidity and mortality. The decision for intervention has to take into account the size and the natural history of the lesion, the risk of rupture, which is high during pregnancy, and the relative risk of surgical or radiological intervention. For splanchnic artery aneurysms, we should recognize that we are not, in reality, well informed about their natural history. For most asymptomatic aneurysms, expectant treatment is acceptable. For large, symptomatic or aneurysms with a high risk of rupture, endovascular treatment has become the first-line therapy. Treatment of VAPAs is always mandatory because of the high risk of rupture. We present our point of view on interventional radiology in the splanchnic arteries, focusing on what has been achieved and the remaining challenges.

Key words: Visceral artery; Aneurysm; False aneurysm; Angiography; Embolization; Stent-graft

Core tip: This editorial deals with interventional radiological techniques in the splanchnic arteries, focusing on

what has been achieved and the remaining challenges. For splanchnic artery aneurysms, we should recognize that we are not, in reality, well informed about their natural history. The indications for the embolization of aneurysms are limited depending on the morphology of the aneurysm and surrounding vessels. Rotational angiography and other recently developed imaging techniques can help analyze the vascular anatomy of every lesion in decision making on the appropriate treatment for each patient when choosing between embolization, surgery and surveillance.

Loffroy R, Favelier S, Pottecher P, Genson PY, Estivalet L, Gehin S, Cercueil JP, Krausé D. Endovascular management of visceral artery aneurysms: When to watch, when to intervene? *World J Radiol* 2015; 7(7): 143-148 Available from: URL: http://www.wjgnet.com/1949-8470/full/v7/i7/143.htm DOI: http://dx.doi.org/10.4329/wjr.v7.i7.143

INTRODUCTION

Visceral aneurysms represent a rare clinical entity; however, 10%-20% will rupture and this is accompanied by a significant mortality rate of 20%-70%, depending on the location of the aneurysm. Their incidence is increasing and controversy still exists regarding their treatment[1]. The decision for intervention has to take into account the size and the natural history of the lesion, the risk of rupture, which is high during pregnancy, and the relative risk of surgical or radiological intervention. For most asymptomatic aneurysms, expectant treatment is acceptable. For large, symptomatic or aneurysms with a high risk of rupture, endovascular treatment has become the first-line therapy[2]. Treatment of visceral artery pseudoaneurysms (VAPAs) is always mandatory because of the high risk of rupture. The purpose of this article is to answer some questions about the current use of interventional techniques in the treatment of visceral artery aneurysms (VAAs) and VAPAs.

WHAT ARE THE CURRENT THRESHOLDS FOR INTERVENTION IN VISCERAL ANEURYSMS?

We can divide the discussion between true VAAs and VAPAs because the thresholds are completely different. For VAPAs due to inflammation or pancreatitis [*e.g.*, splenic, gastroduodenal (GDA), superior mesenteric artery (SMA), hepatic, or even renal aneurysms], trauma, or those occurring after surgery, the thresholds for treatment are very low. Even small aneurysms (2-5 mm) should be treated regardless of diameter because the risk of rupture for VAPAs is not related to their size. The type of aneurysm may (rarely) spontaneously heal, but in most cases, VAPAs will increase over time and eventually rupture. We should treat all of these aneurysms immediately after diagnosis, irrespective of their location or origin[1-3].

For true aneurysms, the treatment threshold is different and depends mainly on anatomic location. The threshold for most true splenic artery aneurysms is 2 cm in diameter at the largest axis. Even if peripheral thrombus is present, these aneurysms should be treated in cases of an overall diameter larger than 2 cm. Women of childbearing age should be treated regardless of the diameter because the risk increase significantly during pregnancy[3].

One of the vascular complications of portal hypertension, which could occur in cirrhotic patients, is the development of intrasplenic or extrasplenic aneurysms. These lesions should not be treated systematically except in cases of aneurysms > 4 cm in diameter and in extrasplenic locations. In most cases, multiple, diffuse, small aneurysms related to portal hypertension should be left untreated and followed by repeat computed tomography (CT) or magnetic resonance imaging (MRI) examinations. Once the portal hypertension and underlying cirrhotic disease is treated (*e.g.*, *via* liver transplantation), the aneurysm may spontaneously decrease and completely disappear over time.

Other types of true aneurysms such as GDAs or those in the pancreaticoduodenal arcades, which can be caused by chronic hyperkinetic flow, should be treated as soon as they are diagnosed because they are at high risk of rupture, even when small in size. In such aneurysms associated with celiac trunk stenosis, inversion of the flow in the pancreaticoduodenal arcades to revascularize the liver or spleen needs to be preserved during the embolization procedure, which is sometimes a technical challenge[4].

For true hepatic or SMA aneurysms, the threshold for treatment is slightly lower than for splenic aneurysms. In most cases, we treat hepatic or SMA aneurysms when the large axis is > 1 to 1.5 cm.

The treatment of renal aneurysms is intended to prevent rupture either in the urinary tract or in the unclosed retroperitoneal space, as well as the development of systemic hypertension or renal failure in cases of intrarenal arteriovenous fistula development. Even small aneurysms could be the cause of changes to intrarenal hemodynamics and systemic hypertension and should, in this case, be treated endovascularly or surgically, depending on the type (saccular or fusiform) and location. In the case of isolated, non-symptomatic aneurysms in the renal arteries, the treatment threshold is around 1 to 1.5 cm[1-4].

For both visceral and renal arteries, extraparenchymal aneurysms take priority over intraparenchymal aneurysms because the risks and severity of major rupture and hemorrhage seem significantly higher for proximal extraparenchymal lesions.

HOW HAVE THRESHOLDS EVOLVED OVER THE LAST TWO DECADES?

The threshold for aneurysm treatment due to pancreaticoduodenal arcade has evolved and is now very

low. This was different 15 to 20 years ago. Considering this type of true aneurysm, the relationship between the celiac trunk or SMA stenosis and the development of hyperkinetic aneurysms was not well known. Only in the last 8 to 10 years has the relationship between these two conditions been established[4].

The threshold for treatment of renal, hepatic, SMA, or splenic aneurysm has been established for 10 or 15 years, and it has not significantly changed. However, we actually can treat all of these types of aneurysms by endovascular approaches instead of a more aggressive, invasive surgical approach. It's easier to treat these aneurysms now due to the evolution of endovascular techniques through a better understanding of peripheral conditions, as well as employment of neurovascular techniques. For the last 10 years, we have been performing peripheral interventions, applying neuro techniques for peripheral purposes with success. We know that the risks of rupture are very low in SMA or hepatic aneurysms < 1 cm, but we can treat these small aneurysms efficiently and safely with the endovascular approach. Most clinicians and patients prefer that these aneurysms are treated, because after treatment, the problem is solved. These patients, if left untreated, should have follow-up with CT scan, MRI, or ultrasonography each year or even every 6 mo.

ARE THERE DIFFERENT THRESHOLDS FOR PATIENTS WITH OTHER UNDERLYING CONDITIONS?

Patients with vasculitis such as Ehlers-Danlos disease type Ⅳ who develop even very small, true aneurysms should be treated regardless of the size because the risk of rupture is very high due to intrinsic defects in the vascular wall. Aneurysms in patients with Ehlers-Danlos syndrome will invariably increase over time and should be treated as soon as the diagnosis has been established, preferentially by endovascular reconstruction or segmental vascular exclusion instead of simple aneurysm coiling[1,2].

IS THERE A RELATIONSHIP BETWEEN THE TREATMENT THRESHOLD AND THE TYPE OF MATERIAL USED?

The threshold to decide if we treat is never directly related to the material we use. For example, a proximal 3-cm-diameter splenic aneurysm can be treated with coiling, stent graft placement, segmental vascular exclusion, or even potentially a flow diverter.

Ten years ago, we only used coils or glue, because we didn't have very smooth and flexible microcoils. We also didn't have flexible stent grafts or flow diverters, and we couldn't use an imaging-guided direct percutaneous approach in cases of inaccessible lesions due to vascular sinuosity or proximal obstruction. With the tools and techniques we have today, by preserving vessel patency, we can conservatively treat even large-neck and fusiform aneurysms that could have only been treated by segmental vascular exclusion before. Now, we can exclude the entire aneurysm and preserve the afferent arteries in more than 90% to 95% of cases. It is particularly important for splenic and renal function that we can treat extraparenchymal or hilar aneurysms while preserving the parent arteries and distal flow[1-3].

WHAT ARE SOME ADVANCEMENTS IN ACCESS TECHNOLOGIES AND TECHNIQUES FOR THE TREATMENT OF VISCERAL ANEURYSMS?

We have now the opportunity to use neuroendovascular tools for peripheral aneurysm exclusion. Over the last 10 years, many neurological techniques have been developed into dedicated peripheral applications. For instance, the use of a balloon remodeling technique was created initially for neurointerventions by Moret *et al*[5] 15 years ago. Ten years ago, one main limiting factor in treating visceral aneurysms with large necks was the risk of coils protruding outside the aneurysm or occluding the parent arteries. The first use of a balloon remodeling technique to increase coil density and avoid protrusion of coils in the parent artery was performed by Moret *et al*[5] in 1997. This technique is routinely used in some centers to overcome limitations due to broad neck, unstable microcatheter, or to treat complex renal/splenic/SMA aneurysms. The combination of Onyx (Covidien) as an embolic agent with Onyx-compatible remodeling balloon has been used by several physicians to treat hilar renal and SMA aneurysms[6]. To preserve the parent artery, we can use bare stents and coiling through the mesh of the stent with a microcatheter and microcoils[7-11]. Alternatively, we can use kissing stents in cases of aneurysms located at bifurcations, which is often the case with renal arteries. To preserve vascularization of the kidney, we use a double-kissing stent or kissing-balloon remodeling technique and detachable coils. Another great technical advancement is the use of detachable coils instead of pushable coils. For neurointerventions, 20 years ago, radiologists started using exclusively detachable coils for cerebral aneurysm embolization, and now there are many types of detachable coils for peripheral applications provided by various companies (*e.g.*, Terumo Interventional Systems, Boston Scientific Corporation, Cook Medical, and Covidien).

This is a significant advancement because it has increased the safety of treatment of even large-necked aneurysms by reducing the risk of periprocedural distal embolization of coils, especially for splenic and renal locations.

Hepatic artery aneurysms are probably the easiest to treat, as there is dual flow to the liver (arterial and portal), and we can we can completely exclude seg-

mentally the parent artery that is responsible for the aneurysm without any risk of ischemia to the liver. Hepatic aneurysms can be treated by different methods including coil packing of the aneurysm sac, segmental coil trapping of the parent artery ("sandwich technique"), placement of a covered stent in cases of proximal or relatively straight distal artery, or a combination of bare stent and microcoils through the mesh[8-10].

The main challenge is with the SMA and renal arteries because we must preserve distal flow and therefore maintain parent vessel patency by using remodeling coils/Onyx techniques, stent grafts, or a combination of bare stent and microcoils. Conversely, in cases of extraparenchymal splenic aneurysm, we use a different approach. The splenic artery is sometimes difficult to navigate, even with small and soft microcatheters. However, in most cases of splenic aneurysm, we can perform segmental splenic artery exclusion by deploying coils distally and proximally. Coil placement on both sides of the aneurysm is safe because there is enough collateralization through the gastric and pancreatic arteries, and this collateralization will revascularize the spleen at the ileum and help to preserve the intrasplenic blood flow.

We believe that the medial or proximal part of the splenic artery can be completely excluded without risk. It is probably the best treatment for splenic aneurysms, especially for pancreatitis-related pseudoaneurysm.

As mentioned previously, pseudoaneurysm due to inflammation, pancreatitis, trauma, and mycotic aneurysm should normally not be treated by packing the aneurysm alone, even if good results have been reported with this technique[12]. These pseudoaneurysms should preferentially be treated by segmental artery exclusion because the aneurysm is secondary to progressive regional arterial wall deterioration. If we only treat the aneurysm, the patient is at risk of aneurysm recurrence on both sides of the occluded neck because the wall is destroyed by the inflammatory process. In this case, the best and only efficient and safe treatment is to completely exclude the parent artery, distally and proximally, to be sure you've completely solved the regional problem. Placement of a covered stent with extensive proximal and distal landing zones could be an acceptable alternative.

Stent grafts may be useful to preserve the distal vascularization. We have used coronary stent grafts because of their high flexibility; they can be navigated through tortuous arteries[9-11]. These balloon-expandable stent grafts are mounted on very thin microcatheters and can reach distal aneurysms. Coronary stent grafts are limited by the length and diameters available, which range between 9 and 22 mm and 2 and 4.5 mm, respectively. Small dedicated stents are now available on the market for visceral aneurysms (V12, Maquet).

Inaccessible small aneurysms or pseudoaneurysms in the GDA or pancreaticoduodenal arcades may also be treated with liquid embolics, such as N-butyl cyanoacrylate glue (Glubran2, GEM) or Onyx instead of coils[6,13]. If we cannot reach a distal aneurysm due to a tortuous access, we place a small catheter as close as possible to the aneurysm and inject a mixture of glue diluted by Lipiodol (Guerbet) in variable ratios depending on the flow and distance between the point of injection and the target. We can inject the glue slowly, moving distally to exclude both the aneurysm and the arterial segments beyond and behind the aneurysm. This is the so-called front-and-back-door occlusion.

In the same way, for inaccessible aneurysms, we can use liquid embolics injected through collaterals when the main artery has been occluded for another reason and the aneurysm still grows or after previous artery occlusion, or if coils have been placed but were not sufficiently packed. The aneurysm remains open because collaterals revascularize the aneurysm, requiring navigation of very thin neuro microcatheters through tortuous collaterals to occlude the aneurysm using Onyx or glue[6,13].

In cases when the aneurysms cannot be accessed by an endovascular approach or if proximal injection of liquid embolic agents is considered too dangerous, we can use a direct percutaneous ultrasound/CT-guided approach. This method could be used not only for intraparenchymal aneurysms in the spleen, liver, kidney, and pancreas, but also for extraparenchymal aneurysms, especially for SMA, GDA, or pancreaticoduodenal aneurysms that we cannot access safely.

Using cone-beam CT imaging guidance or conventional spiral CT, an 18-G guiding needle is first placed from the abdominal or back entry site to the target to stiffen the tract, and a microcatheter is navigated through the external needle into the aneurysm. Thrombin or even glue is slowly injected to get an immediate occlusion. Sometimes, we can fill the aneurysm with microcoils. If the lesion is clearly visible by ultrasonography, it's easy to place the needle through the splenic/renal or hepatic parenchyma into the aneurysm. The needle tip is clearly visible in the aneurysm by using color duplex ultrasonography. This is a major improvement in the treatment of visceral aneurysms inaccessible by an endovascular approach.

ARE THERE ANY OTHER DEVICES OR TECHNIQUES THAT ARE AVAILABLE?

In cases of small aneurysms, there is a risk of perforation when you place the first coils. If this occurs, the coils should be completely placed and detached as quickly as possible to stop the bleeding. When using the balloon technique, inflation of the balloon stops the flow or the bleeding if it occurs and helps solve the problem. During placement of the first coil in a small aneurysm, the remodeling balloon technique is very useful to avoid or address bleeding complications.

Another interesting technical approach to treat pseudoaneurysms with liquids while avoiding distal untargeted embolization is to inject liquid embolic or glue

through the microcatheter just in front of the aneurysm. The exact volume of contrast media necessary to fill the aneurysmal cavity and segmental arteries in front and back is estimated. Before injecting the glue, epinephrine, a vasoconstrictor, is injected to induce occlusive spasm of the artery distal to the aneurysm[13]. Using this technique, there is no risk of glue migration far into the distal arteries and parenchyma.

ARE THERE ANY CLINICAL SCENARIOS IN WHICH A SURGICAL APPROACH IS PREFERRED?

The remaining indications for a surgical approach for visceral aneurysms are few, even for the less common types of fusiform aneurysms. These aneurysms are normally not treated if the dilatation is less than two times the normal diameter of the artery. These may be treated wit a combination of stents and coils, stent grafts (often too rigid), as well as by new devices used for neurointervention, such as flow diverters or multilayer uncovered metallic stents. Due to vascular intima remodeling combined with modification of the hemodynamic flow leading to progressive thrombotic phenomena inside the aneurysm, the placement of such a new device leads to complete aneurysm occlusion in most cases while the arterial lumen is kept patent. Flow diverter stents are more and more often used to treat aneurysms with very large necks or that cannot be managed by a remodeling technique or covered stent placement because of insufficient safe landing zone[14]. When using a covered stent, especially for renal aneurysms, we often do not have sufficient landing zones on both sides of the aneurysm. This angiographic condition seems to be a good indication to use a flow diverter stent because there is no need for a landing zone with flow diverter implantation. Flow diverters keep the side branches patent, which is the main advantage of these devices compared to stent grafts.

Some European physicians have used multilayer stents to treat fusiform renal artery aneurysms or visceral aneurysms that cannot be coiled for technical reasons[14]. Preliminary results of the use of multilayer intra-arterial stents for peripheral applications are very promising. However, flow diverter placement requires dual-antiplatelet therapy for a minimum of 4 to 6 mo because of the risk of platelet aggregation on the dense metallic surface.

For splenic aneurysms, or aneurysms that can be treated by parent artery occlusion, we can also place Amplatzer plugs (St. Jude Medical). Plugs deployed distally and proximally to the aneurysm will lead quickly to complete occlusion of the parent artery[1-4]. This technique, mainly used for splenic aneurysms as well as hepatic aneurysms, seems very promising because it is quick, highly efficient, and probably less expensive compared to other treatment options. Furthermore, Amplatzer vascular plugs are safe in high-flow or short-segmental lesion cases, because the device can be retrieved and repositioned if the initial location is unsatisfactory. The main limiting factor is the rigidity of the device. The AVP Ⅳ family from St. Jude Medical is the most flexible, but we are still limited because the device requires a 4-F, 0.0038-inch inner lumen catheter. A new, more flexible microplug from Reverse Medical, the MVP microvascular plug, is available in two sizes for peripheral vascular use. Comparative trials with conventional microcoils are needed.

WHAT TRIALS ARE NEEDED IN THIS FIELD?

The thresholds for indication to treat are well known, but understanding which type of treatment is best to use remains questionable. It will be interesting to see if we can get better results by using new devices such as flow diverters compared with more conventional coiling or balloon remodeling[5,14]. When we coil an aneurysm, we completely exclude the aneurysm, but the neck remains unclosed even if there is some endothelialization over time. When using flow diverter stents, we do not treat the aneurysm itself, but we treat the arterial wall defect by closing the neck and reinforcing the adjacent side wall.

For standard coiling of simple aneurysms, it will be interesting to know if better results can be obtained in terms of completion and stability of aneurysm occlusion if we use hydrogel-coated coils instead of conventional uncoated coils.

Studies could also compare the mid- and long-term results of coiling with hydrogel-coated coils to flow diverting stents. For cerebral aneurysms, interventional neuro are using more and more flow diverters instead of coiling so why not the same trends in visceral aneurysms?

REFERENCES

1 **Belli AM**, Markose G, Morgan R. The role of interventional radiology in the management of abdominal visceral artery aneurysms. *Cardiovasc Intervent Radiol* 2012; **35**: 234-243 [PMID: 21674280 DOI: 10.1007/s00270-011-0201-3]

2 **Jana M**, Gamanagatti S, Mukund A, Paul S, Gupta P, Garg P, Chattopadhyay TK, Sahni P. Endovascular management in abdominal visceral arterial aneurysms: A pictorial essay. *World J Radiol* 2011; **3**: 182-187 [PMID: 21860714 DOI: 10.4329/wjr.v3.i7.182]

3 **Loffroy R**, Guiu B, Cercueil JP, Lepage C, Cheynel N, Steinmetz E, Ricolfi F, Krausé D. Transcatheter arterial embolization of splenic artery aneurysms and pseudoaneurysms: short- and long-term results. *Ann Vasc Surg* 2008; **22**: 618-626 [PMID: 18504106 DOI: 10.1016/j.avsg.2008.02.018]

4 **Flood K**, Nicholson AA. Inferior pancreaticoduodenal artery aneurysms associated with occlusive lesions of the celiac axis: diagnosis, treatment options, outcomes, and review of the literature. *Cardiovasc Intervent Radiol* 2013; **36**: 578-587 [PMID: 23152034 DOI: 10.1007/s00270-012-0473-2]

5 **Moret J**, Cognard C, Weill A, Castaings L, Rey A. The "Remodelling Technique" in the Treatment of Wide Neck Intracranial Aneurysms. Angiographic Results and Clinical Follow-up in 56 Cases. *Interv Neuroradiol* 1997; **3**: 21-35 [PMID: 20678369]

6 **Bratby MJ**, Lehmann ED, Bottomley J, Kessel DO, Nicholson AA, McPherson SJ, Morgan RA, Belli AM. Endovascular embolization of visceral artery aneurysms with ethylene-vinyl alcohol (Onyx): a case series. *Cardiovasc Intervent Radiol* 2006; **29**: 1125-1128 [PMID: 16625409 DOI: 10.1007/s00270-005-0148-3]

7 **Ikeda O**, Nakasone Y, Tamura Y, Yamashita Y. Endovascular management of visceral artery pseudoaneurysms: transcatheter coil embolization using the isolation technique. *Cardiovasc Intervent Radiol* 2010; **33**: 1128-1134 [PMID: 20857110 DOI: 10.1007/s00270-010-9973-0]

8 **Yasumoto T**, Osuga K, Yamamoto H, Ono Y, Masada M, Mikami K, Kanamori D, Nakamura M, Tanaka K, Nakazawa T, Higashihara H, Maeda N, Tomiyama N. Long-term outcomes of coil packing for visceral aneurysms: correlation between packing density and incidence of coil compaction or recanalization. *J Vasc Interv Radiol* 2013; **24**: 1798-1807 [PMID: 23810652 DOI: 10.1016/j.jvir.2013.04.030]

9 **Künzle S**, Glenck M, Puippe G, Schadde E, Mayer D, Pfammatter T. Stent-graft repairs of visceral and renal artery aneurysms are effective and result in long-term patency. *J Vasc Interv Radiol* 2013; **24**: 989-996 [PMID: 23727420 DOI: 10.1016/j.jvir.2013.03.025]

10 **Manninen HI**, Berg M, Vanninen RL. Stent-assisted coil embolization of wide-necked renal artery bifurcation aneurysms. *J Vasc Interv Radiol* 2008; **19**: 487-492 [PMID: 18375290 DOI: 10.1016/j.jvir.2007.10.026]

11 **Favelier S**, Kretz B, Tanter Y, Loffroy R. Stent-assisted detachable coil embolization of a late-onset wide-necked anastomotic renal allograft artery pseudoaneurysm. *J Vasc Surg* 2012; **56**: 1131 [PMID: 23026424 DOI: 10.1016/j.jvs.2011.09.097]

12 **Loffroy R**, Rao P, Ota S, De Lin M, Kwak BK, Krause D, Geschwind JF. Packing technique for endovascular coil embolisation of peripheral arterial pseudo-aneurysms with preservation of the parent artery: safety, efficacy and outcomes. *Eur J Vasc Endovasc Surg* 2010; **40**: 209-215 [PMID: 20399122 DOI: 10.1016/j.ejvs.2010.03.009]

13 **Morishita H**, Yamagami T, Takeuchi Y, Matsumoto T, Asai S, Masui K, Sato H, Taniguchi F, Sato O, Nishimura T. A new flow control technique using diluted epinephrine in the N-butyl-2-cyanoacrylate embolization of visceral artery pseudoaneurysms secondary to chronic pancreatitis. *Cardiovasc Intervent Radiol* 2012; **35**: 932-937 [PMID: 22037708 DOI: 10.1007/s00270-011-0294-8]

14 **Sfyroeras GS**, Dalainas I, Giannakopoulos TG, Antonopoulos K, Kakisis JD, Liapis CD. Flow-diverting stents for the treatment of arterial aneurysms. *J Vasc Surg* 2012; **56**: 839-846 [PMID: 22840737 DOI: 10.1016/j.jvs.2012.04.020]

P- Reviewer: Murata S, Setacci C, Schoenhagen P
S- Editor: Ji FF **L- Editor**: A **E- Editor**: Liu SQ

World Journal of Radiology

Submit a Manuscript: http://www.wjgnet.com/esps/
Help Desk: http://www.wjgnet.com/esps/helpdesk.aspx
DOI: 10.4329/wjr.v7.i7.149

World J Radiol 2015 July 28; 7(7): 149-156
ISSN 1949-8470 (online)

EDITORIAL

Diffusion-weighted and diffusion-tensor imaging of normal and diseased uterus

Duygu Kara Bozkurt, Murat Bozkurt, Mehmet Ali Nazli, Ilhan Nahit Mutlu, Ozgur Kilickesmez

Duygu Kara Bozkurt, Depatment of Radiology, School of Medicine, Kafkas University, 36000 Kars,Turkey

Murat Bozkurt, Depatment of Obstetrics and Gynecology, School of Medicine, Kafkas University, 36000 Kars, Turkey

Mehmet Ali Nazli, Ilhan Nahit Mutlu, Ozgur Kilickesmez, Department of Diagnostic and Interventional Radiology, Istanbul Training and Research Hospital, 34098 Samatya, Istanbul, Turkey

Author contributions: Kara Bozkurt D and Kilickesmez O had equally contributed to this paper; Kara Bozkurt D and Bozkurt M wrote the paper; Nazli MA and Mutlu IN collected the figures and the literatures; Kilickesmez O approved the final version.

Conflict-of-interest statement: There's no conflict of interest.

Correspondence to: Ozgur Kilickesmez, MD, Associate Professor of Radiology, Department of Diagnostic and Interventional Radiology, Istanbul Training and Research Hospital, Org. Nafiz Gurman St, 34098 Samatya, Istanbul, Turkey. okilickesmez@yahoo.com
Telephone: +90-532-7346196
Fax: +90-216-4693796

Received: February 9, 2015
Peer-review started: February 9, 2015
First decision: March 20, 2015
Revised: April 25, 2015
Accepted: May 7, 2015
Article in press: May 8, 2015
Published online: July 28, 2015

Abstract

Owing to technical advances and improvement of the software, diffusion weighted imaging and diffusion tensor imaging (DWI and DTI) greatly improved the diagnostic value of magnetic resonance imaging (MRI) of the pelvic region. These imaging sequences can exhibit important tissue contrast on the basis of random diffusion (Brownian motion) of water molecules in tissues. Quantitative measurements can be done with DWI and DTI by apparent diffusion coefficient (ADC) and fractional anisotropy (FA) values respectively. ADC and FA values may be changed by various physiological and pathological conditions providing additional information to conventional MRI. The quantitative DWI assists significantly in the differentiation of benign and malignant lesions. It can demonstrate the microstructural architecture and celluler density of the normal and diseased uterine zones. On the other hand, DWI and DTI are useful for monitoring the treatment outcome of the uterine lesions. In this review, we discussed advantages of DWI and DTI of the normal and diseased uterus.

Key words: Magnetic resonance imaging; Diffusion weighted imaging; Diffusion tensor imaging; Uterus

Core tip: Diffusion weighted imaging (DWI) and diffusion tensor imaging (DTI) sequences greatly improved the diagnostic value of magnetic resonance imaging of the uterus with the additional benefits of functional information. They reflect the microstructural architecture and cellular density of the uterine zones and enable quantitative evaluation. Depending on this review, DWI and DTI appear to be applicable and reliable methods for demonstrating physiological changes of the uterus, benign and malignant characteristics of uterine zones

and monitoring the treatment outcome of the uterine diseases.

Kara Bozkurt D, Bozkurt M, Nazli MA, Mutlu IN, Kilickesmez O. Diffusion-weighted and diffusion-tensor imaging of normal and diseased uterus. *World J Radiol* 2015; 7(7): 149-156 Available from: URL: http://www.wjgnet.com/1949-8470/full/v7/i7/149.htm DOI: http://dx.doi.org/10.4329/wjr.v7.i7.149

INTRODUCTION

Diffusion weighted imaging (DWI) is a magnetic resonance imaging (MRI) sequence structured on the basis of diffusion (Brownian motion) of water molecules in the extracellular space and is being increasingly used to evaluate the female pelvis. The quantitative parameter acquired from DWI sequenceis the apparent diffusion coefficient (ADC) value. The basic factors affecting the ADC values are tissue structures, interactions between the molecules and cellular density. Thus, ADC is altered by many physiological and pathological conditions of the body[1].

Uterus is a fibromuscular solid organ under the effect of the hormones and is composed of three layers: the endometrial, the junctional and the myometrial zones. Physiological (menstrual cycle, menopausal period) fluctuations of these zones change the ADC values used in the evaluation of uterine abnormalities[1].

Diffusion is a multi-dimensional process, which occures in different values in different directions depending on the microstructure of the tissues. Since uterine myometrium is composed of smooth muscle bundles and connective tissue diffusion reflects anisotropic features. Though DWI gives information about the direction of diffusion and cellularity of the tissue, anisotropic characteristics of tissues can be assessed appropriately by diffusion tensor imaging (DTI). It can be used to detect water diffusion directionality which in turn shows the microstructural architecture of normal and diseased tissue. Fractional anisotropy (FA) is the main quantitative parameter obtained from DTI data. Initially DTI has been used to show and evaluate the integrity of white matter tracts in neuroradiology. With the improvement of the MRI hardware and softwares, fast imaging techniques, after the use of DWI also DTI was implemented to abdominal imaging for some of the abdominal organs like uterus. The initial researches have been published regarding DTI of the uterus specimens of the patients to whom hysterectomy was performed for medical reasons[2-4] and then *in vivo* on the uterus of the patients[5].

Non-functional (conventional) MRI provides excellent anatomical information of the uterus, however, the morphological appearance still may not differentiate some of the benign and malignant uterine lesions[6]. DWI and DTI which provide functional information and when combined with conventional MRI become a complementary diagnostic tool for the uterus and giving more information for the differentiation and extension of benign and malignant lesions, and for the follow up of treatment outcome after uterine arterial embolization (UAE), oncological therapies[7].

In this paper, we aimed to focus on and review their diagnostic importance of the DWI and DTI techniques of the normal and diseased uterus.

DWI AND DTI TECHNIQUE

Optimal MRI of the female pelvis should be performed on a high field strength MRI system (1.5 or 3 T) using local phased-array coils. High field strenght MRI and phased-array coils increase the signal-to-noise ratio, provide high resolution images for the DWI and DTI sequences. Besides development of ultra-fast pulse sequences such as echo-planar imaging and parallel imaging technique, enabled to prevent motion artefacts and consequently functional MRI of the female pelvis[8].

For conventional MRI T1, T2 and fat saturated T2-weighted fast spin echo sequences followed with pre and post contrast three dimensional gradient-recalled echo volumetric interpolated breath-hold sequences and three plane imaging is necessary which give morphological information about the uterine zones. The addition of DWI and DTI sequences to the conventional MRI gives functional data about the uterus.

DWI is acquired by the measurement of signal loss after a series of two motion-providing gradient (MPG) pulses with the addition of a 180° refocusing radio frequency pulse to both sides for enhancing the variations of molecular diffusion between tissues. The density of MPG pulses is shown by the *b*-value, an paramount criterion affecting the signal intensity of the DWI[7]. An appropriate *b* value is necessary for the female pelvic MRI.

In several studies, DTI has been used to demonstrate fiber structures of the *ex vivo* uterus, because of problematic conditions leading to artefacts such as body motions, heartbeat, intestinal and respiratory movements, and uterine peristalses[2-4]. Fiocchi *et al*[5], examined the DTI of *in vivo* uterus with a 3 T MRI using a 3D tractography algorithm and revealed that DTI is useful for imaging fibre architecture of *in vivo* human uterus.

DWI AND DTI OF NORMAL UTERUS

In reproductive age groups, T1 and T2 signal intensity characteristics of the uterine zones (endometrial, junctional and myometrial) demonstrate variations during ongoing phases of the menstrual cycle and with menauposal status. Physiological fluctuations affect the normal ADC values used in the evaluation of uterine pathologies[6].

On conventional MRI, the endometrial zone reflects high signal on T2-weighted sequences, however not so high like urinary bladder and low signal intensity on

T1-weighted sequences[9]. The junctional zone is the inner band of the myometrium and shows a low signal intensity in comparison to myometrial zone on T2-weighted sequences, probably because of multifactorial reasons[10]. Existence of compact smooth muscles, low water content of the cells, and increased large nuclei are the contributing factors[10,11]. The outer band of myometrial zone shows high signal intensity on T2-weighted sequences than the junctional zone, with high cellular water content and low cell density[9].

The cervix is composed of three different cervical zones that may be identified on high-resolution T2-weighted sequences There is a hyperintense central layer, named endocervical canal including mucosa, secretions, and plica. Outside of this, there is a middle zone, that's characterized by hypointense signal on T2-weighted sequences because of fibrous stroma and smooth muscle. The peripheral exterior zone includes fibromuscular stroma reflecting low-intermediate signal on T2-weighted sequences[12].

The menstrual cycle includes of three different phases. The initial four days of the menstrual phase is nemed as menstruation. On the fifth day the proliferative (follicular) phase begins and continues until the ovulation which is estimated to occure on the 14th day of the menstrual cycle. The secretory (luteal) phase begins with ovulation and lasts on the first day of the next menstrual period[13].

Tsili *et al*[13], reported that the ADC values of the endometrial and myometrial zones were different in the three phases of the cycle (menstrual phase: 1.25 ± 0.27, 1.91 ± 0.35; proliferative phase: 1.39 ± 0.20, 1.72 ± 0.27; secretory phase: 1.50 ± 0.18, 1.87± 0.28, respectively). A wide variation of ADC values of normal endometrial and myometrial zones is detected during different periods of the menstrual cycle. These variations probably depends on the physiologic-histologic fluctuations[14]. In the menstrual period, periodic contractions of the spiral artery walls in the normal endometrial zone, cause interruption of the epithelium and rupture of the vessels. Endometrial discharge caused by the torn ends of venous structures, arteries and glands result in restricted diffusion in the endometrial zone during the menstrual phase. In the secretory phase, expanded uterine glands, prominent arteries in the normal endometrial zone, accompanied by less amount of cells in stratum basalis and higher interstitial fluid can be among the probable explanations for the higher ADC values[13].

Kido *et al*[1], examined both intraindividual and interindividual differences of the ADC values of the normal uterine zones during the phases of the menstrual cycle in young age group. In this report, the ADC values for myometrial and endometrial zones were lower in the menstrual phase in comparison to the periovulatory and the secretoryl phase, although significant variability among individuals was reported. These preliminary results must be kept in mind, that the menstrual cycle and individual differences in reproductive women should be taken into account during the interpretation of the ADC values of uterine zones[1].

Kuang *et al*[6], studied the ADCs of the normal uterine zones during different periods of the menstrual cycle between reproductive women with different ages. The ADC values of the uterine zones were statistically different from each other. Endometrial ADC values of the females in their 30 s were higher than the ones in their 20 s and in their 30 s in the midproliferative and midsecretory periods. Also the ADC values of endometrial zone for all age groups were lower in the midproliferative phase in comparison to midsecretory phase, however the ADC values of the myometrial and junctional zones were not statistically different between the phases and age groups. According to this study patient age, menstrual period and the zone evaluated should be taken into consideration during quantitative evaluation[6].

The relationship of the uterine zonal ADC values were investigated by Fornasa *et al*[15], between the different periods of the cycle. The ADC values of the endometrium calculated on the fifth day of the cycle were lower when compared with periovulatory ADC values at the fundus (mean 0.923 mm^2/s *vs* 1.256 × 10^{-3} mm^2/s) and at the isthmus (mean 1.297 mm^2/s *vs* 1.529 × 10^{-3} mm^2/s). Isthmic endometrial ADC values were higher than the fundal ADC values (mean 1.420 × 10^{-3} mm^2/s *vs* 1.132 mm^2/s). These findings were statistically significant. Physiological fluctuations occurring in the ADC values of the endometrium of normal females should be kept in mind during the interpretation of the DW images of the patients[15].

DTI revealed two basic systems of fibers: circular and longitudinally oriented fibers as shown *ex-vivo*. Examination of the non cesarean scarred uteri showed anisotropy and fiber directions could be depicted[5]. Knowledge of the architectural data can help to understand the details of functionality during gestation and birth. The connective tissue architecture in the uterus of reproductive age is composed of three different layers. The first inner layer is a non-organized cluster-like interweaving of the fiber complex, secondly circular fibers in the middle layer and finally longitudinal fibers in the exterior layer[16]. In the postmenopausal uterus, the cervical region primarily includes well oriented longitudinal fibers[4].

Fiocchi *et al*[5], argued that two third of the caesarean scarred uteri had altered fiber structure in comparison to normal uteri in sutural zone. Numeric data of 13 volunteers (8 nulliparous- Ⅰ group, 5 with caesarean delivery- Ⅱ group) revealed lowest regional fiber number and density in the anterior isthmic portion (respectively 105, 77 and 9.3, 6.7), suture localization, especially in two patients with a big scar caused placental complication at subsequent delivery. The mean FA and ADC of the whole uterus were 0.4 ± 0.0 and 3.4 ± 0.4 × 10^{-3} mm^2/s respectively. The ADC of group Ⅰ was higher than group Ⅱ, but not statistically significant. In this study they concluded that 3 T DTI may show *in-vivo* human uterine fiber structures and may detect significant caesarean scars which may lead to subsequent placental

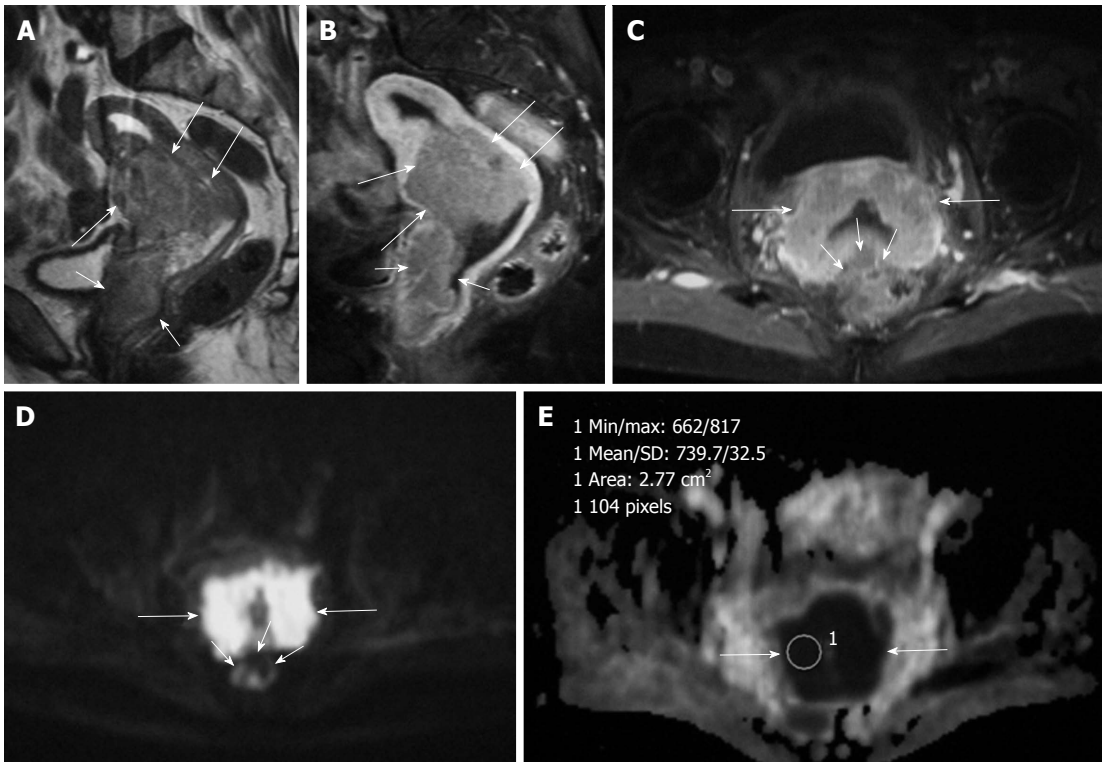

Figure 1 Forty-three years old woman with stage III squamous cell carcinoma of the uterine cervix invading vagina. A: Sagittal T2-weighted image of the uterus shows cervical cancer (long arrows) extending both to the corpus uteri and vagina (short arrows); B: Sagittal contrast-enhanced T1-weighted image with fat suppression shows enhancing cervical cancer (arrows). The tumor invades anterior vaginal wall (short arrows); C: Axial contrast-enhanced T1-weighted image with fat suppression shows enhancing cervical cancer (long arrows). There is suspicious invasion of the mass to the rectum (short arrows); D: Diffusion-weighted imaging with b = 1000 s/mm^2 clearly shows a well-defined hyperintensity mass in the cervical area with no invasion to rectum (short arrows); E: On the apparent diffusion coefficient (ADC) map the tumor is hypointense (arrows). The ADC value within the mass is 0.73 × 10^{-3} mm^2/s.

complications.

DWI AND DTI OF DISEASED UTERUS

The addition of DWI, and DTI sequences which serve as functional imaging in the MRI protocol for the evaluation of uterine pathologies have been offered by several papers[2,3,7,8]. Besides quantitative evaluation with values has been found out to be effective in the discrimination of malignancy from benign lesions[17-20].

Owing to the amount of water and cellular density uterine zones exhibit different signal intensities on the DWI. The endometrial zone and cervix display high signal, however the myometrial zone reflects a lower signal and the junctional zone shows a very low signal. Kilickesmez *et al*[8] reported that the mean ADC values of the volunteers for myometrial zone 1.76 × 10^{-3} mm^2/s, junctional zone 0.99 × 10^{-3} mm^2/s, endometrial zone 1.65 × 10^{-3} mm^2/s, and cervix as 1.71 × 10^{-3} mm^2/s. Malignant lesions mostly display markedly high signal intensity on the DWI, due to water diffusion restriction in high cellular tissues of the malignant lesions[17,21].

Both DWI and DTI of the uterus is generally acquired in the axial slices, since the basic sequences of abdomen is in the axial plane, to decrease the acquisition time for covering whole pelvis along with the uterus.

DWI clearly detects the malignant tumors and metastic lymph nodes with high signal against suppressed background signal of normal tissues, and this sequence may be used like a positron emission tomography image for fast and accurate cancer detection[8] (Figure 1).

Myometrial lesions

The most frequent lesions encountered in the myometrial zone are fibroids. These are benign overgrowths of uterine muscle, reported to be probably to be found in up to 70% of females of reproductive age[22].

Myometrial malignant lesions are leiomyosarcomas and stromal sarcomas[23]. Some of the benign fibroids, in association with different types of degeneration or cellular types may lead to high signal intensity on T2-weighted sequences. Thus, the discrimination of benign and malignant myometrial lesions are challenging on conventional MRI.

Tamai *et al*[24] reported that DWI may be an useful for discriminating uterine sarcomas from benign fibroids. The ADC values of normal myometrial zone and degenerated fibroids were higher than uterine sarcomas and there was no overlap; however, there was an overlap with non-degenerated and cellular fibroids[24]. Pathological examination of the large fibroids with central necrosis revealed fibrosis. This finding was consistent with isotropic diffusion in DTI of the associated lesion. Fibrotic leiomyomas include non-parallel collagen fibrils, whereas

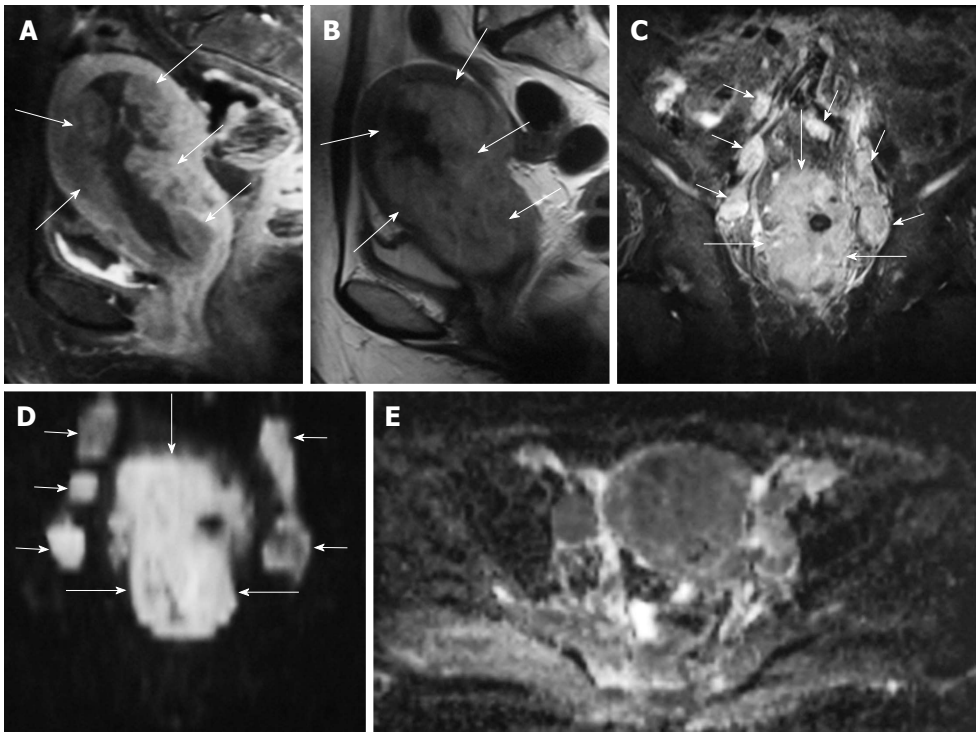

Figure 2 A 57-year-old woman with endometrial carcinoma. A: Sagittal contrast-enhanced T1-weighted image with fat suppression shows enhancing endometrial cancer with infiltration of myometrium (arrows); B: Sagittal T2-weighted image demonstrating hyperintense endometrial cancer with infiltration of myometrium (arrows); C: Coronal fat supressed T2-weighted image reveals a tumor in the corpus uteri (long arrows), and bilateral metastatic lymphadenopathies along the iliac chains (short arrows); D: Coronal DWI (b = 1000 s/mm^2) shows a marked hyperintense tumor in the corpus uteri (long arrows), and bilateral metastatic lymphadenopathies along the iliac chains (short arrows); E: Axial apparent diffusion coefficient map reveals the right sided metastatic lymph node and endometrium with restricted diffusion.

there were well-structured collagen bundles neighbouring to smooth muscle cells in the normal myometrial zone[25,26]. Irregularity of these collagen bundles could be the reason for the lower degree of anisotropy in the fibroids when compared with the neighbouring myometrium.

The ADC values may also be beneficial for determining the therapeutic outcome after UAE, radiotherapy and/or chemotherapy[7]. The effect of UAE or focused ultrasound may be evaluated by the detection of ablated tissue with DWI. The ADC values of fibroids after treatment are lower when compared with initial ADC values[27,28].

Endometrial lesions

The most frequent gynecologic malignancy is endometrial cancer. It should be discriminated from benign hyperplasia of the endometrium along with polyps.

The ADC value of polyps (1.27-1.58 × 10^{-3} mm^2/s) and of normal endometrial zone (1.53 × 10^{-3} mm^2/s) is significantly higher than endometrial cancer (0.88-0.98 × 10^{-3} mm^2/s)[24,29] (Figures 2 and 3).

Histologic grade, stage, level of myometrium invasion, existence of nodal metastases, invasion of lymphoid and vascular structures all effect the prognosis of endometrial cancer. However the most important factor effecting prognosis is the depth of myometrium invasion[30]. The success of DWI has been improved in the assessment of accurate myometrium inavasion detection and in differentiating tumor recurrence from post-theraupetic findings[31]. The first surgical staging of endometrium cancer was proposed in 1988, and than the update of the International Federation of Gynecology and Obstetrics (FIGO) staging was done in 2009[32]. In this revised FIGO staging system, stage Ⅰ A tumors include the tumors invading solely the inner half of the myometrial zone and the tumors confined to endometrium[32,33]. Tumors infiltrating the exterior half of the myometrial zone are defined as stage Ⅰ B tumors. These revisions include simplification of stage Ⅰ disease and determination of cervical infiltration as a distinct stage to increase the diagnostic value of MRI[30].

According to Fujii *et al*[29], the ADC value was 84.6% successful in detecting endometrial cancer. Toba *et al*[2] investigated the feasibility of DTI for evaluating the myometrial invasion of endometrial cancer. The degree of myometrium invasion was subgrouped as stage E (confined to endometrial zone), more than 50%. The ADC values of the cancer, inner or exterior myometrial zones were not statistically different. Tumoral FA values (0.21 ± 0.05) were lower than the inner leyer of the myometrial zone (0.44 ± 0.01) and exterior myometrium (0.32 ± 0.08) (P < 0.01). The inner or exterior myometrial FA values, (0.45 ± 0.05 *vs* 0.43 ± 0.04) were not statistically different in stage E cancers. However, in stage S and D tumors the FA values of the inner or exterior myometrial FA zones were significantly different (0.5 ± 0.05 *vs* 0.3 ± 0.04, P < 0.01; 0.39 ± 0.03

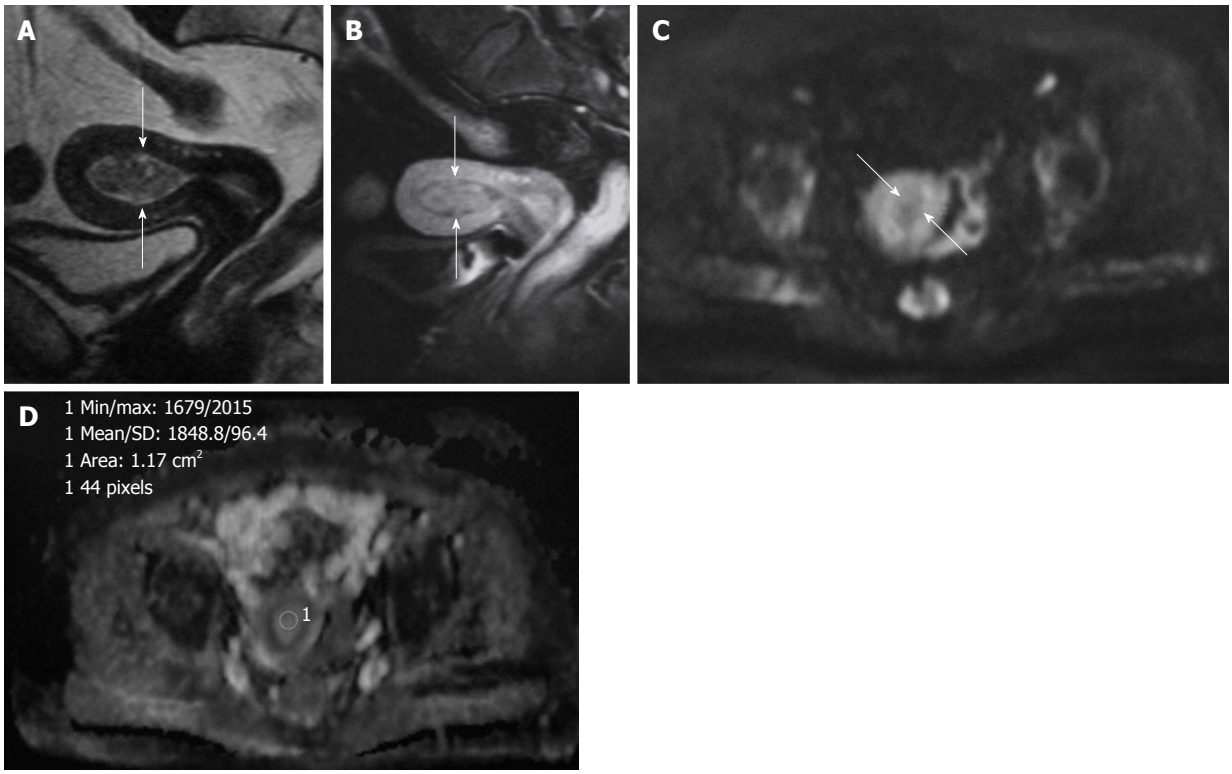

Figure 3 A 42-year-old woman with endometrial polyp. A: Hypointense polyp in the endometrial cavity on sagittal T2-weighted image mimicking low grade endometrial carcinoma (arrows); B: Sagittal contrast-enhanced T1-weighted image with fat suppression shows enhancing endometrial polyp (arrows); C: On the axial DWI (b = 1000 s/mm^2) image, the mass is hypointense clearly excluding malignancy (arrows); D: Corresponding axial apparent diffusion coefficient (ADC) map. The ADC value within the mass is 1.85 × 10^{-3} mm^2/s.

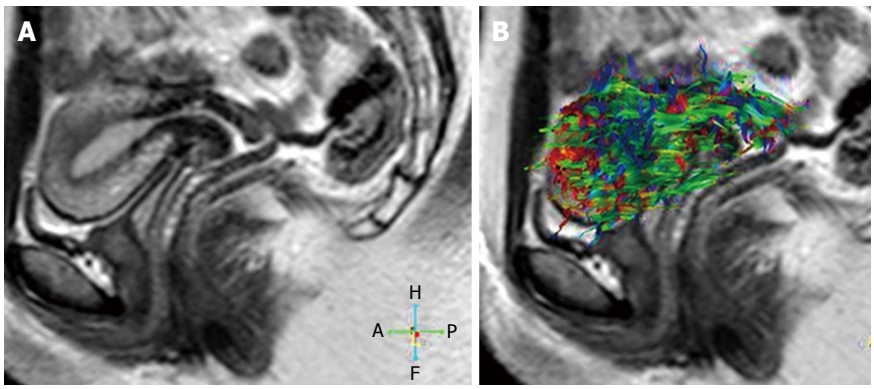

Figure 4 Thirty two years old volunteer. A: Sagittal T2-weighted image of a normal uterus; B: 3D whole tractography image of the normal uterus. Red colors represent a right-left orientation, blue represents a cranio-caudal orientation and green represents an antero-posterior orientation of diffusion. Changes in the intensity of the color represent different strengths of anisotropy.

vs 0.22 ± 0.01, P < 0.01; respectively). Myometrial infiltration of endometrial tumor may be detected with the disruption of the anisotropic layer.

DWI and DTI have a potential role for the discrimination of benign and malignant endometrial masses. It may also give additional information for preoperative assessment and should be performed as a part of routine MRI for endometrial tumors. Besides, DWI is a useful technique increasing the accuracy of staging[30].

Cervical lesions

Cervical cancer is a common gynaecological tumor. However, its incidence has decreased in developed countries as a result of screening with the Papanicolaou test (Pap smear), cervical cancer is still an important cause of tumor-related death in developing countries[34].

ADC measurements made significant supplement for the discrimination of normal cervical zone and cancers preoperatively. Besides there was correlation between tumor type, stage and ADC values[35].

According to McVeigh *et al*[36] the average median ADC of normal cervix was statistically higher than cervical cancers (2.09 × 10^{-3} mm^2/s *vs* 1.09 × 10^{-3} mm^2/s), and returned to the normal level following

chemotherapy and/or radiotherapy.

Kilickesmez *et al*[8] found out a statistically significant difference between the ADC values of malignant (0.88 ± 0.11) and benign (1.55 ± 0.33; $P < 0.01$) uterine lesions. In this study they reported a cut-off ADC level for malignant lesions at 1.05×10^{-3} mm^2/s with a sensitivity, specificity, and accuracy of 95.83%, 94.55%, and 94.94%, respectively. This study demonstrated that quantitative DWI has the potential to discriminate normal and malignant lesions of the uterus.

However, correlation of DWI and DTI with reference sequences is essential for the reason that resolution is relatively low and normal structures such as lymph nodes, bowel loops, and hemorrhage, endometromas, may show high signal like cancers on DWI[8] (Figure 4). This phenomenon may lead to false-positive visual assessment. However, quantitative evaluation with ADC and FA values or correlation of DWI, DTI with reference sequences may overcome this[37].

Although not clearly proved like DWI (low ADC in malignant tumors), quantitative DTI also reveals difference in the FA value of benign *vs* malignant tissue, however statistical significance can be much more less detected. Besides there is confusion regarding FA value alterations which should be evaluated with further studies[2,38,39].

CONCLUSION

According to this review, DWI and DTI emerge to be applicable and reliable sequences for the determination of physiological fluctuations of the uterus, detection of malignant lesions of the uterus and monitoring the therapeutic outcome. When combined with conventional MRI sequences, DWI and DTI provide further data about physiological and pathological conditions of the uterus. DWI and DTI are noninvasive, do not cause radiation exposure or need for contrast injection.

REFERENCES

1 **Kido A**, Kataoka M, Koyama T, Yamamoto A, Saga T, Togashi K. Changes in apparent diffusion coefficients in the normal uterus during different phases of the menstrual cycle. *Br J Radiol* 2010; **83**: 524-528 [PMID: 20505034 DOI: 10.1259/bjr/11056533]

2 **Toba M**, Miyasaka N, Sakurai U, Yamada I, Eishi Y, Kubota T. Diagnostic possibility of diffusion tensor imaging for the evaluation of myometrial invasion in endometrial cancer: an ex vivo study. *J Magn Reson Imaging* 2011; **34**: 616-622 [PMID: 21751283 DOI: 10.1002/jmri.22693]

3 **Thrippleton MJ**, Bastin ME, Munro KI, Williams AR, Oniscu A, Jansen MA, Merrifield GD, McKillop G, Newby DE, Semple SI, Marshall I, Critchley HO. Ex vivo water diffusion tensor properties of the fibroid uterus at 7 T and their relation to tissue morphology. *J Magn Reson Imaging* 2011; **34**: 1445-1451 [PMID: 21953730 DOI: 10.1002/jmri.22793]

4 **Weiss S**, Jaermann T, Schmid P, Staempfli P, Boesiger P, Niederer P, Caduff R, Bajka M. Three-dimensional fiber architecture of the nonpregnant human uterus determined ex vivo using magnetic resonance diffusion tensor imaging. *Anat Rec A Discov Mol Cell Evol Biol* 2006; **288**: 84-90 [PMID: 16345078]

5 **Fiocchi F**, Nocetti L, Siopis E, Currà S, Costi T, Ligabue G, Torricelli P. In vivo 3 T MR diffusion tensor imaging for detection of the fibre architecture of the human uterus: a feasibility and quantitative study. *Br J Radiol* 2012; **85**: e1009-e1017 [PMID: 22744322 DOI: 10.1259/bjr/76693739]

6 **Kuang F**, Ren J, Huan Y, Chen Z, Zhong Q. Apparent diffusion coefficients of normal uterus in premenopausal women with 3.0-T magnetic resonance imaging. *J Comput Assist Tomogr* 2012; **36**: 54-59 [PMID: 22261770 DOI: 10.1097/RCT.0b013e3182418885]

7 **Namimoto T**, Awai K, Nakaura T, Yanaga Y, Hirai T, Yamashita Y. Role of diffusion-weighted imaging in the diagnosis of gynecological diseases. *Eur Radiol* 2009; **19**: 745-760 [PMID: 18839179 DOI: 10.1007/s00330-008-1185-5]

8 **Kilickesmez O**, Bayramoglu S, Inci E, Cimilli T, Kayhan A. Quantitative diffusion-weighted magnetic resonance imaging of normal and diseased uterine zones. *Acta Radiol* 2009; **50**: 340-347 [PMID: 19235579 DOI: 10.1080/02841850902735858]

9 **Wasnik AP**, Mazza MB, Liu PS. Normal and variant pelvic anatomy on MRI. *Magn Reson Imaging Clin N Am* 2011; **19**: 547-566; viii [PMID: 21816330]

10 **Brown HK**, Stoll BS, Nicosia SV, Fiorica JV, Hambley PS, Clarke LP, Silbiger ML. Uterine junctional zone: correlation between histologic findings and MR imaging. *Radiology* 1991; **179**: 409-413 [PMID: 1707545]

11 **Scoutt LM**, Flynn SD, Luthringer DJ, McCauley TR, McCarthy SM. Junctional zone of the uterus: correlation of MR imaging and histologic examination of hysterectomy specimens. *Radiology* 1991; **179**: 403-407 [PMID: 2014282]

12 **Brown MA**, Kubik-huch RA, Reinhold C. Uterus and cervix. In: Semelka RC, editor. 2nd edition, Abdominal pelvic MRI, vol. 1. New Jersey: John Wiley & Sons, Inc, 2006: 1251-1332

13 **Tsili AC**, Argyropoulou MI, Tzarouchi L, Dalkalitsis N, Koliopoulos G, Paraskevaidis E, Tsampoulas K. Apparent diffusion coefficient values of the normal uterus: Interindividual variations during menstrual cycle. *Eur J Radiol* 2012; **81**: 1951-1956 [PMID: 21621360 DOI: 10.1016/j.ejrad.2011.04.057]

14 **Longacre TA**, Bartow SA. A correlative morphologic study of human breast and endometrium in the menstrual cycle. *Am J Surg Pathol* 1986; **10**: 382-393 [PMID: 3717495]

15 **Fornasa F**, Montemezzi S. Diffusion-weighted magnetic resonance imaging of the normal endometrium: temporal and spatial variations of the apparent diffusion coefficient. *Acta Radiol* 2012; **53**: 586-590 [PMID: 22619357 DOI: 10.1258/ar.2012.110717]

16 **Dubrauszky V**, Schwalm H, Fleischer M. [The fibre system of connective tissue in the childbearing age, menopause, and pregnancy]. *Arch Gynakol* 1971; **210**: 276-292 [PMID: 5109671]

17 **Koyama T**, Togashi K. Functional MR imaging of the female pelvis. *J Magn Reson Imaging* 2007; **25**: 1101-1112 [PMID: 17520731]

18 **Ichikawa T**, Erturk SM, Motosugi U, Sou H, Iino H, Araki T, Fujii H. High-B-value diffusion-weighted MRI in colorectal cancer. *AJR Am J Roentgenol* 2006; **187**: 181-184 [PMID: 16794174]

19 **Nasu K**, Kuroki Y, Nawano S, Kuroki S, Tsukamoto T, Yamamoto S, Motoori K, Ueda T. Hepatic metastases: diffusion-weighted sensitivity-encoding versus SPIO-enhanced MR imaging. *Radiology* 2006; **239**: 122-130 [PMID: 16493012]

20 **Takahara T**, Imai Y, Yamashita T, Yasuda S, Nasu S, Van Cauteren M. Diffusion weighted whole body imaging with background body signal suppression (DWIBS): technical improvement using free breathing, STIR and high resolution 3D display. *Radiat Med* 2004; **22**: 275-282 [PMID: 15468951]

21 **Koh DM**, Collins DJ. Diffusion-weighted MRI in the body: applications and challenges in oncology. *AJR Am J Roentgenol* 2007; **188**: 1622-1635 [PMID: 17515386]

22 **Tropeano G**, Amoroso S, Scambia G. Non-surgical management of uterine fibroids. *Hum Reprod Update* 2008; **14**: 259-274 [PMID: 18344356 DOI: 10.1093/humupd/dmn006]

23 **Goto A**, Takeuchi S, Sugimura K, Maruo T. Usefulness of Gd-DTPA contrast-enhanced dynamic MRI and serum determination of LDH and its isozymes in the differential diagnosis of leiomyosarcoma from degenerated leiomyoma of the uterus. *Int J*

Gynecol Cancer 2002; **12**: 354-361 [PMID: 12144683]
24 **Tamai K**, Koyama T, Saga T, Morisawa N, Fujimoto K, Mikami Y, Togashi K. The utility of diffusion-weighted MR imaging for differentiating uterine sarcomas from benign leiomyomas. *Eur Radiol* 2008; **18**: 723-730 [PMID: 17929022]
25 **Catherino WH**, Leppert PC, Stenmark MH, Payson M, Potlog-Nahari C, Nieman LK, Segars JH. Reduced dermatopontin expression is a molecular link between uterine leiomyomas and keloids. *Genes Chromosomes Cancer* 2004; **40**: 204-217 [PMID: 15139000]
26 **Leppert PC**, Baginski T, Prupas C, Catherino WH, Pletcher S, Segars JH. Comparative ultrastructure of collagen fibrils in uterine leiomyomas and normal myometrium. *Fertil Steril* 2004; **82** Suppl 3: 1182-1187 [PMID: 15474093]
27 **Jacobs MA**, Herskovits EH, Kim HS. Uterine fibroids: diffusion-weighted MR imaging for monitoring therapy with focused ultrasound surgery--preliminary study. *Radiology* 2005; **236**: 196-203 [PMID: 15987974]
28 **Liapi E**, Kamel IR, Bluemke DA, Jacobs MA, Kim HS. Assessment of response of uterine fibroids and myometrium to embolization using diffusion-weighted echoplanar MR imaging. *J Comput Assist Tomogr* 2005; **29**: 83-86 [PMID: 15665689]
29 **Fujii S**, Matsusue E, Kigawa J, Sato S, Kanasaki Y, Nakanishi J, Sugihara S, Kaminou T, Terakawa N, Ogawa T. Diagnostic accuracy of the apparent diffusion coefficient in differentiating benign from malignant uterine endometrial cavity lesions: initial results. *Eur Radiol* 2008; **18**: 384-389 [PMID: 17917730]
30 **Beddy P**, O'Neill AC, Yamamoto AK, Addley HC, Reinhold C, Sala E. FIGO staging system for endometrial cancer: added benefits of MR imaging. *Radiographics* 2012; **32**: 241-254 [PMID: 22236905]
31 **Sala E**, Rockall A, Rangarajan D, Kubik-Huch RA. The role of dynamic contrast-enhanced and diffusion weighted magnetic resonance imaging in the female pelvis. *Eur J Radiol* 2010; **76**: 367-385 [PMID: 20810230]
32 **Creasman W**. Revised FIGO staging for carcinoma of the endometrium. *Int J Gynaecol Obstet* 2009; **105**: 109 [PMID: 19345353]
33 **Odicino F**, Pecorelli S, Zigliani L, Creasman WT. History of the FIGO cancer staging system. *Int J Gynaecol Obstet* 2008; **101**: 205-210 [PMID: 18199437]
34 **Solomon D**, Breen N, McNeel T. Cervical cancer screening rates in the United States and the potential impact of implementation of screening guidelines. *CA Cancer J Clin* 2007; **57**: 105-111 [PMID: 17392387]
35 **Demirbaş T**, Cimilli T, Bayramoğlu S, Güner NT, Hocaoğlu E, Inci E. Contribution of diffusion-weighted imaging to diagnosis and staging of cervical cancer. *Balkan Med J* 2014; **31**: 154-157 [PMID: 25207188]
36 **McVeigh PZ**, Syed AM, Milosevic M, Fyles A, Haider MA. Diffusion-weighted MRI in cervical cancer. *Eur Radiol* 2008; **18**: 1058-1064 [PMID: 18193428 DOI: 10.1007/s00330-007-0843-3]
37 **Shen SH**, Chiou YY, Wang JH, Yen MS, Lee RC, Lai CR, Chang CY. Diffusion-weighted single-shot echo-planar imaging with parallel technique in assessment of endometrial cancer. *AJR Am J Roentgenol* 2008; **190**: 481-488 [PMID: 18212236 DOI: 10.2214/AJR.07.2155]
38 **Li C**, Chen M, Li S, Zhao X, Zhang C, Liu M, Zhou C. Diffusion tensor imaging of prostate at 3.0 Tesla. *Acta Radiol* 2011; **52**: 813-817 [PMID: 21586608 DOI: 10.1258/ar.2011.100487]
39 **Kinoshita M**, Hashimoto N, Goto T, Kagawa N, Kishima H, Izumoto S, Tanaka H, Fujita N, Yoshimine T. Fractional anisotropy and tumor cell density of the tumor core show positive correlation in diffusion tensor magnetic resonance imaging of malignant brain tumors. *Neuroimage* 2008; **43**: 29-35 [PMID: 18672074 DOI: 10.1016/j.neuroimage.2008.06.041]

P- Reviewer: Chu JP, Gao BL, Gumustas OG, Nouh MR
S- Editor: Ji FF **L- Editor**: A **E- Editor**: Liu SQ

World Journal of Radiology

Submit a Manuscript: http://www.wjgnet.com/esps/
Help Desk: http://www.wjgnet.com/esps/helpdesk.aspx
DOI: 10.4329/wjr.v7.i7.157

World J Radiol 2015 July 28; 7(7): 157-169
ISSN 1949-8470 (online)

REVIEW

Non-invasive diagnostic imaging of colorectal liver metastases

Pier Paolo Mainenti, Federica Romano, Laura Pizzuti, Sabrina Segreto, Giovanni Storto, Lorenzo Mannelli, Massimo Imbriaco, Luigi Camera, Simone Maurea

Pier Paolo Mainenti, Laura Pizzuti, IBB CNR, 80145 Naples, Italy

Federica Romano, Sabrina Segreto, Massimo Imbriaco, Luigi Camera, Simone Maurea, Advanced Biomedical Science Department, Radiology Section, University of Naples "Federico II", 80145 Naples, Italy

Giovanni Storto, IRCCS, CROB, 85028 Rionero in Vulture, Italy

Lorenzo Mannelli, Radiology Department, Memorial Sloan-Kettering Cancer Center, New York, NY 10022, United States

Author contributions: All authors contributed to this paper.

Conflict-of-interest statement: The review has not been published before, is not under consideration for publication elsewhere and its publication has been approved by all co-authors. All the authors do not have any conflicting interests (including but not limited to commercial, personal, political, intellectual, or religious interests) related to the manuscript.

Correspondence to: Pier Paolo Mainenti, MD, IBB CNR, Via De Amicis, 95, 80145 Naples,
Italy. pierpamainenti@hotmail.com
Telephone: +39-081-7613060
Fax: +39-081-7616013

Received: January 28, 2015
Peer-review started: January 29, 2015
First decision: April 27, 2015
Revised: May 10, 2015
Accepted: June 1, 2015

Article in press: June 2, 2015
Published online: July 28, 2015

Abstract

Colorectal cancer is one of the few malignant tumors in which synchronous or metachronous liver metastases [colorectal liver metastases (CRLMs)] may be treated with surgery. It has been demonstrated that resection of CRLMs improves the long-term prognosis. On the other hand, patients with un-resectable CRLMs may benefit from chemotherapy alone or in addition to liver-directed therapies. The choice of the most appropriate therapeutic management of CRLMs depends mostly on the diagnostic imaging. Nowadays, multiple non-invasive imaging modalities are available and those have a pivotal role in the workup of patients with CRLMs. Although extensive research has been performed with regards to the diagnostic performance of ultrasonography, computed tomography, positron emission tomography and magnetic resonance for the detection of CRLMs, the optimal imaging strategies for staging and follow up are still to be established. This largely due to the progressive technological and pharmacological advances which are constantly improving the accuracy of each imaging modality. This review describes the non-invasive imaging approaches of CRLMs reporting the technical features, the clinical indications, the advantages and the potential limitations of each modality, as well as including some information on the development of new imaging modalities, the role of new contrast media and the feasibility of using parametric image analysis as diagnostic marker of presence of CRLMs.

Key words: Advances in imaging; Colorectal cancer; Liver metastases

Core tip: The present review describes the non invasive imaging approaches of colorectal liver metastases colorectal liver metastases (CRLMs) reporting the technical features, the clinical indications, the advantages and the potential limitations of each modality [ultrasonography, computed tomography (CT); magnetic resonance imaging (MRI), positron emission tomography (PET)/CT, PET/MRI] as well as including some information on the development of new imaging modalities, the role of new contrast media and the feasibility of using parametric image analysis as diagnostic marker of presence of CRLMs.

Mainenti PP, Romano F, Pizzuti L, Segreto S, Storto G, Mannelli L, Imbriaco M, Camera L, Maurea S. Non-invasive diagnostic imaging of colorectal liver metastases. *World J Radiol* 2015; 7(7): 157-169 Available from: URL: http://www.wjgnet.com/1949-8470/full/v7/i7/157.htm DOI: http://dx.doi.org/10.4329/wjr.v7.i7.157

INTRODUCTION

Annually over 130000 new cases of colorectal cancer (CRC) are diagnosed in the United States, representing the third most common cancer in both men and women, with more than 50000 deaths each year[1].

Liver metastases are detected approximately in up to 20%-25% of patients with CRC at the time of diagnosis[2]. The 5-year cumulative rate of metachronous colorectal liver metastases [colorectal liver metastases (CRLMs)] is reported to be 15%[2]. Overall, approximately 50% of patients with CRC will develop liver metastases[3].

CRC is one of the few malignant tumors in which synchronous or metachronous liver metastases may be treated with surgery. CRLMs are resectable in about 20%-30% of the cases[4] with a 5-year survival of about 50%-60% in comparison to a survival of less than 5% of patients with CRLMs not amenable to liver surgery[5].

In patients who are not suitable candidates for surgery, chemotherapy alone or in addition to local hepatic treatments, such as intrahepatic arterial infusion chemotherapy or radiofrequency ablation or laser therapy or cryotherapy, may be performed. These treatments options have been shown to increase survival, too[6-11].

Common to any therapy is the need for pretreatment anatomic planning to assess feasibility and avoid injury to adjacent structures such as vasculature, biliary ducts and surrounding organs.

The surgical criteria, which permit to select the candidates for liver resection, are represented by the size of the lesion, number and location with respect to anatomic landmarks of the CRLMs, as well as the number of segments involved, the volume of the remaining liver and the general clinical parameters[6,7]. Metastases can be completely resected if at least 2 adjacent liver segments can be spared and if the future liver remnant is at least 20% of total pre-resection liver volume[8] in patients with normal liver function and more than 40% in patients with reduced liver function[12,13].

Moreover anatomic variants of hepatic arteries, biliary tree and portal venous system need to be excluded because the surgical resection may be problematic, and thus additional surgery steps may be required[14].

Obviously, diagnostic imaging plays a crucial role in selecting the more appropriate therapy for patients with CRLMs, by detecting the lesions, determining the resectability and assessing the response to treatments.

Even though many non invasive imaging modalities are now available and effective in detection and follow up of CRLMs, such as ultrasonography (US), computed tomography (CT), positron emission tomography (PET) and magnetic resonance imaging (MRI), each offering some advantages as disadvantages over the others, the optimal imaging strategy in patients with CRLMs have still to be designed.

The lack of a worldwide well defined CRLMs imaging protocol is in part due to continuous and rapid technological and pharmacological developments which are progressively improving the performance of each imaging modality.

This review describes the non-invasive imaging approaches of CRLMs reporting the technical features, the clinical indications, the advantages and the potential limitations of each modality, as well as including some information on the development of new imaging modalities, the role of new contrast media and the feasibility of using parametric image analysis as diagnostic marker of presence of CRLMs.

US

Because of its non-invasive character, low cost, no radiation exposure, good patient acceptance and widespread availability, US is often the first choice for screening patients with malignancy and/or suspected liver lesions, and it is widely used in the evaluation of liver metastases[15-19].

In particular, the sensitivity of US for CRLMs detection is variable ranging from 50% to 76%[17,20]; however US sensitivity depends mostly on the size of the lesion and it can be as low as 20% if liver lesions are less than 10 mm[15,16]. Despite of this limitation, in daily practice, US plays still a clinical role in distinguishing two different groups of patients with liver metastases: (1) patients with diffuse metastases who are no longer eligible for curative treatment; and (2) patients without metastases or a very limited number of them. Further diagnostic investigation with tomographic imaging is mandatory for the patients of the group 2 to define the correct therapeutic management.

During the last few years, the contrast-enhanced ultrasound (CEUS) has progressively gained a huge role in the evaluation of liver lesions, improving detection and characterization of both primary or secondary liver lesions[21-28]. The added role of CEUS compared to the baseline US (b-US) has been observed for CRLMs detection, too[29]. A few studies have shown a

significantly better sensitivity of CEUS *vs* b-US in the identification of CRLMs measuring less than 10 mm; moreover CEUS should replace b-US for the detection of CRLMs in patients being treated with neoadjuvant systemic chemotherapy[30-33].

Westwood *et al*[29] in their recent meta-analysis of 19 studies on liver CEUS with Sonovue stated that CEUS shows a similar performance to liver CT and MRI in the characterization of incidentally detected focal liver lesions with lower costs respect to MRI and it may be adequate to rule out CRLMs; in particular, similarly to CT and MRI even with CEUS the CRLMs are better detected in post-contrast portal and late phases[31].

Nevertheless some limitations of CEUS need to be considered. CEUS presents still low sensitivity for very small focal liver lesions (< 5 mm), due to the low spatial resolution, and thus very small CRLMs might be missed[29]. In addition, CEUS does not go beyond certain limitations of the US examinations, like the difficulty in the evaluation of the sub-diaphragmatic liver or the interposition of the intestine, and above all the notable weakness of being operator dependent. Moreover liver steatosis and fibrosis are an important limitation that can increase the possibility of missing deep seated metastases[34]. Finally, another aspect to consider is that CEUS does not offer comprehensive information for surgical planning as both CT and MRI do. Bolondi *et al*[35] report that even if the use of CEUS is largely accepted in clinical practice its role in the diagnostic algorithm of liver lesions has not yet been established.

Beyond the scope of the present review because of the invasive approach, the following US technique merit to be mentioned: the US-guided percutaneous biopsy which allow characterizing indeterminate hepatic lesions and the intra-operative ultra-sonography which offer the highest accuracy rates in CRLMs detection[36,37].

MULTIDETECTOR CT

Multidetector CT MDCT is considered the imaging modality of choice for CRC staging and follow up, because it provides excellent coverage of the entire chest/abdomen/pelvis offering a global one session staging. Nevertheless up to 25% of CRLMs may be missed[38]. The current MDCT devices enable high spatial resolution studies of the entire liver generating slice thickness $\leqslant$ 1 mm and isotropic pixel sizes and, thus, allowing high quality reformatted multiplanar (MPR) and volumetric three-dimensional rendering (3D VR) reconstructions. The resulting high definition images define accurately the main features of each lesion, as the sizes, the margins, the segmental spatial distribution, the relation with the vascular and biliary structure, and the volume of the remaining liver.

The additional diagnostic value of using thin collimation in the detection of hepatic lesions is debated. Some authors have demonstrated that the use of a thinner section thickness (*i.e.*, 2.5 mm *vs* $\geqslant$ 5 mm slice thickness) at CT improves the detection of hepatic lesions[39], as well as, the accuracy of 16-MDCT using a 1.5 mm collimation might be superior to previous CT techniques in differentiating between hepatic metastases and hepatic cysts[40]. On the contrary, other authors reported that image reconstruction with MDCT at collimations less than 5 mm did not improve sensitivity in the detection of hepatic metastases 1.5 cm or smaller[41], as well as, a slice thickness $\leqslant$ 1 mm does not improve hepatic lesion detection and it provides a significant increase of image noise[42]. As a result of the above information, a CRLMs protocol scanning of 2-4 mm of collimation may be recommended.

The value of unenhanced scans lies mainly in the characterization of small lesions as being solid or cystic or in the identification of calcified CRLMs. About the contrast-enhanced (ce) scanning protocol, the venous phase is well recognized as the optimal timing to detect CRLMs. Arterial and equilibrium phase CT have no incremental value compared to hepatic venous phase MDCT in the detection of CRLMs, as a result a multiphasic scanning protocol implies an unjustified additional radiation exposure[43,44]. Moreover the single portal venous phase contrast enhanced MDCT (ce-MDCT) scanning protocol enables accurate preoperative assessment of the local CRC staging (T and N), too[45].

The performance of MDCT in the CRLMs detection is variable showing unsatisfactory sensitivity and specificity values for lesions < 10 mm[46] or in presence of fatty liver which is often a consequence of chemotherapy[47]. Furthermore, incidental findings such as small hemangiomas and cysts measuring less than 10 mm in size can be difficult to differentiate from metastases because of volume averaging[48,49].

Contrast medium allergies as well as renal impairment may limit the use of the ce-CT; however they do not represent absolute contraindications because of the possibility of a supporting therapy.

MRI

Currently, MRI represents the most accurate modality for evaluating CRLMs; it provides anatomic details and has a high detection rate, even for lesions smaller than 10 mm[38,48-51].

The recent technological advances (high magnetic field strength > 1 T, high gradients, parallel imaging techniques, fast dynamic sequences, breath-hold sequences) have improved the liver application of MRI increasing the signal-to-noise ratio, the contrast-to-noise ratio (CNR), the spatial resolution and the image quality as well as reducing the scan times.

The unenhanced standard MRI protocol for detecting and characterizing focal liver lesions includes both T1- and T2-weighted images. For T1-weighted imaging, the in-phase and opposed-phase gradient-recalled echo (GRE) sequences are acquired to assess the presence of parenchymal fatty infiltration or focal sparing of diffuse fatty infiltration. For T2-weighted imaging, the turbo-spin echo (TSE) or the fast spin echo without and with

fat suppression are preferred over the single-shot TSE pulse sequences, because the latter do not offer an optimal soft tissue contrast. For detection of focal lesions a TE of approximately 80-100 ms is adopted, however a heavily T2-weighted sequences with a time of echo of approximately 160-180 ms may help in differentiation between solid and non-solid lesions (*e.g.*, metastasis/HCC *vs* haemangioma/cyst)[52-54].

Recent clinically important advances in MRI include the addition of diffusion-weighted imaging (DWI). DWI is a functional technique that looks at the Brownian motion of water in tissues. In biological tissues, the Brownian motion is restricted by interactions with cell membranes and macromolecules on a microscopic level as well as it is modified by any architectural tissue changes[55]. Increased tissue cellularity observed in tumors restricts Brownian motion, which can be quantified by calculation of the apparent diffusion coefficient (ADC) on derived ADC parametric maps. Of note, ADC has been shown to be inversely correlated with tumor cellularity and it can be considered a quantitative biomarker parameter of pathology. Metastases tend to restrict diffusion and the addition of DWI to the standard liver MRI protocol improves sensitivity and specificity for lesion detection and characterization[56-58]. The added value of DWI is even more evident in the detection of CRLMs $\leqslant$ 1 cm with sensitivity of 92% compared to 71% of late phase hepato-biliary contrast agent MRI[59]. Hence, these sequences are now routinely included in a liver MRI protocols.

Successively, the contrast-enhanced sequences are performed. Three different groups of MRI contrast agents for hepatic imaging are available: the non-specific extracellular gadolinium chelates, the organs-specific (reticulo-endothelial) and the liver-specific intracellular (hepato-biliary) contrast agents.

Non-specific gadolinium chelates

Extracellular gadolinium chelates are the contrast agent more frequently used for MRI. Several agents with similar properties are on the market, including gadopentetate dimeglumine (Magnevist, Schering, Berlin, Germany), Gd-DTPA-BMA (Omniscan®, GE Healthcare, Chalfont St. Giles, United Kingdom) and Gd-DOTA (Dotarem, Guerbet, Aulnay-sous-Bois, France).

Non-specific extracellular gadolinium chelates have pharmacokinetics similar to those of iodinated contrast agents and are excreted almost exclusively by passive glomerular filtration through the kidneys. Because of their small size, gadolinium chelates are rapidly cleared from the intravascular space into the extracellular interstitial space according to the concentration difference of the contrast agent between the two compartments. The transfer of the molecules occurs in the opposite direction, when the concentration gradient inverts[60].

About the contrast-enhanced scanning protocol, the T1-weighted 3D-GRE breath hold (BH) sequences are obtained during the arterial, portal venous phase and the equilibrium phase. The following considerations have to be reported about the differences between MRI and CT contrast-enhanced scanning protocol: the exposure to ionizing radiation suggests to use single phase CT protocol and to reserve multiphasic studies only when really necessary; although the MRI of the liver is the most accurate modality for detecting CRLMs, in the clinical practice it is frequently used after a staging whole-body ce-MDCT to solve problems of differential diagnosis; that is why a multiphasic MRI liver protocol may be necessary to characterize correctly a liver lesion defined as undetermined at ce-MDCT.

Gadolinium-based contrast agents may cause collateral effects, such as acute non-renal adverse reactions (*e.g.*, anaphylactoid reactions), acute renal adverse reactions (*e.g.*, contrast induced nephropathy), delayed adverse reactions [nephrogenic systemic fibrosis (NSF)] and problems at the site of injection (*e.g.*, local necrosis)[60]. NSF is a rare potentially fatal disease that has been observed in patients with severe renal insufficiency exposed to gadolinium contrast agent. To prevent the risk of NSF it is suggested to avoid the intravenous (*iv*) administration of gadolinium contrast agents in patients who have a glomerular filtration rate lower than 30 mL/min per 1.73 m^2 as well as in those who are on dialysis or have acutely renal impairment. This point represents a recommendation rather than an absolute contraindication.

Reticulo-endothelial contrast agents

All reticuloendothelial system (RES) agents are super-paramagnetic iron oxide-based contrast agents (SPIO). SPIO particles are taken up by RES cells of the normal liver parenchyma, the spleen and the lymph nodes. They shorten T2 and T2* relaxation times resulting in a loss of signal intensity in normal liver parenchyma. On the opposite, malignant liver lesions do not have a substantial number of RES cells and appear as hyperintense lesions with distinct borders in contrast to the hypointense liver parenchyma after application of SPIO on T2-weighted MRI.

Although SPIO agents have showed high accuracy in the detection of liver lesions[40,61-64], hepatocyte-specific contrast agents are preferred to these molecules in clinical practice[65].

Hepato-biliary contrast agents

Hepatobiliary agents represent a heterogeneous group of paramagnetic molecules of which a fraction is taken up by hepatocytes and excreted into the bile. On T1 weighted images, lesions not containing hepatocytes are hypointense to the surrounding enhanced parenchyma during the hepato-biliary phase (HBP). Presently, the hepatobiliary agents actually available are mangafodipir trisodium (MT, Teslascan®, GE Healthcare), godobenate dimeglumine (Gd-BOPTA, Multihance®, Bracco) and gadoxetic acid (Gd-EOB-DTPA, Primovist®, Schering).

MT has limited assessment of vascular structures due to its inability to be administered as a bolus. Gd-BOPTA and Gd-EOB-DTPA show biphasic liver enhancement

with an early vascular and extracellular phase allowing arterial, portal venous and equilibrium phase and a delayed HBP with a peak to 20-40 min for Gd-EOB-DTPA and 60-90 min for Gd-BOPTA. The advantages of the Gd-EOB-DTPA over Gd-BOPTA are the higher biliary excretion approximately close to the 50% of the delivered dose respect to 3%-5%, the high relaxivity, the earlier onset and the longer duration of contrast, which facilitates imaging and image quality[65,66].

HBP improves the sensitivity of MRI in the detection of CRLMs[59]. In addition hepatocyte-specific contrast agents allow detection of the "disappearing liver metastases"[13], which mimic a complete response to neoadjuvant chemotherapy leading to a mismatch between imaging response and true pathological complete response. A false complete imaging response is more often observed with CT and PET-CT[67], while the current data suggest that MRI with hepato-biliary contrast agents represent the most appropriate imaging modality for assessment of patients with CRLMs treated with neoadjuvant chemotherapy[68].

Despite of the great ability of MRI in detection of CRLMs, above all with the introduction of DWI and HBP, this modality still presents some limitations in patients who have difficulty holding their breath. Motion artefacts can heavily degrade images especially in dynamic acquisitions. Different sequences can be performed to study dynamic and HBP such as volumetric interpolated BH examination (Siemens Healthcare, Erlangen, Germany), liver acquisition with acceleration volume acquisition (GE Healthcare, Waukesha, Wis), or enhanced high-resolution isotropic volume excitation (Philips Healthcare, Best, the Netherlands) or respiratory-triggered T1-WI, this latter independent from patient's collaboration[69]. Recently Yoon *et al*[70] have evaluated in a large number of patients the image quality and diagnostic performance in evaluation of focal liver lesions of the respiratory-triggered 3D T1W-GRE sequence compared to standard BH T1W-GRE in HBP. Their results demonstrate that in no-collaborative patients respiratory-triggered 3D T1W-GRE images showed clearer liver margins and intrahepatic vascular structures as well as better image quality, so providing a better diagnostic performance. Overall image quality of respiratory-triggered 3D T1W-GRE was also better than that of BH T1W-GRE in patients with sufficient breath-holding capacity (n = 309, 3.96 ± 0.88, 3.81 ± 0.6, respectively, $P < 0.001$).

^{18}F-FDG-PET AND ^{18}F-FDG-PET/CT

^{18}F-FDG-PET is the most sensitive non-invasive imaging modality for the detection of CRLMs on a per patient basis[15,38,49,50]; however PET is limited by the low spatial resolution, the lack of clear anatomic landmarks, and the physiological uptake of the parenchyma which can mask small hepatic lesions. As a result, the detection of CRLMs by ^{18}F-FDG-PET is directly related to the size of the liver metastases: 14% of hepatic lesions ⩽ 15 mm[71] and 5%-36% of hepatic lesion ⩽ 10 mm[72-74] were identified by ^{18}F-FDG-PET.

Therefore, to overcome the above limitations, PET has been combined with CT to realize the hybrid modality PET/CT. This combination provides simultaneous functional and anatomic diagnostic information. The combination of PET with CT improves the distinction of physiological ^{18}F-FDG uptake from pathology and also aids the localization of metastases within the segmental anatomy of the liver, but does not overcome the intrinsic limits of PET modality such as the poor spatial resolution or the inaccurate identification of small non-hyper-metabolic lesions. That is why performing the CT of the PET/CT examination with the administration of *iv* iodinated contrast medium improves the performance of the PET/CT modality. ^{18}F-FDG-PET/ce-CT increases significantly the detection of CRLMs compared with ^{18}FDG-PET/CT[75].

^{18}F-FDG-PET does not require breath holding during acquisition, thus respiratory movements may reduce conspicuity of small liver lesions with potential errors in the detection of focal sub-diaphragmatic ^{18}F-FDG uptakes and respiratory phase mismatch between the PET and CT data. Revheim *et al*[76] have recently investigated the added role of two tailored ^{18}F-FDG-PET liver protocols [prolonged liver acquisition time (PL-PET) and repeated breath-hold respiratory gated liver acquisition (RGL-PET)] to a standard whole body (sWB) ^{18}F-FDG-PET/CT protocol to improve detection of CRLMs. The PL-PET protocol lasted 8 min and covered the liver with two bed positions, while patients of the RGL-PET protocol were asked to alternate breaths and BHs for 10 min. The addition of tailored liver-specific ^{18}F-FDG PET protocols to sWB-PET scan improved the detection of CRLMs compared to sWB-PET alone; more lesions were detected and a higher CRLMs SUV max was measured, with a substantial reduction of the background noise related to physiologic liver uptake.

The role of PET/CT in CRLMs is yet evolving. Due to the high cost and an additional radiation exposure, ^{18}F-FDG-PET/CT is reserved for the detection of occult extra-hepatic disease in patients with CRLMs amenable of surgical resection to avoid the morbidity of a futile invasive therapy[77].

Moreover further clinical roles of ^{18}F-FDG-PET/CT may be the following: (1) identification of the primary colorectal neoplasm and evaluation of its local extent[78,79]; (2) after a curative resection, the detection of local or distant recurrence of the disease[80] as well as solving ambiguous cases of unexplained CEA rise without conventional radiological explanation and in their prognostic stratification[81]; and (3) metabolic monitoring of the tumor response to the therapy[82].

^{18}F-FDG-PET/MRI

As stated above, both PET and CT show a few limitations in the evaluation of liver lesions; recently PET/MRI has been proposed as an alternative hybrid imaging modality.

Because of the great sensitivity of MRI in recognizing small liver metastases, its combination with the metabolic data obtained by PET may lead to an improved diagnostic accuracy.

Nowadays, the role of PET-MRI in evaluating CRLMs is becoming a topic of major interest, however at present insufficient data is available because hybrid devices are present in few highly specialized centers.

Recent studies have enrolled patients with CRLMs to evaluate the performance of PET-MRI[83-85]. Drzezga *et al*[85] compared PET/CT and PET-MRI in 32 oncologic patients, four of those had CRC and with seven liver lesions. Overall conclusion of this study was that PET/MRI was comparable to PET/CT. Quick *et al*[86] studied 80 patients who underwent a double-scanning protocol with PET/ MRI and PET/CT with 195 tracer-avid lesions and rated image quality. Their results show that integrated PET/MR hybrid imaging is feasible in clinical setting with similar detection rates as those of PET/CT. Partovi *et al*[87] and Kershah *et al*[88] investigated the role of PET/MRI in 120 patients with various primary neoplasms (13 CRCs) who underwent double-scanning protocol with PET/MR and PET/CT in a sequential design following a single-tracer injection of FDG. They observed that hybrid PET-MRI imaging led to a better diagnostic confidence in the characterization of focal liver lesions, taking advantage from the synergic evaluation of ADC and SUVmax. Nielsen *et al*[89] investigated the possible role of PET/MRI in evaluation of therapeutic response in twenty patients with CRLMs treated with radiofrequency or microwave ablation. The sensitivity of MRI in detecting small intrahepatic lesions combined with the ability of ^{18}F-FDG-PET to visualize enhanced metabolism at the ablation site suggests that ^{18}F-FDG-PET/MRI could potentially improve the accuracy of early detection of progressive disease, and thus allow swifter and more effective decision-making regarding appropriate treatment.

NON-CONVENTIONAL PARAMETRIC IMAGING OF CRLMs

This section is dedicated to morphological and functional liver parametric imaging proposed for detecting occult CRLMs and predicting which patients are at risk to develop metachronous liver disease. At present, the real role of parametric images has to be further investigated, as a result they are not routinely performed in the diagnostic clinical management of patients with CRC.

Different studies[90,91] have focused on methods targeting liver perfusion to individuate occult CRLMs before they become overt on morphological imaging. Changes of liver hemodynamics may indeed be related to the presence of occult liver metastases and may also predict the development of metachronous ones. It is well known that the liver receives a dual blood supply from the portal and systemic circulation. Normally in healthy subjects approximately two thirds of this blood supply is carried by the portal vein and one third by the common hepatic artery. During the onset of liver metastases this relation changes because of the increase of arterial blood flow (arterialization) and decrease of portal venous inflow[92].

Imaging can allow recognizing and quantifying these perfusional changes occurring in the liver microvasculature even before any visible morphological signs. For this purpose, doppler perfusion index (DPI) is an US measure of the ratio of arterial hepatic blood flow to total hepatic blood flow[93,94]. Kopljar *et al*[95] compared two different groups with and without liver metastases and observed that patients with liver metastases showed greater DPI determined by increased arterial hepatic blood flow associated to a smaller portal cross-sectional area portal blood flow. The strong operator dependence of the technique represents the major limit of this method.

Perfusion CT allows evaluation hepatic hemodynamic changes and provides quantitative perfusional data useful for the precocious detection of liver metastases[96]. However, to produce reliable enhancement curves the perfusion CT necessitates of multiple high temporal resolution acquisitions after administration of *iv* contrast medium, this leads to radiation overexposure; moreover the breathing cycle can cause severe motion and distortion artifacts[97].

Thanks to the lack of ionizing exposure, perfusion MRI seems to be more promising as a reliable tool for the evaluation of focal and global perfusion indexes[98]. The perfusion parameters evaluated with dynamic contrast-enhanced MRI are essentially represented by Ktrans (volume transfer constant) and Kep (rate constant). Ktrans is the rate constant of contrast agent transfer from the plasma compartment into the extracellular extravascular space, whereas Kep is the rate constant of contrast agent that escape from the extracellular extravascular space back into the plasma compartment. De Bruyne *et al*[99] found that a decrease in Ktrans of more than 40% after bevacizumab-containing chemotherapy was associated with better progression-free survival. Further investigations are needed to understand the real role of perfusion MRI in CRLMs.

Different authors[100-103] have investigated the role of CT texture analysis (TA) to identify the early changes in liver texture heralding the possible presence of occult liver micro-metastases. Texture analysis does not require any additional phase and it can be easily obtained from routinely acquired clinical CT data. This technique is based on the assumption that presence of liver occult lesions can be suspected by the amount of spatial heterogeneity on CT which can be assessed quantifying the texture parameters. These parameters go beyond human visual evaluation and include as main explored values the brightness (quantitative measurement of the mean grey level intensity), entropy (grade of inhomogeneity) and uniformity (distribution of grey levels). As different studies are investigating the potential role of TA, it is debated which is the more appropriate CT phase to analyze. Ganeshan *et al*[100] applied TA to non-

contrast enhanced CT scan of patients with CRC showing significant changes of TA parameters in the non diseased part of the liver of patients with CRLMs compared to those without. Similar results are reached even using TA on routinely acquired portal phase images[101-103]. The exact reasons to explain the relationship between an altered texture in apparently disease-free liver areas and the presence of occult micro-metastases or the development of metachronous live metastases are not quite clear. Probably the alterations of texture features are related to subtle tumor-induced structural and/or hemodynamic changes.

As it has been well demonstrated that the presence of micro-metastasis is related to subtle changes in liver hemodynamics, some authors are investigating the role of blood oxygenation level dependent MRI in early detection of CRLMs. Barash *et al*[104,105] evaluated in mice the pathological changes in liver perfusion assessing the hemodynamic response imaging (HRI), a method that involves hypercapnic challenge with brief inhalation of 5% CO_2 followed by hyperoxic challenge with brief inhalation of carbogen. They demonstrated that during CO_2 enrichment there is an increase in portal flow compared to arterial hepatic flow, and that the higher deoxyhemoglobin levels produced a decrease in fMRI signal intensity. Conversely hyperoxia signifies vascular density and tissue perfusion. Edrei *et al*[106,107] more recently applied this method to demonstrate in a mouse model the early hemodynamic changes that occur in CRLMs, and their modification with advance of liver involvement. The HRI method showed enhanced sensitivity for small CRLM (1-2 mm) detection compared with ce-MRI (82% *vs* 38%, respectively) as well as it demonstrated hemodynamic changes occurring during CRLMs antiangiogenic treatment.

DETECTION OF CRLMs: WHICH IS THE MOST ACCURATE MODALITY?

A huge literature is available about the performances of each imaging modality in the evaluation of CRLMs; as a consequence, we will describe mostly the data of meta-analysis reports in this section.

Kinkel *et al*[15] performed a meta-analysis including papers published between 1985 and 2000 and concluded that, at equivalent specificity ($\geqslant$ 85%), ^{18}F-FDG-PET (90%; CI: 80, 97) is the most sensitive non invasive imaging modality compared to US (55%; CI: 41, 68), CT (72%; CI: 63, 80) and MR (76%; CI: 57, 91) for the detection of hepatic metastases from colorectal, gastric and esophageal cancers on a patient basis.

Bipat *et al*[49] performed a meta-analysis including papers published between 1990 and 2003 and concluded that ^{18}F-FDG-PET is the most sensitive diagnostic tool for the detection of hepatic metastases from CRC on a per patient basis, but not on a per lesion basis. On a per patient basis, the sensitivity of CT, MR, ^{18}F-FDG-PET were 64% (CI: 55, 72), 65% (CI: 58, 70) and 76% (CI: 61, 86), respectively. For lesion of 1 cm or larger SPIO-enhanced MRI was the most accurate modality.

Niekel *et al*[38] performed a meta-analysis including papers published between 1990 and 2010 and concluded that, MRI is the preferred fist-line modality for evaluating CRLMs in patients who have not previously undergone therapy; it provides anatomic details and has a high detection rate for lesions smaller than 10 mm. ^{18}F-FDG-PET can be used as the second line-modality because it is valuable in the evaluation of extra-hepatic disease. The role of ^{18}F-FDG-PET/CT was not clear owing the small number of studies. At equivalent specificity, the sensitivity of CT, MR and ^{18}F-FDG-PET was 75% (CI: 69, 79), 80% (CI: 75, 62) and 81% (CI: 66, 91), respectively, on a per lesion basis, and 84% (CI: 67, 93), 88% (CI: 65, 97) and 94% (CI: 92, 96), respectively, on a per patient basis.

van Kessel *et al*[68] performed a meta-analysis including papers published between 2005 and 2011 and concluded that, MRI is the most appropriate imaging modality for preoperative assessment of patients with CRLMs treated with neoadjuvant chemotherapy. The sensitivity of CT, MRI, ^{18}F-FDG-PET and ^{18}F-FDG-PET/CT were 70% (CI: 47, 62), 86% (CI: 70, 94), 54% (CI: 47, 62) and 52% (CI: 38, 65), respectively, on a per patient basis.

Seo *et al*[108] reported the comparison of Gd-EOB-DTPA-MRI and ^{18}F-FDG-PET/ce-CT in 68 patients with 103 CRLMs and concluded that Gd-EOB-DTPA-MRI is more accurate than ^{18}F-FDG-PET/ce-CT, especially for detection of small ($\leqslant$ 1 cm) lesions. The sensitivity, the specificity, the positive and negative predictive values on a patients basis were 100%, 71%, 97% and 100% respectively for Gd-EOB-DTPA-MRI, and 93%, 71%, 97% and 57% respectively for ^{18}F-FDG-PET/ce-CT.

Muhi *et al*[109] reported the comparison of ce-CT, ce-US, SPIO-MRI and Gd-EOB-DTPA-MRI in 111 patients with CRC, 46 of whom presented 112 hepatic metastases. The sensitivity of ce-US, ce-CT, SPIO-MRI and Gd-EOB-DTPA-MRI, was 73%, 63%, 80% and 95%, respectively, considering all the lesions, and 41%, 26%, 63% and 92%, respectively, considering the lesions $\leqslant$ 10 mm. The sensitivity of MRI was significantly better than the other modalities. Although the sensitivity of Gd-EOB-DTPA-MRI was superior to that of SPIO-MRI especially for lesions $\leqslant$ 10 mm, the difference was not statistically significant. No significant differences in positive predictive value were disclosed between any of the images sets for all the lesions, lesions > 1 cm and lesions $\leqslant$ 1 cm.

Berger-Kulemann *et al*[47] evaluated the performance of ce-MDCT and gadoxetic acid enhanced MRI in the detection of CRLMs in patients with diffuse fatty infiltration of the liver. MDCT identified 49 (72%) and MRI 66 (97%) of 68 lesions confirmed by hystopathology. Statistical analysis showed that the MRI was superior to MDCT with a significant difference considering all the lesions ($P < 0.001$) and small lesions ($\leqslant$ 1 cm; $P < 0.001$), while there was no-significant difference between

the two modalities in the detection of lesions > 1 cm.

Zech *et al*[110] reported that Gd-EOB-DTPA-MRI can lead to cost savings respect to extracellular-contrast-medium-MRI by improving pre-operative planning, reducing additional imaging and decreasing intra-operative changes.

Chen *et al*[111] performed a meta-analysis including 13 papers published between 2011 and 2012 (6/13 papers dealt with CRLMs) and concluded that, Gd-EOB-DTPA-MRI presents high sensitivity (93%; CI: 90, 95) and specificity (95%; CI: 91, 97) for detection of CRLMs.

Maffione *et al*[112] have evaluated the diagnostic performance of ^{18}F-FDG PET and PET/CT for staging liver metastases in patients with CRC including in their meta-analysis studies published from 2004 to 2014. They conclude that ^{18}F-FDG-PET/CT is highly accurate for the detection of CRLMs on a per-patient basis (pooled sensitivity and specificity of 93%) while on a per-lesion basis results were lower (pooled sensitivity and specificity of 60% and 79%). Comparing PET with different imaging modalities their results show that PET had a lower sensitivity than MRI and CT on a per-patient basis (93%, 100% and 98%) and a per-lesion basis (66%, 89% and 79%). In contrast, PET appeared more specific than MRI and CT (86%, 81% and 67%).

Maas *et al*[80] published a meta-analysis comparing PET, PET-CT and CT for whole body staging in patients with suspected recurrence of CRC. The Authors found PET and PET-CT to have the highest diagnostic performance with an area under the curve of 0.94 for both PET and PET-CT compared to 0.83 for CT scan. PET/CT appears as the whole body technique of choice because of its greater ability respect to CT to identify extra-hepatic and additional sites of disease and also for the detection of local recurrence.

MANAGEMENT OF CRLMS: WHICH IMAGING PROTOCOL?

The main clinical scenarios to be managed in patients with CRLMs are the following: (1) detection of liver metastases as part of global staging of newly diagnosed CRC; and (2) pre-surgical planning of CRLMs resection; c) surveillance/monitoring of treatment response of the CRLMs.

Although the optimal imaging strategy is not well established, yet, we will suggest a diagnostic algorithm for each clinical scenario underscoring in part information just reported above.

Detection of CRLMs of newly diagnosed CRC

ce-CT is currently regarded as the standard for one session whole-body staging, including the liver, for initially diagnosed CRC patients. However, as stated above, ce-CT may miss up to 25% of CRLMs also using a multiphasic acquisition protocol and its performance worsens in presence of hepatic steatosis[47]. Furthermore, ce-CT shows limitations in characterizing small (< 1 cm) hypoattenuating lesions, which may be defined as indeterminate or "too-small-to-characterize" (TSCT)[46].

Currently, liver MRI is increasingly used to evaluate CRLMs. The higher accuracy of MRI in comparison with CT and PET/CT for detection of CRLMs, especially for lesions < 1 cm, has been just largely mentioned in the previous section. However, it is unclear which CRC patients should receive liver MRI in addition to standard staging CT. Recently, Han *et al*[113] have investigated the clinical impact of liver MRI in staging evaluation of newly diagnosed CRC patients in three ce-CT groups of patients: (1) patients who demonstrate diminutive indeterminate hypoattenuating TSCT lesions; (2) patients with metastasis-negative hepatic findings; and (3) suspicious or non-TSCT indeterminate lesions. The Authors concluded that liver MRI provides little benefit for detecting synchronous CRLMs in the groups 1 and 2, while it has a significant impact in the group 3. Moreover in the setting of hepatic steatosis, MRI with hepato-biliary contrast agents is superior to ce-MDCT in detecting CRLMs[47].

Both US and PET/CT play a marginal role. As stated above, US may be used to identify patients with diffuse liver metastases who may not need further hepatic diagnostic investigation, whereas PET/CT show a high performance in identifying patients with liver metastases.

Pre-surgical planning of CRLMs resection

The current National Comprehensive Cancer Network (NCCN) guidelines state that liver MRI can be consider to further evaluate patients diagnosed with potentially resectable CRLMs on CT[114]. This recommendation takes into account the fact that liver MRI is most reliable in defining the number, the size and the location of CRLMs, may detect additional CRLMs that are undiagnosed on CT and therefore may change the treatment plan. Moreover it provides information about the volume of the future liver remnant, of the biliary ductal system and of the hepatic parenchyma, such as steatosis, iron deposition, fibrosis, that may impair liver function.

ce-MDCT and ce-MRI angiography have shown similar performance for preoperative hepatic vascular anatomic evaluation[115], however CT may have some advantages over MRI as rapid acquisition, less susceptibility to motion, thin collimation, which assure excellent MPR and 3D images. ce-MDCT may be preferred to ce-MRI angiography in situations where detailed vascular information is necessary prior to complex hepatic resection.

^{18}F-FDG-PET/CT may be recommended for the detection of occult extra-hepatic disease prior of CRLMs surgical resection to avoid not useful invasive treatment.

Surveillance/monitoring of the treatment response of the CRLMs

As diagnostic imaging can help identify the best therapeutic strategy for treatment of CRLMs, equally it plays a key role in assessing response to treatment.

The criteria for monitoring CRLMs response to chemotherapy are the response evaluation criteria in solid tumors, which consist of a simple single dimension measurement of tumor size with efficacy determined by tumor shrinkage[116]. In the evaluation of patients with CRLMs treated with chemotherapy, ce-MRI should be preferred to both ce-MDCT and ^{18}F-FDG-PET/CT for the following reasons: (1) the steatosis induced by chemotherapy decreases the liver-to-lesion contrast, hindering the detection and delineation of the lesions on ce-MDCT; and (2) the necrosis, the reduction of the size of the lesions and the decrease in metabolic activity of cancer cells hamper the diagnostic performance of ^{18}F-FDGPET/CT; it is still not clear if the disappearance of metabolic activity of a lesion can be considered a complete response[117,118]. Today, MRI with DWI and liver specific contrast agents provide the most sensitive tool for detecting CRLMs in patients who have undergone neoadjuvant chemotherapy.

After systemic or local therapy, the change in size of the CRLMs may not be representative of a response, because the initial post-treatment examinations often fail to demonstrate shrinkage of the tumor. In such cases radiologists can misinterpret a slight increase in size of a recently treated lesion as tumor progression, whereas it is often sign of early response to anti-angiogenic treatment. The CT "pseudo-progression" is defined as the increase in size of a lesion after treatment associated with a reduction of attenuation, due to intra-lesional edema, together with a decrease in the tumor markers[119]. In these instances, the evaluation of changes in size and enhancement of the lesion as well as following the lesion up over time, preferably using the same modality, helps determine the efficacy of the treatment[120].

After a local hepatic treatment, the current NCCN guidelines[114] suggest surveillance imaging with CT or MRI every 3-6 mo for 2 years, then every 6 mo for 3-5 years. The NCCN guidelines do not recommend PET/CT for assessing treatment response, because of false-negative (necrotic lesions) and false-positive (inflammation and surgery) results may occur.

CONCLUSION

Several imaging techniques are available in management of CRLMs.

US plays a marginal role due to the operator-dependence, the lack of panoramic view and the low sensitivity for lesions < 10 mm. US may select patients with diffuse secondary liver involvement who do not benefit of further hepatic imaging.

Actually, ce-MDCT is the preferred imaging modality for initial global staging, allowing also an optimal pre-treatment planning for curative CRLMs resection.

MRI provides additional information respect to ce-MDCT when suspicious or non-TSCT indeterminate hepatic lesions are present on ce-MDCT, in presence of hepatic steatosis or in the post-chemotherapy liver evaluation.

^{18}F-FDG-PET/CT may be proposed to detect occult extra-hepatic disease prior of CRLMs resection to avoid inappropriate surgical treatment.

^{18}F-PET-MRI may represent the future elective diagnostic tool because it combines the high accuracy for CRLMs detection of MRI with the high performance of extra-hepatic metastases evaluation of PET.

Non-conventional parametric imaging may play a future role for detecting occult CRLMs and predicting which patients are at risk to develop metachronous liver disease, but these techniques have to be further investigated.

REFERENCES

1 **American Cancer Society**. Cancer Facts & Figures 2014. Atlanta: American Cancer Society, 2014. [Accessed 2014 Jan 21]. Available from: URL: http://www.cancer.org/research/cancerfactsstatistics/index

2 **Manfredi S**, Lepage C, Hatem C, Coatmeur O, Faivre J, Bouvier AM. Epidemiology and management of liver metastases from colorectal cancer. *Ann Surg* 2006; **244**: 254-259 [PMID: 16858188 DOI: 10.1097/01.sla.0000217629.94941.cf]

3 **Kanas GP**, Taylor A, Primrose JN, Langeberg WJ, Kelsh MA, Mowat FS, Alexander DD, Choti MA, Poston G. Survival after liver resection in metastatic colorectal cancer: review and meta-analysis of prognostic factors. *Clin Epidemiol* 2012; **4**: 283-301 [PMID: 23152705 DOI: 10.2147/CLEP.S34285]

4 **Simmonds PC**, Primrose JN, Colquitt JL, Garden OJ, Poston GJ, Rees M. Surgical resection of hepatic metastases from colorectal cancer: a systematic review of published studies. *Br J Cancer* 2006; **94**: 982-999 [PMID: 16538219 DOI: 10.1038/sj.bjc.6603033]

5 **Tzeng CW**, Aloia TA. Colorectal liver metastases. *J Gastrointest Surg* 2013; **17**: 195-201; quiz p.201-202 [PMID: 23054896 DOI: 10.1007/s11605-012-2022-3]

6 **Fong Y**, Cohen AM, Fortner JG, Enker WE, Turnbull AD, Coit DG, Marrero AM, Prasad M, Blumgart LH, Brennan MF. Liver resection for colorectal metastases. *J Clin Oncol* 1997; **15**: 938-946 [PMID: 9060531]

7 **Nakamura S**, Suzuki S, Baba S. Resection of liver metastases of colorectal carcinoma. *World J Surg* 1997; **21**: 741-747 [PMID: 9276706 DOI: 10.1007/s002689900300]

8 **Alberts SR**, Poston GJ. Treatment advances in liver-limited metastatic colorectal cancer. *Clin Colorectal Cancer* 2011; **10**: 258-265 [PMID: 21820974 DOI: 10.1016/j.clcc.2011.06.008]

9 **Tanada M**, Saeki T, Takashima S, Mogami H, Hyoudou I, Jinno K. [Intrahepatic arterial infusion chemotherapy for the colon cancer patients with liver metastases--a comparison of arterial embolization chemotherapy versus continuous arterial infusion chemotherapy]. *Gan To Kagaku Ryoho* 1996; **23**: 1440-1442 [PMID: 8854774]

10 **Dodd GD**, Soulen MC, Kane RA, Livraghi T, Lees WR, Yamashita Y, Gillams AR, Karahan OI, Rhim H. Minimally invasive treatment of malignant hepatic tumors: at the threshold of a major breakthrough. *Radiographics* 2000; **20**: 9-27 [PMID: 10682768 DOI: 10.1148/radiographics.20.1.g00ja019]

11 **Ruers T**, Bleichrodt RP. Treatment of liver metastases, an update on the possibilities and results. *Eur J Cancer* 2002; **38**: 1023-1033 [PMID: 11978527]

12 **Clavien PA**, Petrowsky H, DeOliveira ML, Graf R. Strategies for safer liver surgery and partial liver transplantation. *N Engl J Med* 2007; **356**: 1545-1559 [PMID: 17429086]

13 **Shah KN**, Clary BM. Selection of Patients with Colorectal/Liver Metastases for Surgical Intervention: Current Issues and Challenges. *Curr Surg Rep* 2014; **2**: 1-7 [DOI: 10.1007/s40137-014-0065-y]

14 **Catalano OA**, Singh AH, Uppot RN, Hahn PF, Ferrone CR, Sahani

DV. Vascular and biliary variants in the liver: implications for liver surgery. *Radiographics* 2008; **28**: 359-378 [PMID: 18349445 DOI: 10.1148/rg.282075099]

15 **Kinkel K**, Lu Y, Both M, Warren RS, Thoeni RF. Detection of hepatic metastases from cancers of the gastrointestinal tract by using noninvasive imaging methods (US, CT, MR imaging, PET): a meta-analysis. *Radiology* 2002; **224**: 748-756 [PMID: 12202709 DOI: 10.1148/radiol.2243011362]

16 **Wernecke K**, Rummeny E, Bongartz G, Vassallo P, Kivelitz D, Wiesmann W, Peters PE, Reers B, Reiser M, Pircher W. Detection of hepatic masses in patients with carcinoma: comparative sensitivities of sonography, CT, and MR imaging. *AJR Am J Roentgenol* 1991; **157**: 731-739 [PMID: 1892027 DOI: 10.2214/ajr.157.4.1892027]

17 **Glover C**, Douse P, Kane P, Karani J, Meire H, Mohammadtaghi S, Allen-Mersh TG. Accuracy of investigations for asymptomatic colorectal liver metastases. *Dis Colon Rectum* 2002; **45**: 476-484 [PMID: 12006929]

18 **Clarke MP**, Kane RA, Steele G, Hamilton ES, Ravikumar TS, Onik G, Clouse ME. Prospective comparison of preoperative imaging and intraoperative ultrasonography in the detection of liver tumors. *Surgery* 1989; **106**: 849-855 [PMID: 2554519]

19 **Ohlsson B**, Tranberg KG, Lundstedt C, Ekberg H, Hederström E. Detection of hepatic metastases in colorectal cancer: a prospective study of laboratory and imaging methods. *Eur J Surg* 1993; **159**: 275-281 [PMID: 8103361]

20 **Ong KO**, Leen E. Radiological staging of colorectal liver metastases. *Surg Oncol* 2007; **16**: 7-14 [PMID: 17499498]

21 **Albrecht T**, Hohmann J, Oldenburg A, Skrok J, Wolf KJ. Detection and characterisation of liver metastases. *Eur Radiol* 2004; **14** Suppl 8: P25-P33 [PMID: 15700330]

22 **Albrecht T**, Hoffmann CW, Schmitz SA, Schettler S, Overberg A, Germer CT, Wolf KJ. Phase-inversion sonography during the liver-specific late phase of contrast enhancement: improved detection of liver metastases. *AJR Am J Roentgenol* 2001; **176**: 1191-1198 [PMID: 11312180 DOI: 10.2214/ajr.176.5.1761191]

23 **Albrecht T**, Blomley MJ, Burns PN, Wilson S, Harvey CJ, Leen E, Claudon M, Calliada F, Correas JM, LaFortune M, Campani R, Hoffmann CW, Cosgrove DO, LeFevre F. Improved detection of hepatic metastases with pulse-inversion US during the liver-specific phase of SHU 508A: multicenter study. *Radiology* 2003; **227**: 361-370 [PMID: 12649417 DOI: 10.1148/radiol.2272011833]

24 **Esteban JM**, Mollá MA, Tomás C, Maldonado L. Improved detection of liver metastases with contrast-enhanced wideband harmonic imaging: comparison with CT findings. *Eur J Ultrasound* 2002; **15**: 119-126 [PMID: 12423737 DOI: 10.1016/S0929-8266(02)00032-0]

25 **Quaia E**, D'Onofrio M, Palumbo A, Rossi S, Bruni S, Cova M. Comparison of contrast-enhanced ultrasonography versus baseline ultrasound and contrast-enhanced computed tomography in metastatic disease of the liver: diagnostic performance and confidence. *Eur Radiol* 2006; **16**: 1599-1609 [PMID: 16552507 DOI: 10.1007/s00330-006-0192-7]

26 **Dalla Palma L**, Bertolotto M, Quaia E, Locatelli M. Detection of liver metastases with pulse inversion harmonic imaging: preliminary results. *Eur Radiol* 1999; **9** Suppl 3: S382-S387 [PMID: 10602934 DOI: 10.1007/PL00014079]

27 **Celli N**, Gaiani S, Piscaglia F, Zironi G, Camaggi V, Leoni S, Righini R, Bolondi L. Characterization of liver lesions by real-time contrast-enhanced ultrasonography. *Eur J Gastroenterol Hepatol* 2007; **19**: 3-14 [PMID: 17206071 DOI: 10.1097/01.meg.0000250585.53608.3c]

28 **Larsen LP**, Rosenkilde M, Christensen H, Bang N, Bolvig L, Christiansen T, Laurberg S. The value of contrast enhanced ultrasonography in detection of liver metastases from colorectal cancer: a prospective double-blinded study. *Eur J Radiol* 2007; **62**: 302-307 [PMID: 17194561 DOI: 10.1016/j.ejrad.2006.11.033]

29 **Westwood M**, Joore M, Grutters J, Redekop K, Armstrong N, Lee K, Gloy V, Raatz H, Misso K, Severens J, Kleijnen J. Contrast-enhanced ultrasound using SonoVue® (sulphur hexafluoride microbubbles) compared with contrast-enhanced computed tomography and contrast-enhanced magnetic resonance imaging for the characterisation of focal liver lesions and detection of liver metastases: a systematic review and cost-effectiveness analysis. *Health Technol Assess* 2013; **17**: 1-243 [PMID: 23611316 DOI: 10.3310/hta17160]

30 **Rafaelsen SR**, Jakobsen A. Contrast-enhanced ultrasound vs multidetector-computed tomography for detecting liver metastases in colorectal cancer: a prospective, blinded, patient-by-patient analysis. *Colorectal Dis* 2011; **13**: 420-425 [PMID: 20412096 DOI: 10.1111/j.1463-1318.2010.02288.x]

31 **Cantisani V**, Ricci P, Erturk M, Pagliara E, Drudi F, Calliada F, Mortele K, D'Ambrosio U, Marigliano C, Catalano C, Marin D, Di Seri M, Longo F, Passariello R. Detection of hepatic metastases from colorectal cancer: prospective evaluation of gray scale US versus SonoVue® low mechanical index real time-enhanced US as compared with multidetector-CT or Gd-BOPTA-MRI. *Ultraschall Med* 2010; **31**: 500-505 [PMID: 20408122 DOI: 10.1055/s-0028-1109751]

32 **Larsen LP**, Rosenkilde M, Christensen H, Bang N, Bolvig L, Christiansen T, Laurberg S. Can contrast-enhanced ultrasonography replace multidetector-computed tomography in the detection of liver metastases from colorectal cancer? *Eur J Radiol* 2009; **69**: 308-313 [PMID: 18068925 DOI: 10.1016/j.ejrad.2007.10.023]

33 **Konopke R**, Bunk A, Kersting S. Contrast-enhanced ultrasonography in patients with colorectal liver metastases after chemotherapy. *Ultraschall Med* 2008; **29** Suppl 4: S203-S209 [PMID: 18833498 DOI: 10.1055/s-2008-1027795]

34 **Cantisani V**, Grazhdani H, Fioravanti C, Rosignuolo M, Calliada F, Messineo D, Bernieri MG, Redler A, Catalano C, D'Ambrosio F. Liver metastases: Contrast-enhanced ultrasound compared with computed tomography and magnetic resonance. *World J Gastroenterol* 2014; **20**: 9998-10007 [PMID: 25110428 DOI: 10.3748/wjg.v20.i29.9998]

35 **Bolondi L**. The appropriate allocation of CEUS in the diagnostic algorithm of liver lesions: a debated issue. *Ultrasound Med Biol* 2013; **39**: 183-185 [PMID: 23140590]

36 **Choti MA**, Sitzmann JV, Tiburi MF, Sumetchotimetha W, Rangsin R, Schulick RD, Lillemoe KD, Yeo CJ, Cameron JL. Trends in long-term survival following liver resection for hepatic colorectal metastases. *Ann Surg* 2002; **235**: 759-766 [PMID: 12035031]

37 **Rojas Llimpe FL**, Di Fabio F, Ercolani G, Giampalma E, Cappelli A, Serra C, Castellucci P, D'Errico A, Golfieri R, Pinna AD, Pinto C. Imaging in resectable colorectal liver metastasis patients with or without preoperative chemotherapy: results of the PROMETEO-01 study. *Br J Cancer* 2014; **111**: 667-673 [PMID: 24983362 DOI: 10.1038/bjc.2014.351]

38 **Niekel MC**, Bipat S, Stoker J. Diagnostic imaging of colorectal liver metastases with CT, MR imaging, FDG PET, and/or FDG PET/CT: a meta-analysis of prospective studies including patients who have not previously undergone treatment. *Radiology* 2010; **257**: 674-684 [PMID: 20829538 DOI: 10.1148/radiol.10100729]

39 **Weg N**, Scheer MR, Gabor MP. Liver lesions: improved detection with dual-detector-array CT and routine 2.5-mm thin collimation. *Radiology* 1998; **209**: 417-426 [PMID: 9807568]

40 **Kim YK**, Ko SW, Hwang SB, Kim CS, Yu HC. Detection and characterization of liver metastases: 16-slice multidetector computed tomography versus superparamagnetic iron oxide-enhanced magnetic resonance imaging. *Eur Radiol* 2006; **16**: 1337-1345 [PMID: 16453115 DOI: 10.1007/s00330-005-0140-y]

41 **Haider MA**, Amitai MM, Rappaport DC, O'Malley ME, Hanbidge AE, Redston M, Lockwood GA, Gallinger S. Multi-detector row helical CT in preoperative assessment of small (< or = 1.5 cm) liver metastases: is thinner collimation better? *Radiology* 2002; **225**: 137-142 [PMID: 12354997 DOI: 10.1148/radiol.2251011225]

42 **Kulinna C**, Helmberger T, Kessler M, Reiser M. [Improvement in diagnosis of liver metastases with the multi-detector CT]. *Radiologe* 2001; **41**: 16-23 [PMID: 11220094 DOI: 10.1007/s001170050923]

43 **Ch'en IY**, Katz DS, Jeffrey RB, Daniel BL, Li KC, Beaulieu CF, Mindelzun RE, Yao D, Olcott EW. Do arterial phase helical CT images improve detection or characterization of colorectal liver

metastases? *J Comput Assist Tomogr* 2011; **21**: 391-397 [PMID: 9135646 DOI: 10.1097/00004728-199705000-00010]

44 **Wicherts DA**, de Haas RJ, van Kessel CS, Bisschops RH, Takahara T, van Hillegersberg R, Bipat S, Rinkes IH, van Leeuwen MS. Incremental value of arterial and equilibrium phase compared to hepatic venous phase CT in the preoperative staging of colorectal liver metastases: an evaluation with different reference standards. *Eur J Radiol* 2011; **77**: 305-311 [PMID: 19695807 DOI: 10.1016/j.ejrad.2009.07.026]

45 **Mainenti PP**, Cirillo LC, Camera L, Persico F, Cantalupo T, Pace L, De Palma GD, Persico G, Salvatore M. Accuracy of single phase contrast enhanced multidetector CT colonography in the preoperative staging of colo-rectal cancer. *Eur J Radiol* 2006; **60**: 453-459 [PMID: 16965883 DOI: 10.1016/j.ejrad.2006.08.001]

46 **Bajpai SK**, Sahani D. Recent progress in imaging of colorectal cancer liver metastases. *Curr Colorectal Cancer Rep* 2009; **5**: 99-107 [DOI: 10.1007/s11888-009-0015-8]

47 **Berger-Kulemann V**, Schima W, Baroud S, Koelblinger C, Kaczirek K, Gruenberger T, Schindl M, Maresch J, Weber M, Ba-Ssalamah A. Gadoxetic acid-enhanced 3.0 T MR imaging versus multidetector-row CT in the detection of colorectal metastases in fatty liver using intraoperative ultrasound and histopathology as a standard of reference. *Eur J Surg Oncol* 2012; **38**: 670-676 [PMID: 22652037 DOI: 10.1016/j.ejso.2012.05.004]

48 **Bipat S**, Niekel MC, Comans EF, Nio CY, Bemelman WA, Verhoef C, Stoker J. Imaging modalities for the staging of patients with colorectal cancer. *Neth J Med* 2012; **70**: 26-34 [PMID: 22271811]

49 **Bipat S**, van Leeuwen MS, Comans EF, Pijl ME, Bossuyt PM, Zwinderman AH, Stoker J. Colorectal liver metastases: CT, MR imaging, and PET for diagnosis--meta-analysis. *Radiology* 2005; **237**: 123-131 [PMID: 16100087 DOI: 10.1148/radiol.2371042060]

50 **Mainenti PP**, Mancini M, Mainolfi C, Camera L, Maurea S, Manchia A, Tanga M, Persico F, Addeo P, D'Antonio D, Speranza A, Bucci L, Persico G, Pace L, Salvatore M. Detection of colorectal liver metastases: prospective comparison of contrast enhanced US, multidetector CT, PET/CT, and 1.5 Tesla MR with extracellular and reticulo-endothelial cell specific contrast agents. *Abdom Imaging* 2010; **35**: 511-521 [PMID: 19562412 DOI: 10.1007/s00261-009-9555-2]

51 **Blyth S**, Blakeborough A, Peterson M, Cameron IC, Majeed AW. Sensitivity of magnetic resonance imaging in the detection of colorectal liver metastases. *Ann R Coll Surg Engl* 2008; **90**: 25-28 [PMID: 18201494 DOI: 10.1308/003588408X242303]

52 **Schima W**, Saini S, Echeverri JA, Hahn PF, Harisinghani M, Mueller PR. Focal liver lesions: characterization with conventional spin-echo versus fast spin-echo T2-weighted MR imaging. *Radiology* 1997; **202**: 389-393 [PMID: 9015063]

53 **Bennett GL**, Petersein A, Mayo-Smith WW, Hahn PF, Schima W, Saini S. Addition of gadolinium chelates to heavily T2-weighted MR imaging: limited role in differentiating hepatic hemangiomas from metastases. *AJR Am J Roentgenol* 2000; **174**: 477-485 [PMID: 10658728 DOI: 10.2214/ajr.174.2.1740477]

54 **Cittadini G**, Santacroce E, Giasotto V, Rescinito G. [Focal liver lesions: characterization with quantitative analysis of T2 relaxation time in TSE sequence with double echo time]. *Radiol Med* 2004; **107**: 166-173 [PMID: 15031682]

55 **Patterson DM**, Padhani AR, Collins DJ. Technology insight: water diffusion MRI--a potential new biomarker of response to cancer therapy. *Nat Clin Pract Oncol* 2008; **5**: 220-233 [PMID: 18301415 DOI: 10.1038/ncponc1073]

56 **Bruegel M**, Holzapfel K, Gaa J, Woertler K, Waldt S, Kiefer B, Stemmer A, Ganter C, Rummeny EJ. Characterization of focal liver lesions by ADC measurements using a respiratory triggered diffusion-weighted single-shot echo-planar MR imaging technique. *Eur Radiol* 2008; **18**: 477-485 [PMID: 17960390 DOI: 10.1007/s00330-007-0785-9]

57 **Parikh T**, Drew SJ, Lee VS, Wong S, Hecht EM, Babb JS, Taouli B. Focal liver lesion detection and characterization with diffusion-weighted MR imaging: comparison with standard breath-hold T2-weighted imaging. *Radiology* 2008; **246**: 812-822 [PMID: 18223123 DOI: 10.1148/radiol.2463070432]

58 **Kenis C**, Deckers F, De Foer B, Van Mieghem F, Van Laere S, Pouillon M. Diagnosis of liver metastases: can diffusion-weighted imaging (DWI) be used as a stand alone sequence? *Eur J Radiol* 2012; **81**: 1016-1023 [PMID: 21377305 DOI: 10.1016/j.ejrad.2011.02.019]

59 **Löwenthal D**, Zeile M, Lim WY, Wybranski C, Fischbach F, Wieners G, Pech M, Kropf S, Ricke J, Dudeck O. Detection and characterisation of focal liver lesions in colorectal carcinoma patients: comparison of diffusion-weighted and Gd-EOB-DTPA enhanced MR imaging. *Eur Radiol* 2011; **21**: 832-840 [PMID: 20886339 DOI: 10.1007/s00330-010-1977-2]

60 **Bellin MF**, Van Der Molen AJ. Extracellular gadolinium-based contrast media: an overview. *Eur J Radiol* 2008; **66**: 160-167 [PMID: 18358659 DOI: 10.1016/j.ejrad.2008.01.023]

61 **del Frate C**, Bazzocchi M, Mortele KJ, Zuiani C, Londero V, Como G, Zanardi R, Ros PR. Detection of liver metastases: comparison of gadobenate dimeglumine-enhanced and ferumoxides-enhanced MR imaging examinations. *Radiology* 2002; **225**: 766-772 [PMID: 12461259 DOI: 10.1148/radiol.2253011854]

62 **Ward J**, Robinson PJ, Guthrie JA, Downing S, Wilson D, Lodge JP, Prasad KR, Toogood GJ, Wyatt JI. Liver metastases in candidates for hepatic resection: comparison of helical CT and gadolinium- and SPIO-enhanced MR imaging. *Radiology* 2005; **237**: 170-180 [PMID: 16126930 DOI: 10.1148/radiol.2371041444]

63 **Kim YK**, Lee JM, Kim CS, Chung GH, Kim CY, Kim IH. Detection of liver metastases: gadobenate dimeglumine-enhanced three-dimensional dynamic phases and one-hour delayed phase MR imaging versus superparamagnetic iron oxide-enhanced MR imaging. *Eur Radiol* 2005; **15**: 220-228 [PMID: 15624108 DOI: 10.1007/s00330-004-2570-3]

64 **Maurea S**, Mainenti PP, Tambasco A, Imbriaco M, Mollica C, Laccetti E, Camera L, Liuzzi R, Salvatore M. Diagnostic accuracy of MR imaging to identify and characterize focal liver lesions: comparison between gadolinium and superparamagnetic iron oxide contrast media. *Quant Imaging Med Surg* 2014; **4**: 181-189 [PMID: 24914419 DOI: 10.3978/j.issn.2223-4292.2014.01.02]

65 **Hamm B**, Staks T, Mühler A, Bollow M, Taupitz M, Frenzel T, Wolf KJ, Weinmann HJ, Lange L. Phase I clinical evaluation of Gd-EOB-DTPA as a hepatobiliary MR contrast agent: safety, pharmacokinetics, and MR imaging. *Radiology* 1995; **195**: 785-792 [PMID: 7754011]

66 **Dahlström N**, Persson A, Albiin N, Smedby O, Brismar TB. Contrast-enhanced magnetic resonance cholangiography with Gd-BOPTA and Gd-EOB-DTPA in healthy subjects. *Acta Radiol* 2007; **48**: 362-368 [PMID: 17453513 DOI: 10.1080/02841850701196922]

67 **Auer RC**, White RR, Kemeny NE, Schwartz LH, Shia J, Blumgart LH, Dematteo RP, Fong Y, Jarnagin WR, D'Angelica MI. Predictors of a true complete response among disappearing liver metastases from colorectal cancer after chemotherapy. *Cancer* 2010; **116**: 1502-1509 [PMID: 20120032 DOI: 10.1002/cncr.24912]

68 **van Kessel CS**, Buckens CF, van den Bosch MA, van Leeuwen MS, van Hillegersberg R, Verkooijen HM. Preoperative imaging of colorectal liver metastases after neoadjuvant chemotherapy: a meta-analysis. *Ann Surg Oncol* 2012; **19**: 2805-2813 [PMID: 22396005 DOI: 10.1245/s10434-012-2300-z]

69 **Tran PV**, Jhaveri KS. Comparison of high spatial resolution respiratory triggered inversion recovery-prepared spoiled gradient echo sequence with standard breathhold T1 sequence MRI of the liver using gadoxetic acid. *J Magn Reson Imaging* 2013; **37**: 700-706 [PMID: 23335396 DOI: 10.1002/jmri.23864]

70 **Yoon JH**, Lee JM, Lee ES, Baek J, Lee S, Iwadate Y, Han JK, Choi BI. Navigated three-dimensional T1-weighted gradient-echo sequence for gadoxetic acid liver magnetic resonance imaging in patients with limited breath-holding capacity. *Abdom Imaging* 2015; **40**: 278-288 [PMID: 25112454]

71 **Ruers TJ**, Langenhoff BS, Neeleman N, Jager GJ, Strijk S, Wobbes T, Corstens FH, Oyen WJ. Value of positron emission tomography with [F-18]fluorodeoxyglucose in patients with

colorectal liver metastases: a prospective study. *J Clin Oncol* 2002; **20**: 388-395 [PMID: 11786565 DOI: 10.1200/JCO.20.2.388]

72 **Rappeport ED**, Loft A, Berthelsen AK, von der Recke P, Larsen PN, Mogensen AM, Wettergren A, Rasmussen A, Hillingsoe J, Kirkegaard P, Thomsen C. Contrast-enhanced FDG-PET/CT vs. SPIO-enhanced MRI vs. FDG-PET vs. CT in patients with liver metastases from colorectal cancer: a prospective study with intraoperative confirmation. *Acta Radiol* 2007; **48**: 369-378 [PMID: 17453514 DOI: 10.1080/02841850701294560]

73 **Fong Y**, Saldinger PF, Akhurst T, Macapinlac H, Yeung H, Finn RD, Cohen A, Kemeny N, Blumgart LH, Larson SM. Utility of 18F-FDG positron emission tomography scanning on selection of patients for resection of hepatic colorectal metastases. *Am J Surg* 1999; **178**: 282-287 [PMID: 10587184 DOI: 10.1016/S0002-9610(99)00187-7]

74 **Sahani DV**, Kalva SP, Fischman AJ, Kadavigere R, Blake M, Hahn PF, Saini S. Detection of liver metastases from adenocarcinoma of the colon and pancreas: comparison of mangafodipir trisodium-enhanced liver MRI and whole-body FDG PET. *AJR Am J Roentgenol* 2005; **185**: 239-246 [PMID: 15972430 DOI: 10.2214/ajr.185.1.01850239]

75 **Badiee S**, Franc BL, Webb EM, Chu B, Hawkins RA, Coakley F, Singer L. Role of IV iodinated contrast material in 18F-FDG PET/CT of liver metastases. *AJR Am J Roentgenol* 2008; **191**: 1436-1439 [PMID: 18941082 DOI: 10.2214/AJR.07.3750]

76 **Revheim ME**, Haugvik SP, Johnsrud K, Mathisen Ø, Fjeld JG, Skretting A. Respiratory gated and prolonged acquisition 18F-FDG PET improve preoperative assessment of colorectal liver metastases. *Acta Radiol* 2015; **56**: 397-403 [PMID: 24682406 DOI: 10.1177/0284185114529563]

77 **Ruers TJ**, Wiering B, van der Sijp JR, Roumen RM, de Jong KP, Comans EF, Pruim J, Dekker HM, Krabbe PF, Oyen WJ. Improved selection of patients for hepatic surgery of colorectal liver metastases with (18)F-FDG PET: a randomized study. *J Nucl Med* 2009; **50**: 1036-1041 [PMID: 19525451 DOI: 10.2967/jnumed.109.063040]

78 **Mainenti PP**, Salvatore B, D'Antonio D, De Falco T, De Palma GD, D'Armiento FP, Bucci L, Pace L, Salvatore M. PET/CT colonography in patients with colorectal polyps: a feasibility study. *Eur J Nucl Med Mol Imaging* 2007; **34**: 1594-1603 [PMID: 17492447 DOI: 10.1007/s00259-007-0422-5]

79 **Mainenti PP**, Iodice D, Segreto S, Storto G, Magliulo M, De Palma GD, Salvatore M, Pace L. Colorectal cancer and 18FDG-PET/CT: what about adding the T to the N parameter in loco-regional staging? *World J Gastroenterol* 2011; **17**: 1427-1433 [PMID: 21472100 DOI: 10.3748/wjg.v17.i11.1427]

80 **Maas M**, Rutten IJ, Nelemans PJ, Lambregts DM, Cappendijk VC, Beets GL, Beets-Tan RG. What is the most accurate whole-body imaging modality for assessment of local and distant recurrent disease in colorectal cancer? A meta-analysis : imaging for recurrent colorectal cancer. *Eur J Nucl Med Mol Imaging* 2011; **38**: 1560-1571 [PMID: 21468765 DOI: 10.1007/s00259-011-1785-1]

81 **Giacomobono S**, Gallicchio R, Capacchione D, Nardelli A, Gattozzi D, Lettini G, Molinari L, Mainenti P, Cammarota A, Storto G. F-18 FDG PET/CT in the assessment of patients with unexplained CEA rise after surgical curative resection for colorectal cancer. *Int J Colorectal Dis* 2013; **28**: 1699-1705 [PMID: 23846517 DOI: 10.1007/s00384-013-1747-0]

82 **Storto G**, Nicolai E, Salvatore M. [18F]FDG-PET-CT for early monitoring of tumor response: when and why. *Q J Nucl Med Mol Imaging* 2009; **53**: 167-180 [PMID: 19293765]

83 **Partovi S**, Kohan A, Gaeta C, Rubbert C, Vercher-Conejero JL, Jones RS, O'Donnell JK, Wojtylak P, Faulhaber P. Image quality assessment of automatic three-segment MR attenuation correction vs. CT attenuation correction. *Am J Nucl Med Mol Imaging* 2013; **3**: 291-299 [PMID: 23638340]

84 **Schwenzer NF**, Schmidt H, Claussen CD. Whole-body MR/PET: applications in abdominal imaging. *Abdom Imaging* 2012; **37**: 20-28 [PMID: 22002195 DOI: 10.1007/s00261-011-9809-7]

85 **Drzezga A**, Souvatzoglou M, Eiber M, Beer AJ, Fürst S, Martinez-Möller A, Nekolla SG, Ziegler S, Ganter C, Rummeny EJ, Schwaiger M. First clinical experience with integrated whole-body PET/MR: comparison to PET/CT in patients with oncologic diagnoses. *J Nucl Med* 2012; **53**: 845-855 [PMID: 22534830 DOI: 10.2967/jnumed.111.098608]

86 **Quick HH**, von Gall C, Zeilinger M, Wiesmüller M, Braun H, Ziegler S, Kuwert T, Uder M, Dörfler A, Kalender WA, Lell M. Integrated whole-body PET/MR hybrid imaging: clinical experience. *Invest Radiol* 2013; **48**: 280-289 [PMID: 23442775 DOI: 10.1097/RLI.0b013e3182845a08]

87 **Partovi S**, Kohan A, Paspulati RM, Ros PR, Herrmann KA. PET/MRI in Colorectal cancer. In: Carrio I, Ros P. PET/MRI Methodology and Clinical Applications. *Springer* 2014; 7: 95-108

88 **Kershah S**, Partovi S, Traughber BJ, Muzic RF, Schluchter MD, O'Donnell JK, Faulhaber P. Comparison of standardized uptake values in normal structures between PET/CT and PET/MRI in an oncology patient population. *Mol Imaging Biol* 2013; **15**: 776-785 [PMID: 23632951 DOI: 10.1007/s11307-013-0629-8]

89 **Nielsen K**, Scheffer HJ, Pieters IC, van Tilborg AA, van Waesberghe JH, Oprea-Lager DE, Meijerink MR, Kazemier G, Hoekstra OS, Schreurs HW, Sietses C, Meijer S, Comans EF, van den Tol PM. The use of PET-MRI in the follow-up after radiofrequency- and microwave ablation of colorectal liver metastases. *BMC Med Imaging* 2014; **14**: 27 [PMID: 25103913 DOI: 10.1186/1471-2342-14-27]

90 **Sheafor DH**, Killius JS, Paulson EK, DeLong DM, Foti AM, Nelson RC. Hepatic parenchymal enhancement during triple-phase helical CT: can it be used to predict which patients with breast cancer will develop hepatic metastases? *Radiology* 2000; **214**: 875-880 [PMID: 10715061]

91 **Miles KA**, Colyvas K, Griffiths MR, Bunce IH. Colon cancer: risk stratification using hepatic perfusion CT. *Eur Radiol* 2004; **14** (Suppl 2): 129

92 **Ridge JA**, Bading JR, Gelbard AS, Benua RS, Daly JM. Perfusion of colorectal hepatic metastases. Relative distribution of flow from the hepatic artery and portal vein. *Cancer* 1987; **59**: 1547-1553 [PMID: 3828954]

93 **Leen E**, Goldberg JA, Robertson J, Sutherland GR, McArdle CS. The use of duplex sonography in the detection of colorectal hepatic metastases. *Br J Cancer* 1991; **63**: 323-325 [PMID: 1997115]

94 **Leen E**, Goldberg JA, Robertson J, Sutherland GR, Hemingway DM, Cooke TG, McArdle CS. Detection of hepatic metastases using duplex/color Doppler sonography. *Ann Surg* 1991; **214**: 599-604 [PMID: 1953113]

95 **Kopljar M**, Brkljacic B, Doko M, Horzic M. Nature of Doppler perfusion index changes in patients with colorectal cancer liver metastases. *J Ultrasound Med* 2004; **23**: 1295-1300 [PMID: 15448318]

96 **Anzidei M**, Napoli A, Zaccagna F, Cartocci G, Saba L, Menichini G, Cavallo Marincola B, Marotta E, Di Mare L, Catalano C, Passariello R. Liver metastases from colorectal cancer treated with conventional and antiangiogenetic chemotherapy: evaluation with liver computed tomography perfusion and magnetic resonance diffusion-weighted imaging. *J Comput Assist Tomogr* 2011; **35**: 690-696 [PMID: 22082538 DOI: 10.1097/RCT.0b013e318230d905]

97 **Meijerink MR**, van Waesberghe JH, van der Weide L, van den Tol P, Meijer S, van Kuijk C. Total-liver-volume perfusion CT using 3-D image fusion to improve detection and characterization of liver metastases. *Eur Radiol* 2008; **18**: 2345-2354 [PMID: 18491094 DOI: 10.1007/s00330-008-0996-8]

98 **Kanematsu M**, Goshima S, Watanabe H, Kondo H, Kawada H, Noda Y, Moriyama N. Diffusion/perfusion MR imaging of the liver: practice, challenges, and future. *Magn Reson Med Sci* 2012; **11**: 151-161 [PMID: 23037559]

99 **De Bruyne S**, Van Damme N, Smeets P, Ferdinande L, Ceelen W, Mertens J, Van de Wiele C, Troisi R, Libbrecht L, Laurent S, Geboes K, Peeters M. Value of DCE-MRI and FDG-PET/CT in the prediction of response to preoperative chemotherapy with bevacizumab for colorectal liver metastases. *Br J Cancer* 2012; **106**: 1926-1933 [PMID: 22596235 DOI: 10.1038/bjc.2012.184]

100 **Ganeshan B**, Miles KA, Young RC, Chatwin CR. Texture analysis

in non-contrast enhanced CT: impact of malignancy on texture in apparently disease-free areas of the liver. *Eur J Radiol* 2009; **70**: 101-110 [PMID: 18242909 DOI: 10.1016/j.ejrad.2007.12.005]

101 **Miles KA**, Ganeshan B, Griffiths MR, Young RC, Chatwin CR. Colorectal cancer: texture analysis of portal phase hepatic CT images as a potential marker of survival. *Radiology* 2009; **250**: 444-452 [PMID: 19164695 DOI: 10.1148/radiol.2502071879]

102 **Rao SX**, Lambregts DM, Schnerr RS, van Ommen W, van Nijnatten TJ, Martens MH, Heijnen LA, Backes WH, Verhoef C, Zeng MS, Beets GL, Beets-Tan RG. Whole-liver CT texture analysis in colorectal cancer: Does the presence of liver metastases affect the texture of the remaining liver? *United European Gastroenterol J* 2014; **2**: 530-538 [PMID: 25452849 DOI: 10.1177/2050640614552463]

103 **Ganeshan B**, Miles KA. Quantifying tumour heterogeneity with CT. *Cancer Imaging* 2013; **13**: 140-149 [PMID: 23545171 DOI: 10.1102/1470-7330.2013.0015]

104 **Barash H**, Gross E, Edrei Y, Pappo O, Spira G, Vlodavsky I, Galun E, Matot I, Abramovitch R. Functional magnetic resonance imaging monitoring of pathological changes in rodent livers during hyperoxia and hypercapnia. *Hepatology* 2008; **48**: 1232-1241 [PMID: 18629804 DOI: 10.1002/hep.22394]

105 **Barash H**, Gross E, Matot I, Edrei Y, Tsarfaty G, Spira G, Vlodavsky I, Galun E, Abramovitch R. Functional MR imaging during hypercapnia and hyperoxia: noninvasive tool for monitoring changes in liver perfusion and hemodynamics in a rat model. *Radiology* 2007; **243**: 727-735 [PMID: 17463135]

106 **Edrei Y**, Gross E, Corchia N, Tsarfaty G, Galun E, Pappo O, Abramovitch R. Vascular profile characterization of liver tumors by magnetic resonance imaging using hemodynamic response imaging in mice. *Neoplasia* 2011; **13**: 244-253 [PMID: 21390187]

107 **Edrei Y**, Freiman M, Sklair-Levy M, Tsarfaty G, Gross E, Joskowicz L, Abramovitch R. Quantitative functional MRI biomarkers improved early detection of colorectal liver metastases. *J Magn Reson Imaging* 2014; **39**: 1246-1253 [PMID: 24006217 DOI: 10.1002/jmri.24270]

108 **Seo HJ**, Kim MJ, Lee JD, Chung WS, Kim YE. Gadoxetate disodium-enhanced magnetic resonance imaging versus contrast-enhanced 18F-fluorodeoxyglucose positron emission tomography/computed tomography for the detection of colorectal liver metastases. *Invest Radiol* 2011; **46**: 548-555 [PMID: 21577131 DOI: 10.1097/RLI.0b013e31821a2163]

109 **Muhi A**, Ichikawa T, Motosugi U, Sou H, Nakajima H, Sano K, Sano M, Kato S, Kitamura T, Fatima Z, Fukushima K, Iino H, Mori Y, Fujii H, Araki T. Diagnosis of colorectal hepatic metastases: comparison of contrast-enhanced CT, contrast-enhanced US, superparamagnetic iron oxide-enhanced MRI, and gadoxetic acid-enhanced MRI. *J Magn Reson Imaging* 2011; **34**: 326-335 [PMID: 21780227 DOI: 10.1002/jmri.22613]

110 **Zech CJ**, Grazioli L, Jonas E, Ekman M, Niebecker R, Gschwend S, Breuer J, Jönsson L, Kienbaum S. Health-economic evaluation of three imaging strategies in patients with suspected colorectal liver metastases: Gd-EOB-DTPA-enhanced MRI vs. extracellular contrast media-enhanced MRI and 3-phase MDCT in Germany, Italy and Sweden. *Eur Radiol* 2009; **19** Suppl 3: S753-S763 [PMID: 19484243 DOI: 10.1007/s00330-009-1432-4]

111 **Chen L**, Zhang J, Zhang L, Bao J, Liu C, Xia Y, Huang X, Wang J. Meta-analysis of gadoxetic acid disodium (Gd-EOB-DTPA)-enhanced magnetic resonance imaging for the detection of liver metastases. *PLoS One* 2012; **7**: e48681 [PMID: 23144927 DOI: 10.1371/journal.pone.0048681]

112 **Maffione AM**, Lopci E, Bluemel C, Giammarile F, Herrmann K, Rubello D. Diagnostic accuracy and impact on management of (18)F-FDG PET and PET/CT in colorectal liver metastasis: a meta-analysis and systematic review. *Eur J Nucl Med Mol Imaging* 2015; **42**: 152-163 [PMID: 25319712 DOI: 10.1007/s00259-014-2930-4]

113 **Han K**, Park SH, Kim KW, Kim HJ, Lee SS, Kim JC, Yu CS, Lim SB, Joo YS, Kim AY, Ha HK. Use of liver magnetic resonance imaging after standard staging abdominopelvic computed tomography to evaluate newly diagnosed colorectal cancer patients. *Ann Surg* 2015; **261**: 480-486 [PMID: 24866542]

114 National Comprehensive Cancer Network Oncologic Guidelines. Colon cancer. Version 2. 2012. Available from: URL: http://nccn.org

115 **Sahani D**, Mehta A, Blake M, Prasad S, Harris G, Saini S. Preoperative hepatic vascular evaluation with CT and MR angiography: implications for surgery. *Radiographics* 2004; **24**: 1367-1380 [PMID: 15371614 DOI: 10.1148/rg.245035224]

116 **Therasse P**, Arbuck SG, Eisenhauer EA, Wanders J, Kaplan RS, Rubinstein L, Verweij J, Van Glabbeke M, van Oosterom AT, Christian MC, Gwyther SG. New guidelines to evaluate the response to treatment in solid tumors. European Organization for Research and Treatment of Cancer, National Cancer Institute of the United States, National Cancer Institute of Canada. *J Natl Cancer Inst* 2000; **92**: 205-216 [PMID: 10655437 DOI: 10.1093/jnci/92.3.205]

117 **Catenacci DV**, Kozloff M, Kindler HL, Polite B. Personalized colon cancer care in 2010. *Semin Oncol* 2011; **38**: 284-308 [PMID: 21421118]

118 **Chibaudel B**, Maindrault-Goebel F, Lledo G, Mineur L, André T, Bennamoun M, Mabro M, Artru P, Carola E, Flesch M, Dupuis O, Colin P, Larsen AK, Afchain P, Tournigand C, Louvet C, de Gramont A. Can chemotherapy be discontinued in unresectable metastatic colorectal cancer? The GERCOR OPTIMOX2 Study. *J Clin Oncol* 2009; **27**: 5727-5733 [PMID: 19786657 DOI: 10.1200/JCO.2009.23.4344]

119 **Chung WS**, Park MS, Shin SJ, Baek SE, Kim YE, Choi JY, Kim MJ. Response evaluation in patients with colorectal liver metastases: RECIST version 1.1 versus modified CT criteria. *AJR Am J Roentgenol* 2012; **199**: 809-815 [PMID: 22997372]

120 **Schima W**, Ba-Ssalamah A, Kurtaran A, Schindl M, Gruenberger T. Post-treatment imaging of liver tumours. *Cancer Imaging* 2007; **7** Spec No A: S28-S36 [PMID: 17921098 DOI: 10.1102/1470-7330.2007.9047]

P- Reviewer: Kita K **S- Editor**: Ji FF
L- Editor: A **E- Editor**: Liu SQ

World Journal of Radiology

Submit a Manuscript: http://www.wjgnet.com/esps/
Help Desk: http://www.wjgnet.com/esps/helpdesk.aspx
DOI: 10.4329/wjr.v7.i7.170

World J Radiol 2015 July 28; 7(7): 170-179
ISSN 1949-8470 (online)

MINIREVIEWS

Perfusion computed tomography in renal cell carcinoma

Chandan J Das, Usha Thingujam, Ananya Panda, Sanjay Sharma, Arun Kumar Gupta

Chandan J Das, Usha Thingujam, Ananya Panda, Sanjay Sharma, Arun Kumar Gupta, Department of Radiology, All India Institute of Medical Sciences, Ansari Nagar, New Delhi 110029, India

Author contributions: Das CJ, Thingujam U and Panda A contributed equally to conception, article design, literature search, article drafting, critical revision and image preparation; Das CJ and Sharma S helped with the article concept and revision; Das CJ and Gupta AK helped in article preparation and final approval of version of article to be published.

Conflict-of-interest statement: None.

Correspondence to: Dr. Chandan J Das, MD, DNB, MNAMS, Assistant Professor, Department of Radiology, All India Institute of Medical Sciences, Room No. 63, Ansari Nagar, New Delhi 110029, India. docchandan17@gmail.com
Telephone: +91-11-26594889
Fax: +91-11-26588663

Received: December 1, 2014
Peer-review started: December 2, 2014
First decision: February 7, 2015
Revised: March 30, 2015
Accepted: June 4, 2015
Article in press: June 8, 2015
Published online: July 28, 2015

Abstract

Various imaging modalities are available for the diagnosis, staging and response evaluation of patients with renal cell carcinoma (RCC). While contrast enhanced computed tomography (CT) is used as the standard of imaging for size, morphological evaluation and response assessment in RCC, a new functional imaging technique like perfusion CT (pCT), goes down to the molecular level and provides new perspectives in imaging of RCC. pCT depicts regional tumor perfusion and vascular permeability which are indirect parameters of tumor angiogenesis and thereby provides vital information regarding tumor microenvironment. Also response evaluation using pCT may predate the size criteria used in Response Evaluation Criteria in Solid Tumors, as changes in the perfusion occurs earlier following tissue kinase inhibitors before any actual change in size. This may potentially help in predicting prognosis, better selection of therapy and more accurate and better response evaluation in patients with RCC. This article describes the techniques and role of pCT in staging and response assessment in patients with RCCs.

Key words: Angiogenesis; Anti-angiogenic therapy; Perfusion computed tomography; Renal cell carcinoma

Core tip: Perfusion computed tomography is a functional imaging technique. It can be used to predict the histologic grade and early as well as more accurate response evaluation in renal cell carcinoma (RCC). This has the potential to help in better selection of therapy and improve prognosis in RCC.

Das CJ, Thingujam U, Panda A, Sharma S, Gupta AK. Perfusion computed tomography in renal cell carcinoma. *World J Radiol* 2015; 7(7): 170-179 Available from: URL: http://www.wjgnet.com/1949-8470/full/v7/i7/170.htm DOI: http://dx.doi.org/10.4329/wjr.v7.i7.170

INTRODUCTION

Renal cell carcinoma (RCC) is the most common primary tumor of the kidney. Hypervascularity is

an important feature of primary RCC as well as its metastases. Angiogenesis plays an important role in the growth of the primary tumor and the spread of distant metastases.

Depending on the histologic type and the stage of tumors, the treatment options vary from surgery to chemotherapy. With the advent of new anti-angiogenic agents acting at a molecular level, the treatment of RCC has undergone a paradigm shift. These drugs include sorafenib, sunitinib, pazopanib, and axitinib that target key growth factors like the vascular endothelial growth factor and tyrosine kinase, monoclonal antibody (*e.g.,* bevacizumab), and mammalian target of rapamycin inhibitors (*e.g.,* temsirolimus and everolimus).

The evaluation of the treatment response in patients on these drugs is a challenge. Because of their cytostatic nature, most of these agents produce no significant change in the size of tumor as compared to earlier agents which were cytotoxic. Thus traditional response evaluation based only on size will not be accurate in predicting actual response.

Hence there is a need for tumor evaluation with new functional imaging techniques like perfusion computed tomography (pCT) and dynamic contrast enhanced magnetic resonance imaging. These make feasible grading of the tumor, prognosticating and targeted therapy. These are predicted based on certain perfusion parameters, namely blood flow (BF), blood volume (BV), mean transit time (MTT) and permeability (PMB) which shall be dealt in detail in the subsequent paragraphs. Also different histologic types of tumors have been shown to have different perfusion parameters which will have an impact on the prognosis[1].

PCT: PRINCIPLE

pCT is based on the temporal changes in tissue attenuation after intravenous administration of iodinated contrast media. Tissue iodine concentration determines enhancement and is an indirect reflection of tissue vascularity and vascular physiology[2,3]. Two phases are seen in tissue enhancement based on the contrast dynamics and contrast distribution in the intravascular and extravascular compartment[2]. Initial phase contrast enhancement is due to intravascular space distribution and lasts for approximately 40 to 60 s[2-4]. Contrast extravasation from the intravascular to the extravascular compartment across the capillary basement membrane marks the onset of the second phase.

BF and BV determine the first phase, whereas vascular PMB to the contrast media is the main determining factor during the second phase[2]. In pCT, images are taken in quick succession in the region of interest during these two phases. A tissue attenuation curve is plotted after recording the temporal changes in tissue attenuation. Quantification of tissue perfusion is done by applying proper mathematical modeling[2].

Table 1 Protocol for dynamic perfusion computed tomography acquisition

No. of scans	Cycle time (s)	Accumulated time since start of scan (s)
3	3	9
9	1.5	22.5
5	3	37.5
5	6	68.0
22 (in total)		Examination time: 68

PCT: TECHNIQUE

pCT protocol consists of a baseline image acquisition without contrast enhancement. Dynamic acquisition performed sequentially after intravenous injection of contrast media follows subsequently[2].

Unenhanced CT acquisition

An unenhanced CT scan of the upper abdomen covering the kidneys is initially performed to locate the renal lesion. It also acts as a localizer to further select the region of interest in the contrast-enhanced dynamic imaging phase. Larger coverage (8-16 cm) is currently obtained with the use of newer scanners having increased rows of detectors[2].

Dynamic CT acquisition

Images are acquired every 3 to 5 s (Table 1) in the initial cine phase for a total of approximately 40 to 60 s during the first-pass study[2-4]. For obtaining PMB measurements, a second phase lasting from 2 to 10 min is supplemented after the first-pass study[2,3]. The second phase images are acquired every 10 to 20 s[2].

In the pCT study, a predefined scan volume (80 mm for shuttle axial technique and 40 mm for cine technique) in the Z-axis is selected to cover the lesion[5]. For lesions smaller than 20 mm, cine technique is useful. One hundred milliliters of non-ionic iodinated contrast is administered intravenously for the pCT study maintaining a flow rate of 5 mL/s followed by 40 mL of normal saline flush at the same flow rate[5].

In cine mode acquisition, 8 contiguous sections, collimated to 5 mm, with temporal resolution of 1 s by are obtained without table movement using the following parameters: 100 Kv, 80 mAs, rotation time 0.5 s, and scan field of view of 50 cm[5]. Whereas in shuttle-mode acquisition, 8 contiguous sections, collimated to 5 mm, with temporal resolution of 2.8 s are obtained with table movement (21 passes) and using following parameters: 100 Kv, 80 mAs, rotation time 0.4 s, and scan field of view of 50 cm[5]. In order to include both first-pass enhancement and delayed phase, the total duration of scan is approximately 60 s. After pCT scans, a conventional contrast enhanced CT of the abdomen and thorax is performed immediately. Excretory phase CT urography may be obtained after 5 to 10 min after the contrast media injection whenever required[5].

Table 2 Computed tomography perfusion parameters[2-4]

Perfusion parameters	Definition	Unit	Biomarker
Regional blood flow	Blood flow per unit volume or mass of tissue	mL/100 mL per minute	Tumour vascularization
Regional tumour blood volume	Ratio of blood volume to tumour volume	mL/100 mL	Tumour vascularization
Permeability/blood flow extraction (PMB/PS/k-trans)	Rate of transfer of contrast agent from the intravascular to the extravascular compartment	mL/100 gm per minute	Vascular immaturity
Mean transit time	Average time taken to travel from artery to vein	s	Perfusion pressure
Time to peak	Time from arrival of the contrast in major arterial vessels to thepeak enhancement	s	Perfusion pressure
Maximum peak intensity	Maximum increase in tissue density after contrast injection	HU	Tissue blood volume

Table 3 Perfusion computed tomography parameter values for kidney (renal cell carcinoma *vs* normal renal cortex)[7]

	Normal renal cortex (mean ± SD)	Renal cell carcinoma (mean ± SD)	*t* value	*P* value
Blood flow (mL/min per 100 g)	454.32 ± 110.90	261.96 ± 175.86	-7.620	0.000
Blood volume (mL/100 g)	23.53 ± 5.71	17.17 ± 8.34	-5.193	0.000
Mean transit time (s)	3.62 ± 1.38	7.08 ± 3.42	7.670	0.000
Permeability (mL/min per 100 g)	63.95 ± 18.85	25.07 ± 13.20	-14.193	0.000

PCT: IMAGE INTERPRETATION

Post processing is done to correct for the motion artifacts and the data are analyzed at a work station. The slice showing the maximal transverse tumor diameter is chosen for further analysis. An arterial input is defined by putting a circular region-of-interest (ROI) over the abdominal aorta at the level of the renal vessels. Similarly, ROIs are also placed manually (covering 1 cm^2) over the renal tumor and the normal renal cortex of the affected kidney or the contralateral kidney. Tumor ROI is placed in solid enhancing area avoiding necrosis, calcification, hemorrhage and cysts.

A tissue time attenuation curve is generated using in-built software. Perfusion parameters (BV, BF, MTT, PMB, MIP) are also calculated. The perfusion parameters are obtained and their definitions have been enumerated in Table 2.

Histogram analysis in pCT

Differentiation between the different tumor types on the basis of qualitative interpretation of contrast enhancement patterns may be possible but quantitative methods of measuring enhancement provides a higher degree of accuracy[6]. Quantitative method is associated with less subjective variability. ROI-based method of assessing enhancement has demonstrated high accuracy in differentiating clear cell RCC (ccRCC) from papillary RCC (pRCC)[6]. Limitations of ROI-based methods include invariability in ROI placement amongst different observers, difficulty in selecting the exact location of ROI and technical problems such as misregistration between pre- and post-contrast acquisitions[6].

Therefore, to overcome the limitations of ROI placement, a tool that can perform automatic registration, lesion segmentation, and whole-lesion (WL) enhancement analysis is needed. Furthermore, histogram distribution has been used to discriminate ccRCC from pRCC using analysis of the WL enhancement pattern[6]. Whole lesion parameter of third quartile enhancement has been found to have the highest accuracy (area under curve 0.98), with sensitivity of 96% and specificity of 90%[6]. Special software is used to obtain a histogram of the voxel-based enhancement values and computation of the mean, median, and third quartile enhancement of the sorted values done. Histogram distribution parameters like kurtosis and skewness off-line are subsequently obtained from the values computed[6].

pCT parameters in normal kidneys

Chen *et al*[7] have reported CT perfusion values for normal renal cortex; the average BF was reported to be 454.32 mL/100 mL per minute (Figure 1). Difference between BF, BV, MTT, and PMB of normal renal cortex and RCC are shown in Table 3. Perfusion parameters in two representative cases are shown in Table 4.

pCT in renal tumours

Predicting the histologic grade: Pre-operative tumor histotyping using perfusion parameters can be used to prognosticate patients and is important in patients with small renal tumors. Chen *et al*[7] found that mean values of BF, BV were significantly higher and mean MTT was significantly lower in ccRCC than in pRCC ($P < 0.05$ (Figures 1 and 2).

Similarly Gigli *et al*[1] have shown a correlation between tumor histological subtype and perfusion index. Significant differences in perfusion values were found in ccRCC of different Fuhrman grades. High perfusion index corresponded with high microvessel density (MVD) while those with lower MVD showed lower perfusion indices.

Previous studies have shown that there was a significant difference in PS and MTT values of malignant lesions (ccRCCs, pRCCs, and chromophobe RCCs) and the normal renal cortex ($P < 0.001$ and $P = 0.029$, respectively) but BF and BV values did not differ

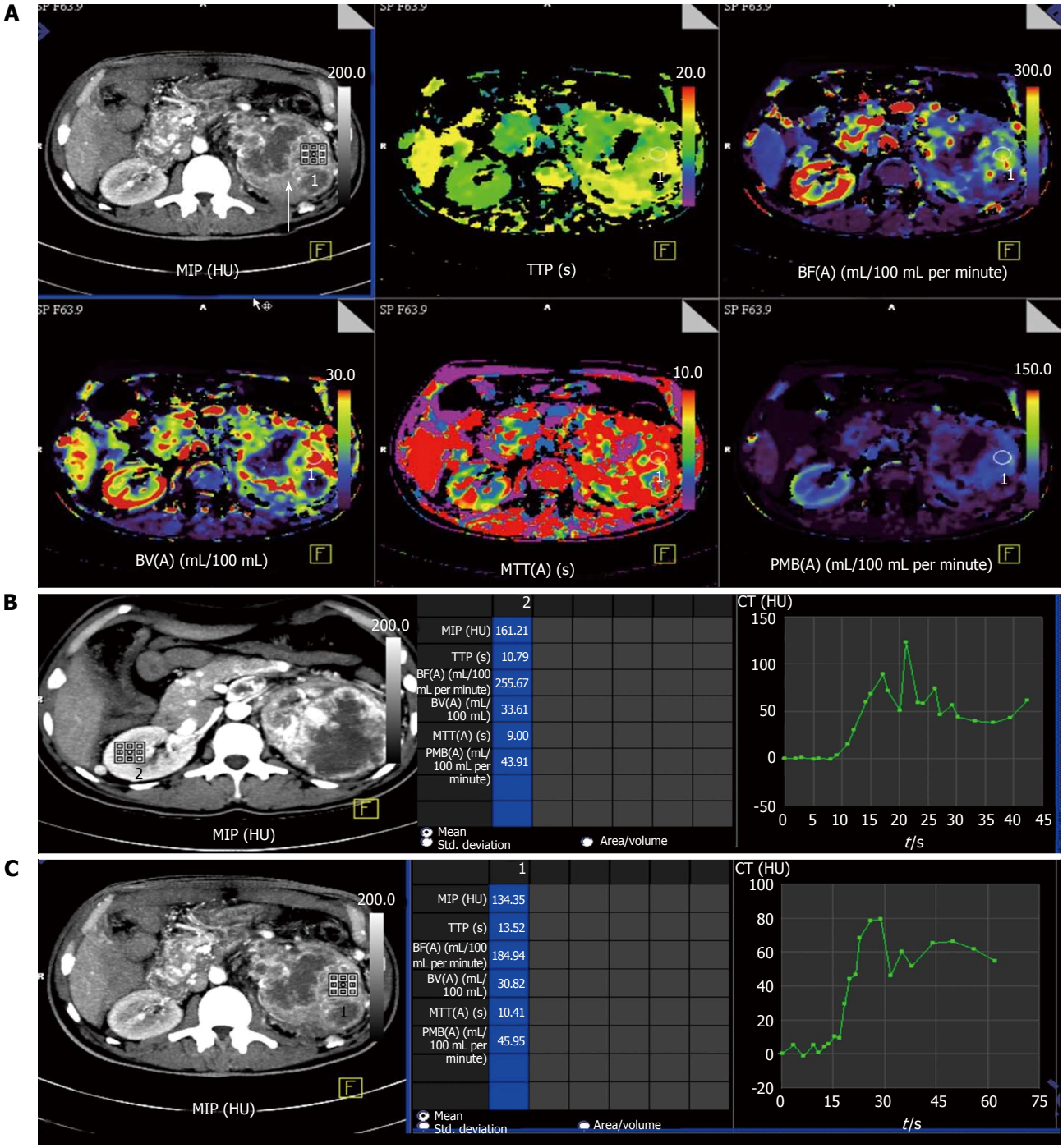

Figure 1 Perfusion computed tomography in normal renal parenchyma *vs* renal cell carcinoma in a 50-year-old man with left renal cell carcinoma (clear cell type). A: Contrast computed tomography (CT) images showed a large, hyperenhancing mass in left kidney with central necrosis (arrow). Colour-coded perfusion maps show various perfusion parameters in normal right kidney and diseased left kidney. Red being the region with highest perfusion parameter with purple being the least; B: Time attenuation curve and the perfusion parameters in normal right kidney. Normal renal parenchyma is seen to have high perfusion in the range of 255 mL/100 mL per minute; C: Time attenuation curve and perfusion parameters in the left renal cell carcinoma. There is delayed wash-out of contrast in the region of the tumour as depicted in the graph. MIP: Maximum peak intensity; TTP: Time to peak; BF: Blood flow; BV: Blood volume; MTT: Mean transit time; PMB: Permeanbility.

significantly[8,9]. Also the permeability surface area product, MTT, and BF values were reported to be significantly lower in malignant lesions as compared with oncocytomas[8].

BF and BV are two perfusion parameters which have been found to have significant histological correlation ($P < 0.01$) with MVD as a prognostic marker for RCCs and the neoangiogenesis associated with RCCs[8]. The difference in normal cortex and tumoral PS values has been found to best predict RCCs with a cutoff greater than 2.5 mL/100 g per minute having sensitivity, specificity, and accuracy of 100%, 66.67%, and 95.92%[5]. Hence, evaluation of the different perfusion parameters can depict histologic grade of RCCs.

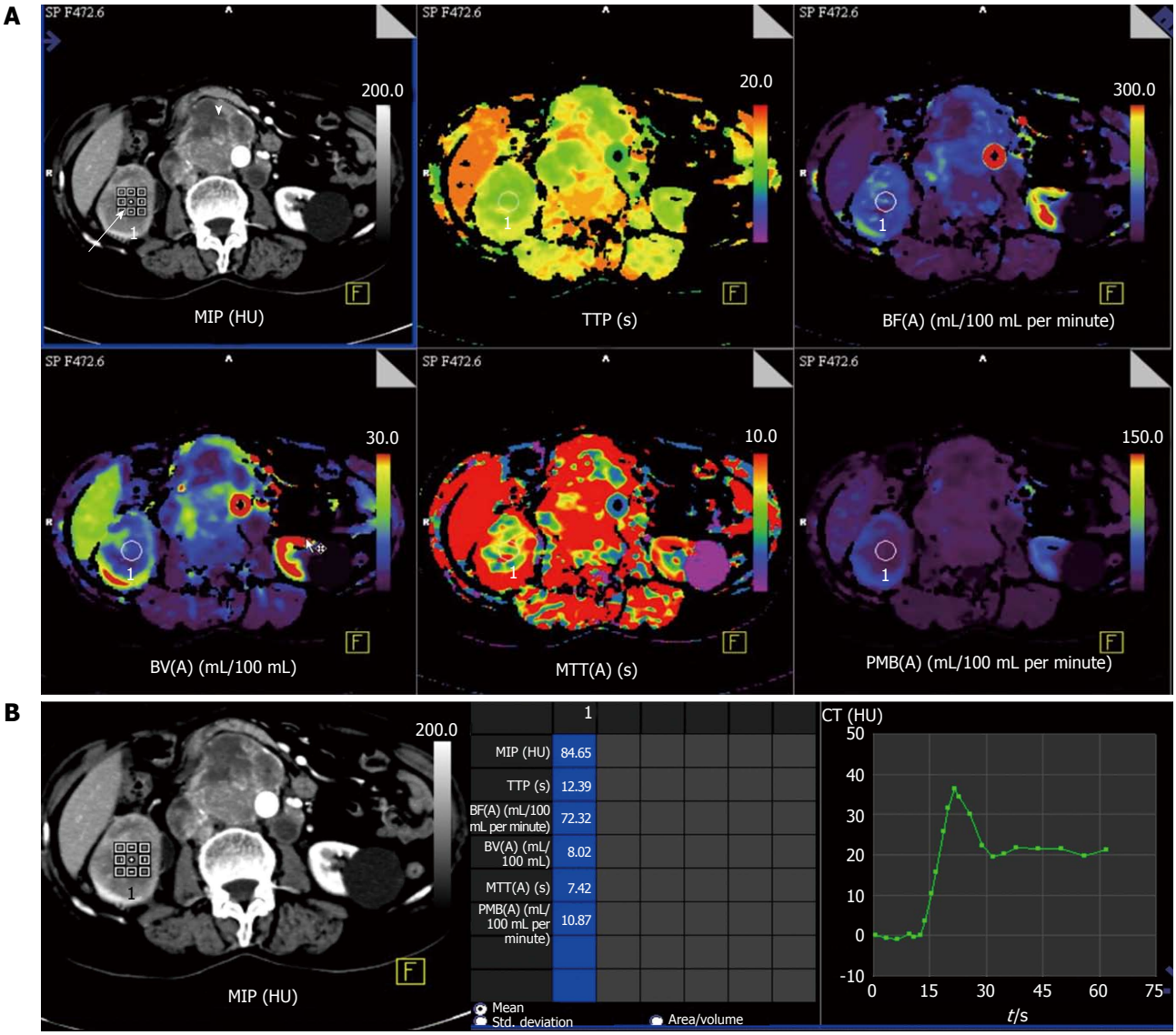

Figure 2 Perfusion computed tomography in a 63-year-old lady with right renal cell carcinoma (chromophobe type). A: Contrast computed tomography (CT) images show tumor in right kidney (white arrow) with retroperitoneal nodal metastases (arrowhead). Colour-coded perfusion maps show the perfusion parameters; B: Time attenuation curve and perfusion parameters with region-of-interest in the right renal cell carcinoma depict delayed wash-out of contrast. MIP: Maximum peak intensity; TTP: Time to peak; BF: Blood flow; BV: Blood volume; MTT: Mean transit time; PMB: Permeanbility.

Table 4 Response evaluation using changes in computed tomography perfusion parameters in two representative cases

	Date of study		MIP (HU)	TTP (s)	BF (mL/100 mL per minute)	BV (mL/100 mL)	MTT (s)	PMB (mL/100 mL per minute)
Case 1	2013-4-2	Normal cortex	120	11.1	202.9	31.6	8.7	47.1
		Renal tumour	134	13.5	184.9	30.8	10.4	45.95
	2013-9-11	Normal cortex	121	13.2	209	30.2	9.2	50.2
		Renal tumour	79	11.5	174	13.2	5	18.1
	2013-11-20	Normal cortex	130	10.8	229	32	9.6	45.3
		Renal tumour	42	12.3	5.7	1.2	12.4	8.2
Case 2	2013-10-23	Normal cortex	157	11.9	236	27.8	8.9	43.7
		Renal tumour	88	12.3	64.4	9.3	8.9	18.7
	2013-12-26	Normal cortex	140	15.2	170.9	29.5	10.5	42.1
		Renal tumour	82.7	14.8	60.9	7.9	8.4	13.8
	2013-8-3	Normal cortex	216	12.5	315	38	72	55.2
		Renal tumour	84.6	12.3	72.3	8	7.4	10.8

BF: Blood flow; BV: Blood volume; MTT: Mean transit time; PMB: Permeability; MIP: Maximum peak intensity; TTP: Time to peak.

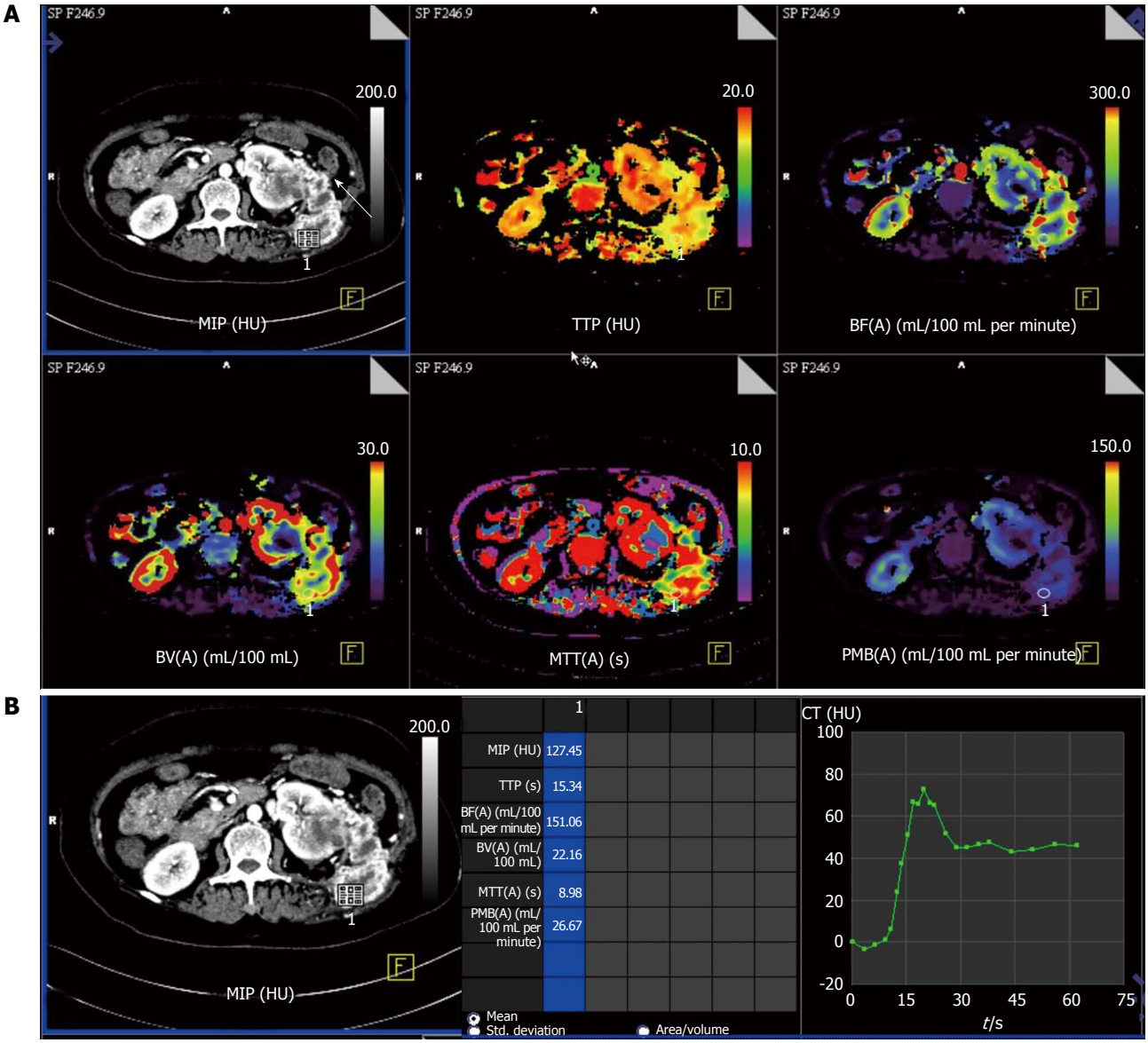

Figure 3 Perfusion computed tomography in a 55-year-old lady with metastatic left renal cell carcinoma. A: Contrast computed tomography (CT) images show heterogeneous necrotic mass in left kidney with abdominal wall metastatic deposit in left lumbar region (arrow) and colour-coded perfusion maps show the perfusion parameters; B: Time attenuation curve and perfusion parameters with region-of-interest placed in the metastatic left lumbar lesion depict delayed wash-out of contrast from the tumour deposit. MIP: Maximum peak intensity; TTP: Time to peak; BF: Blood flow; BV: Blood volume; MTT: Mean transit time; PMB: Permeanbility.

Response evaluation with anti-angiogenic therapy: Predicting response assessment with anti-angiogenic therapy can be done with pCT (*e.g.,* colorectal)[10]. It is known that growth of primary tumor as well as seeding of distant metastasis in patients with renal tumors requires angiogenesis. By inhibiting angiogenesis, it is possible to target both the primary tumor as well as metastases.

The role of several antiangiogenic therapies in RCC are currently being evaluated in clinical trials[11-14]. However, these anti-angiogenic therapies are predominantly cytostatic in action rather than cytotoxic and induce disease stabilization rather than tumor regression (Figures 3-5). Thereby, traditional response assessment based on size criteria by using the Response Evaluation Criteria in Solid Tumors (RECIST) is rendered inadequate for follow-up and prognostication of patients on anti-angiogenic therapy. In such instances, functional evaluation with pCT can play a major role. There are few studies highlighting the role of pCT for assessing effect of antiangiogenesis[15-17].

Significant differences in pCT parameters have been described between treated tumors and control tumors in a rat model by Kan *et al*[16]. There was significant difference in these parameters after interventional therapy as compared with the pre-therapy in an investigation in a rabbit model[17].

Maksimovic *et al*[18] in their study using tyrosine kinase inhibitor sorafenib found that perfusion parameters changes appear much earlier before changes in size during therapy. Also early disease progression identification seen as new areas of tumour perfusion

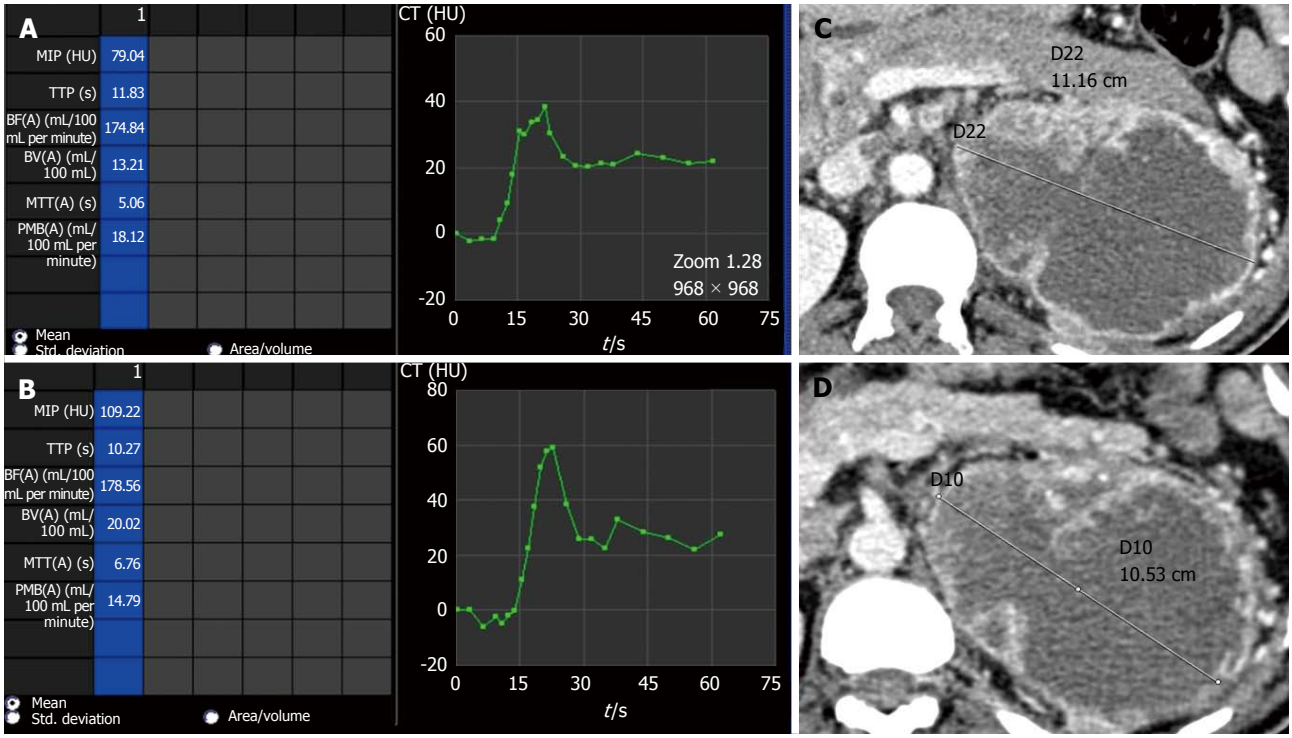

Figure 4 Perfusion parameters *vs* size evaluation in depicting partial response. Comparison of perfusion parameters in a case of left side clear cell renal cell carcinoma after start of anti-angiogenic therapy. Follow-up scan at 6 mo interval (B) showed at 6 mo interval shows decrease in permeability as compared to baseline scan (A) suggestive of partial response. However, no change in size of lesion noted between baseline (C) and follow-up (D) scans which would have been labelled as stable disease. MIP: Maximum peak intensity; TTP: Time to peak; BF: Blood flow; BV: Blood volume; MTT: Mean transit time; PMB: Permeanbility; CT: Computed tomography.

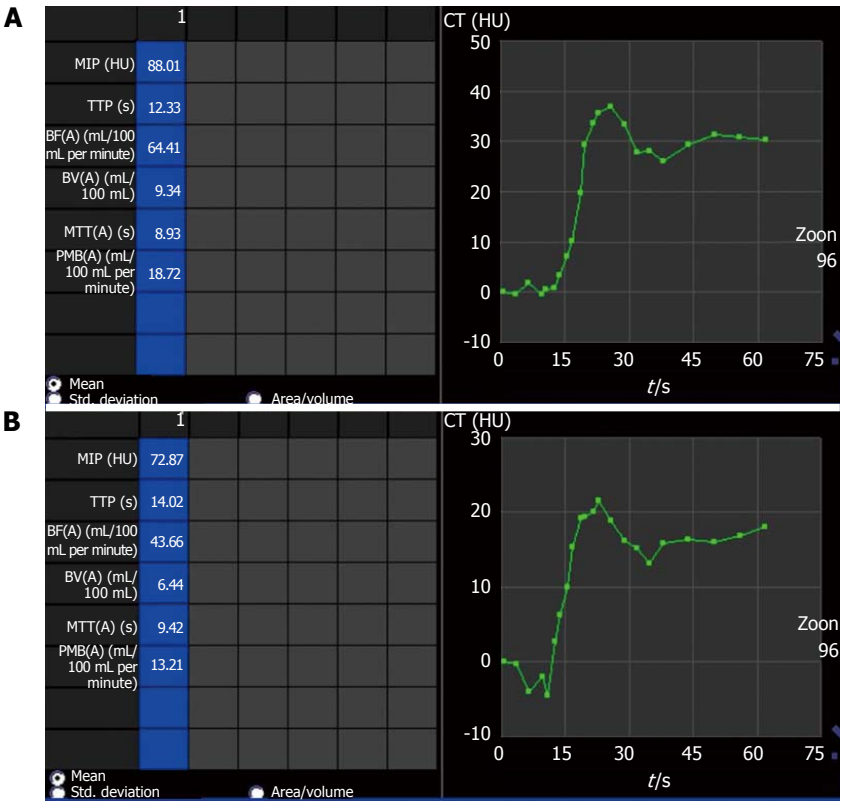

Figure 5 Perfusion parameters showing partial response with anti-angiogenic therapy. Comparison of perfusion parameters in right side chromophobe renal cell carcinoma (same patient as shown in Figure 2) after start of anti-angiogenic therapy shows partial response as permeability (PMB) in follow-up scan (B) at 6 mo interval decreased compared to baseline scan (A). The PMB measured 18.72 mL/100 mL per minute at baseline (A) while in follow-up scan (B), PMB was 13.2 mL/100 mL per minute. There was no interval change in lesion size and would have been labeled as stable disease in absence of perfusion parameters. MIP: Maximum peak intensity; TTP: Time to peak; BF: Blood flow; BV: Blood volume; MTT: Mean transit time; CT: Computed tomography.

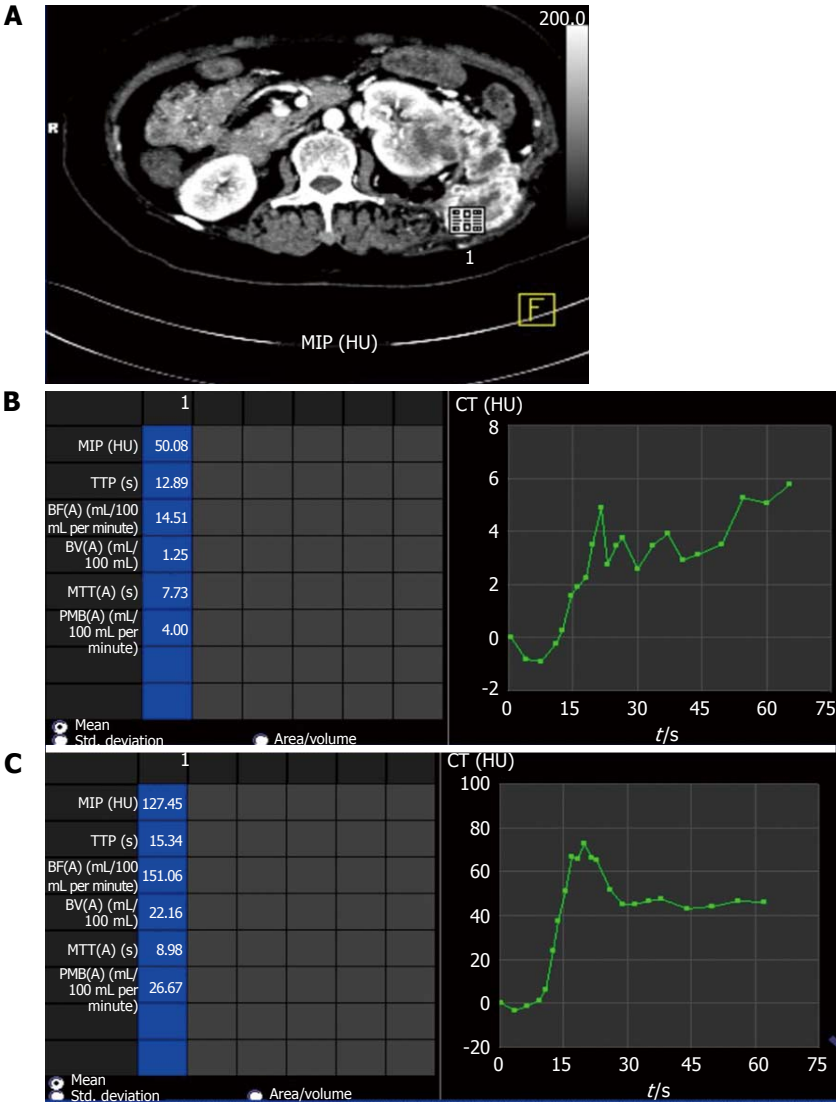

Figure 6 Perfusion parameters showing progressive disease with anti-angiogenic therapy. Comparison of perfusion parameters in left metastatic renal cell carcinoma (A) after start of anti-angiogenic therapy at 6 mo interval shows progressive disease as permeability (PMB) at baseline scan (B) was 4.00 mL/10 mL per minute which increased to 26.67 mL/100 mL per minute in follow-up scan (C). There was also increase in size and extent of lesions during this interval (not shown). MIP: Maximum peak intensity; TTP: Time to peak; BF: Blood flow; BV: Blood volume; MTT: Mean transit time; CT: Computed tomography.

would enable clinicians to change therapy. A targeted biopsy and therapy by identification of the specific area at an early stage can be performed[19].

Perfusion parameters can also be utilized to prognosticate response to therapy. Patients responding to antiangiogenic therapy had higher baseline values of BF and BV than in those patients whose perfusion parameters remained stable throughout follow-up[20].

Significant decrease in BF, BV and PMB can be seen in those patients responding to antiangiogenic therapy (case 1 in Table 4) (Figures 3 and 4) while those showing progression showed increase in these perfusion parameters over serial follow-up (case 2 in Table 4) (Figure 5).

Evaluation of metastases: Metastases are commonly seen in RCCs. Most are hematogenous and are highly vascular. Amongst the different histologic subtypes, ccRCCs have the highest risk of developing metastatic disease and is seen in more than 90% of cases[21]. Since maximum anatomic coverage during pCT is limited, hence evaluation of distant metastasis is challenging considering the increasing radiation burden with increase in the region covered. However, evaluation of RCC metastases is made possible in most cases because of the characteristic distribution of these metastases in lung bases, liver, adrenal glands, pancreas, retroperitoneal lymph nodes (Figure 2) and lumbar fossa (Figure 6)[22]. The renal metastases show similar contrast enhancement as the parent tumor and may be evaluated for treatment response by using pCT.

Pitfalls of pCT

As true for any imaging technique, pCT also has certain technical limitations. These include high radiation burden as shown in Table 5 because of the repetitive scans

Table 5 Comparison of the acquisition parameters and dose in dynamic acquisition of perfusion computed tomography and normal contrast enhanced computed tomography chest and abdomen in our institute

	Dynamic acquisition	Chest and abdomen scan (routine)
Exposure time (s)	33	14.24
Scan length (mm)	155	655
Collimation (mm)	1.2	0.6
KVp	100	100
Ma	523	211
CTDI vol (mGy)	180.1	7.2
DLP (mGycm)	2789.69	458.68

CTDI vol: Computed tomography dose index volumetric; DLP: Dose length product.

acquired over a period of time and limited anatomic coverage. As the scan has to be repeated within a short span of time, the actual anatomic length that can be covered is limited (maximum up to about 20 cm). This imposes a limitation on the evaluation of distant metastases which may be present in such patients.

CONCLUSION

pCT is an evolving imaging modality which provides deeper insights into the molecular behavior of tumor angiogenesis and thereby facilitating targeted therapy. It has revolutionized oncologic imaging by prognosticating and evaluating therapy response at an earlier stage. Other potential benefits include identifying tumor histological subtype and predicting potentially aggressive tumors which can help clinicians to better plan the therapy of patients. As an emerging technique, pCT is currently used in evaluation of malignancies of different body parts such as kidneys, brain, lung, liver, pancreas and colon. In the future, pCT is likely to become the *in vivo* biomarker for tumor behavior and response evaluation in malignant lesions of different body parts.

REFERENCES

1 **Gigli F**, Zattoni F, Zamboni G, Valotto C, Bernardin L, Mucelli RP, Zattoni F. [Correlation between pathologic features and perfusion CT of renal cancer: a feasibility study]. *Urologia* 2010; **77**: 223-231 [PMID: 21234864]

2 **Miles KA**. Tumour angiogenesis and its relation to contrast enhancement on computed tomography: a review. *Eur J Radiol* 1999; **30**: 198-205 [PMID: 10452718 DOI: 10.1016/S0720-048X(99)00012-1]

3 **Miles KA**, Griffiths MR. Perfusion CT: a worthwhile enhancement? *Br J Radiol* 2003; **76**: 220-231 [PMID: 12711641 DOI: 10.1259/bjr/13564625]

4 **Miles KA**. Functional CT imaging in oncology. *Eur Radiol* 2003; **13** Suppl 5: M134-M138 [PMID: 14989624 DOI: 10.1016/S0959-8049(02)00386-6]

5 **Mazzei FG**, Mazzei MA, Cioffi Squitieri N, Pozzessere C, Righi L, Cirigliano A, Guerrini S, D'Elia D, Ambrosio MR, Barone A, del Vecchio MT, Volterrani L. CT perfusion in the characterisation of renal lesions: an added value to multiphasic CT. *Biomed Res Int* 2014; **2014**: 135013 [PMID: 25184133 DOI: 10.1155/2014/135013]

6 **Chandarana H**, Rosenkrantz AB, Mussi TC, Kim S, Ahmad AA, Raj SD, McMenamy J, Melamed J, Babb JS, Kiefer B, Kiraly AP. Histogram analysis of whole-lesion enhancement in differentiating clear cell from papillary subtype of renal cell cancer. *Radiology* 2012; **265**: 790-798 [PMID: 23175544 DOI: 10.1148/radiol.12111281]

7 **Chen Y**, Zhang J, Dai J, Feng X, Lu H, Zhou C. Angiogenesis of renal cell carcinoma: perfusion CT findings. *Abdom Imaging* 2010; **35**: 622-628 [PMID: 19763683 DOI: 10.1007/s00261-009-9565-0]

8 **Chen C**, Liu Q, Hao Q, Xu B, Ma C, Zhang H, Shen Q, Lu J. Study of 320-slice dynamic volume CT perfusion in different pathologic types of kidney tumor: preliminary results. *PLoS One* 2014; **9**: e85522 [PMID: 24465588 DOI: 10.1371/journal.pone.0085522]

9 **Reiner CS**, Roessle M, Thiesler T, Eberli D, Klotz E, Frauenfelder T, Sulser T, Moch H, Alkadhi H. Computed tomography perfusion imaging of renal cell carcinoma: systematic comparison with histopathological angiogenic and prognostic markers. *Invest Radiol* 2013; **48**: 183-191 [PMID: 23328912 DOI: 10.1097/RLI.0b013e31827c63a3]

10 **Sahani DV**, Kalva SP, Hamberg LM, Hahn PF, Willett CG, Saini S, Mueller PR, Lee TY. Assessing tumor perfusion and treatment response in rectal cancer with multisection CT: initial observations. *Radiology* 2005; **234**: 785-792 [PMID: 15734934 DOI: 10.1148/radiol.2343040286]

11 **Dhanabal M**, Ramchandran R, Volk R, Stillman IE, Lombardo M, Iruela-Arispe ML, Simons M, Sukhatme VP. Endostatin: yeast production, mutants, and antitumor effect in renal cell carcinoma. *Cancer Res* 1999; **59**: 189-197 [PMID: 9892206]

12 **Morita T**, Shinohara N, Tokue A. Antitumour effect of a synthetic analogue of fumagillin on murine renal carcinoma. *Br J Urol* 1994; **74**: 416-421 [PMID: 7529632 DOI: 10.1111/j.1464-410X.1994.tb00415.x]

13 **Fujioka T**, Hasegawa M, Ogiu K, Matsushita Y, Sato M, Kubo T. Antitumor effects of angiogenesis inhibitor 0-(chloroacetylcarbamoyl) fumagillol (TNP-470) against murine renal cell carcinoma. *J Urol* 1996; **155**: 1775-1778 [PMID: 8627882 DOI: 10.1016/S0022-5347(01)66196-2]

14 **Stadler WM**, Kuzel T, Shapiro C, Sosman J, Clark J, Vogelzang NJ. Multi-institutional study of the angiogenesis inhibitor TNP-470 in metastatic renal carcinoma. *J Clin Oncol* 1999; **17**: 2541-2545 [PMID: 10561320]

15 **Koukourakis MI**, Mavanis I, Kouklakis G, Pitiakoudis M, Minopoulos G, Manolas C, Simopoulos C. Early antivascular effects of bevacizumab anti-VEGF monoclonal antibody on colorectal carcinomas assessed with functional CT imaging. *Am J Clin Oncol* 2007; **30**: 315-318 [PMID: 17551312 DOI: 10.1097/01.coc.0000258119.90805.ca]

16 **Kan Z**, Phongkitkarun S, Kobayashi S, Tang Y, Ellis LM, Lee TY, Charnsangavej C. Functional CT for quantifying tumor perfusion in antiangiogenic therapy in a rat model. *Radiology* 2005; **237**: 151-158 [PMID: 16183931 DOI: 10.1148/radiol.2363041293]

17 **Zhang J**, Wang R, Lou H, Zou Y, Zhang M. Functional computed tomographic quantification of angiogenesis in rabbit VX2 soft-tissue tumor before and after interventional therapy. *J Comput Assist Tomogr* 2008; **32**: 697-705 [PMID: 18830097 DOI: 10.1097/RCT.0b013e31815b7dcf]

18 **Maksimovic O**, Schraml C, Hartmann JT, Bitzer M, Claussen CD, Pintoffl J, Horger M. Evaluation of response in malignant tumors treated with the multitargeted tyrosine kinase inhibitor sorafenib: a multitechnique imaging assessment. *AJR Am J Roentgenol* 2010; **194**: 5-14 [PMID: 20028898 DOI: 10.2214/AJR.09.2744]

19 **Sabir A**, Schor-Bardach R, Wilcox CJ, Rahmanuddin S, Atkins MB, Kruskal JB, Signoretti S, Raptopoulos VD, Goldberg SN. Perfusion MDCT enables early detection of therapeutic response to antiangiogenic therapy. *AJR Am J Roentgenol* 2008; **191**: 133-139 [PMID: 18562736 DOI: 10.2214/AJR.07.2848]

20 **Fournier LS**, Oudard S, Thiam R, Trinquart L, Banu E, Medioni J, Balvay D, Chatellier G, Frija G, Cuenod CA. Metastatic renal

carcinoma: evaluation of antiangiogenic therapy with dynamic contrast-enhanced CT. *Radiology* 2010; **256**: 511-518 [PMID: 20551183 DOI: 10.1148/radiol.10091362]

21 **Motzer RJ**, Bacik J, Mariani T, Russo P, Mazumdar M, Reuter V. Treatment outcome and survival associated with metastatic renal cell carcinoma of non-clear-cell histology. *J Clin Oncol* 2002; **20**: 2376-2381 [PMID: 11981011 DOI: 10.1200/JCO.2002.11.123]

22 **Bianchi M**, Sun M, Jeldres C, Shariat SF, Trinh QD, Briganti A, Tian Z, Schmitges J, Graefen M, Perrotte P, Menon M, Montorsi F, Karakiewicz PI. Distribution of metastatic sites in renal cell carcinoma: a population-based analysis. *Ann Oncol* 2012; **23**: 973-980 [PMID: 21890909 DOI: 10.1093/annonc/mdr362]

P- Reviewer: Cerwenka HR, Chen F, Nouh MR
S- Editor: Tian YL **L- Editor**: A **E- Editor**: Liu SQ

World Journal of Radiology

Submit a Manuscript: http://www.wjgnet.com/esps/
Help Desk: http://www.wjgnet.com/esps/helpdesk.aspx
DOI: 10.4329/wjr.v7.i7.180

World J Radiol 2015 July 28; 7(7): 180-183
ISSN 1949-8470 (online)

CASE REPORT

Isolated renal hydatid presenting as a complex renal lesion followed by spontaneous hydatiduria

Anil Bhaya, Archana P Shinde

Anil Bhaya, Department of Radio Diagnosis, Apple Hospitals and Research Institute Ltd., Kolhapur 416001, India

Archana P Shinde, Department of Pathology, Apple Hospitals and Research Institute Ltd., Kolhapur 416001, India

Author contributions: Bhaya A contributed to concept, design, preparation of manuscript, literature search and final review; Shinde AP contributed to patient diagnosis, provided diagnostic inputs.

Institutional review board statement: As this was an outpatient and study observational case report on only one patient hence IRB approval was not obtained.

Informed consent statement: All involved subjects have provided their written/verbal consent for performance of all diagnostic studies and inclusion in this case report. The subject has been made aware that all identifying data has been removed and kept confidential.

Conflict-of-interest statement: The authors declare no financial, professional or personal conflict of interest.

Correspondence to: Dr. Anil Bhaya, MD, DNB, CCST, Senior Consultant and HOD Advanced Imaging, Department of Radio Diagnosis, Apple Hospitals and Research Institute Ltd., 525/E, Vyapari Peth, Shahupuri, Kolhapur 416001, Maharashtra, India. anilbhaya@hotmail.com
Telephone: +91-231-2651207
Fax: +91-231-2654850

Received: February 26, 2015
Peer-review started: February 27, 2015
First decision: March 20, 2015
Revised: April 14, 2015
Accepted: May 7, 2015
Article in press: May 8, 2015
Published online: July 28, 2015

Abstract

Echinococcosis is a zoonotic disease. Liver is the most common site of involvement. Renal involvement is seen in 2% to 3% of patients. Computed tomography findings in renal hydatid typically include: a cyst with thick or calcified wall, unilocular cyst with detached membrane, a multiloculated cyst with mixed internal density and daughter cysts with lower density than maternal matrix. Rarely type Ⅳ hydatid cysts may mimic hypovascular renal cell carcinoma. We report a case of previously asymptomatic middle aged female who presented with mild intermittent pain and a complex renal lesion on imaging which was considered to be a hypovascular renal carcinoma or urothelial neoplasm. However, by serendipity, the patient had spontaneous hydatiduria and later was definitively diagnosed and stented. Hydatid disease should always be considered amongst the top differential diagnosis of an isolated "complex" renal lesion which remains indeterminate on imaging.

Key words: Hydatidoses; Echinococcosis; Hydatiduria; Kidney diseases; Cystic; Hydatid; Renal

Core tip: Renal hydatid is generally secondary to disseminated hydatidoses or associated with hepatic involvement. Isolated renal involvement is far less common and reported in less than 5% of all hydatid cases. Without appropriate history a subset of renal hydatid, especially type 4 cyst may simulate cystic renal/urothelial neoplasm or other complex cystic lesions

such as abscess. Radiologists must harbour a high index of suspicion and look for subtle imaging signs such as calcification and non enhancing "solid" component to include this diagnosis in the differential of complex renal lesion. Absence of relevant history or hepatic involvement should not prevent diagnosticians from entertaining this rare diagnosis.

Bhaya A, Shinde AP. Isolated renal hydatid presenting as a complex renal lesion followed by spontaneous hydatiduria. *World J Radiol* 2015; 7(7): 180-183 Available from: URL: http://www.wjgnet.com/1949-8470/full/v7/i7/180.htm DOI: http://dx.doi.org/10.4329/wjr.v7.i7.180

INTRODUCTION

Hydatid disease is mainly caused by Echinococcus granulosus[1]. It often manifests as a slow growing cystic lesion. We report a case of renal hydatid disease suspicious for complex cyst/urothelial neoplasm on computed tomography (CT) scan. The patient was extensively investigated and later presented with spontaneous hydatiduria.

CASE REPORT

A 42-year-old female patient, resident of central India presented with mild right lumbar pain over one month. There was no dysuria, vomiting or fever. Routine laboratory investigations were within normal range except for urinary pus cells (10-12/hpf). Ultrasonography (USG) revealed a complex hetero-echoic lesion in the right kidney (Figure 1).

CT scan revealed a poorly demarcated lobulated, isodense lesion on plain images becoming better delineated on contrast study and measuring 2.2 (craniocaudal) cm × 2.8 (anteroposterior) cm × 3.5 (transverse) cm within interpolar region. The lesion exhibited few small irregular calcific foci and mild contrast enhancement. In addition, a hypo-attenuating, non-enhancing cystic area was noted adjacent to the lesion (Figure 2).

The right kidney revealed delayed contrast excretion. The previously noted cystic component did not opacify on the delayed scan. The left kidney was normal. The ureters and bladder were normal (Figure 3).

This was provisionally diagnosed as renal abscess possibly tubercular. The differential diagnosis of urothelial neoplasm was communicated to the referring general physician and urological consultation was strongly recommended.

A few days later she reported passage of fleshy/mucoid matter per urethra which she collected in a container. These were submitted for histopathological analysis. In view of high index of suspicion of a neoplastic lesion, the patient underwent ureteroscopy following which a double J stent was placed. Urine did not reveal any malignant cells. The patient improved clinically and was discharged on a course of antibiotics.

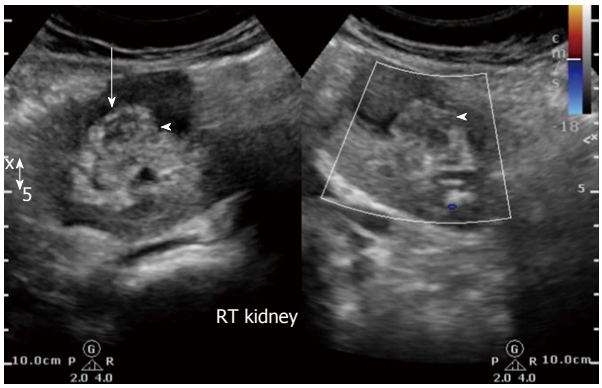

Figure 1 Initial ultrasound image reveals heteroechoic indeterminate renal sinus/renal pelvic lesion (white arrow). Doppler revealed negligible vascularity.

Histopathology

Gross examination: Multiple flat membranous pieces, the largest measuring 2 cm × 1 cm × 0.3 cm. These were greyish white, translucent and soft with smooth surfaces (Figure 4).

Microscopic examination: Lamellated layer with focal calcification and occasional brood capsules consistent with hydatid cyst (Figure 5).

Follow up

Serological test for Echinococcus antibody was done and reported as positive. The patient remained asymptomatic. Follow up USG a month later revealed resolution of the lesion. The right kidney appeared normal without hydronephrosis (Figure 6). The left kidney and bladder were normal. No lesions were detected in the liver or spleen. The chest radiograph was unremarkable.

DISCUSSION

Echinococcosis is a zoonotic disease and is endemic in Mediterranean and other sheep rearing countries. However, due to increasing travel and tourism it may be found even in developed countries. In India, annual incidence of Hydatid disease per 100000 persons vary from 1 to 200[1]. The liver is most common site of involvement[2]. Renal involvement is seen in 2% to 3%[2,3].

Gharbi *et al*[4], classified hydatid cysts based upon sonographic morphology into five types (Table 1)[5].

Type 4 hydatid cysts have heterogeneous appearance similar to pseudotumor. CT scan is reportedly a problem solving modality in these cases especially as it is sensitive to calcifications and enhancement of the cyst wall[6].

Imaging spectrum of CT Renal hydatid varies and depends on stage of cyst. Typical CT findings for renal hydatidoses include a cyst with thick or calcified wall, a unilocular cyst with detached membrane, a multiloculated cyst with mixed internal density and daughter cysts with lower density than maternal matrix[4,6].

Despite multimodality imaging, in a subset of

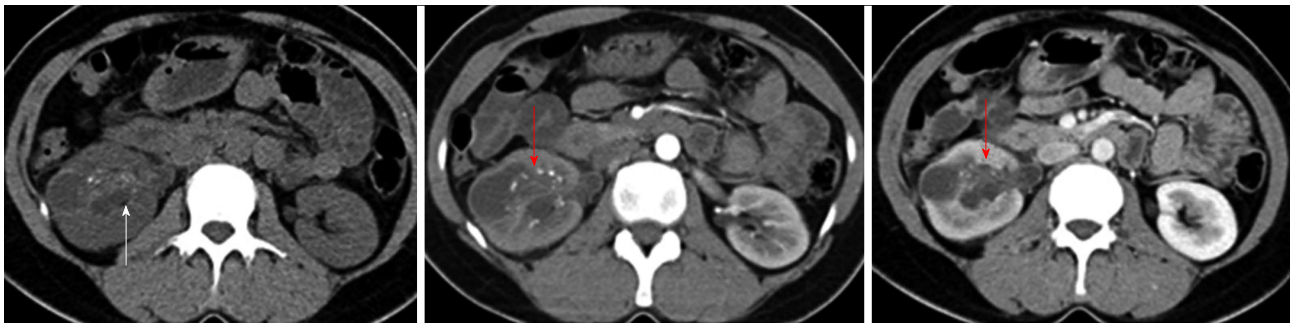

Figure 2 Composite of non contrast axial MDCT-post contrast corticomedullary and post contrast nephrographic phases reveals poorly enhancing isodense lesion within the renal pelvis exhibiting calcific specks (white arrow) and hypo-attenuating lesion along its lateral aspect (red arrows). Subtle thickening of the urothelial walls is present.

Figure 3 Delayed oblique coronal multiplanar reformat MDCT image shows the lesion as a filling defect within the collecting system. The lesion and laterally placed cortical cyst are inseparable. Additionally, persistent nephrogram is noted.

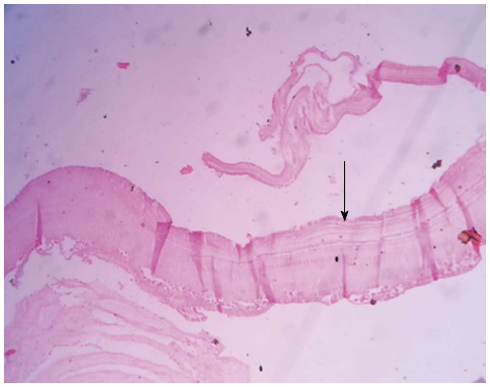

Figure 5 Microscopy (magnification 100 ×) revealed characteristic hydatid lamellated layer (arrow) with occasional brood capsules.

Figure 4 Photograph of the fleshy membranes passed spontaneously by the patient few days after ureteroscopy.

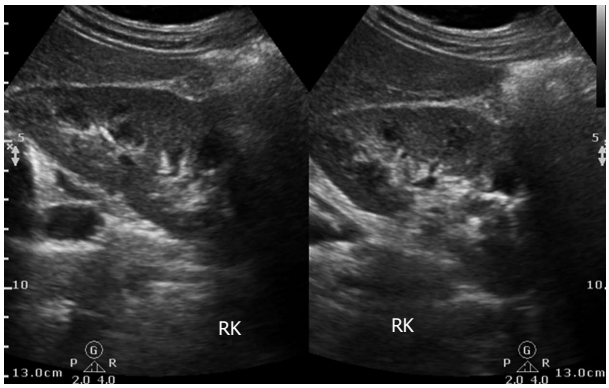

Figure 6 Follow up ultrasound revealed normal right kidney.

patients, no definitive diagnosis can be made and the differential diagnosis often includes infected renal cysts, abscess, pyonephrosis and neoplasms[7,8]. Rarely Type IV hydatid cysts may mimic hypo vascular renal cell carcinoma[9].

On the other hand, in endemic countries, unusual neoplasms such as mucinous cystadenoma/carcinoma may be misdiagnosed as renal hydatid[10].

Hydatiduria accompanies 10%-20% of cases of renal hydatidoses and is basically microscopic. Gross

Table 1 Sonographic appearance of hydatid cysts in Gharbi classification[5]

Type Ⅰ	Well-defined, purely anechoic lesions that may be indistinguishable from simple renal cysts. Multiple echogenic foci due to hydatid sands may be seen in the cyst (22%)
Type Ⅱ	Focal or diffuse detachment of the inner germinal layer results in a floating membrane inside the cyst (4%)
Type Ⅲ	Multiseptated cysts with multiple daughter cysts (54%)
Type Ⅳ	Heterogeneous, solid appearance with infolded membranes, and internal echoes (12%)
Type Ⅴ	Solid appearance, calcifications in the cyst wall, and germinative membranes (8%)

passage of hydatid cysts in urine though near diagnostic is rather uncommon and infrequently reported. We came across only two reports of gross hydatiduria in the Indian scenario - one with extensive liver and renal hydatid while the other revealed cystic renal lesion following investigation for hydatiduria. Both did not report any dilemma on imaging unlike our case[11,12].

Histologically, Hydatid cyst comprises of pericyst or fibrous layer, middle lamellated membrane and inner germinal layer which produces scolices. In patients with ruptured cysts and hydatiduria the membranes do not reveal pericyst[12].

Isolated renal hydatid involvement presents a further diagnostic challenge (as occurred in our patient). In our opinion, hydatid cyst should always be considered in the differential diagnosis of isolated complex cystic renal lesion. Absence of relevant history or hepatic involvement should not prevent diagnosticians from entertaining this rare diagnosis.

Renal hydatid may present with unusual imaging characteristics, resembling complex cyst or hypovascular solid-cystic neoplasm. This is particularly relevant in non-endemic countries wherein the Radiologists may not be aware of these unusual imaging features resulting in delayed and/or misdiagnosis.

COMMENTS

Case characteristics

Middle aged lady with non colicky right lumbar pain.

Clinical diagnosis

Neither tenderness nor any mass felt.

Differential diagnosis

Chronic renal infection, renal stone disease or occult neoplasm.

Laboratory diagnosis

Urine analysis revealed mild pyuria suggestive of urinary tract infection.

Imaging diagnosis

Ultrasound and computed tomography scan suspicious for urothelial cystic neoplasm.

Pathological diagnosis

Histopathology and microscopy suggestive of ruptured hydatid cyst.

Treatment

Albendazole 15 mg/kg per day for 28 d followed by 2 wk interval and repeated total three cycles.

Related reports

Enzyme-linked immunosorbent assay ELISA for detection of anti-Echinococcus antibodies (immunoglobulin G) was positive.

Peer-review

This is an interesting case.

REFERENCES

1 **Eckert J**, Deplazes P. Biological, epidemiological, and clinical aspects of echinococcosis, a zoonosis of increasing concern. *Clin Microbiol Rev* 2004; **17**: 107-135 [PMID: 14726458 DOI: 10.1128/CMR.17.1.107-135.2004]

2 **Silber SJ**, Moyad RA. Renal echinococcus. *J Urol* 1972; **108**: 669-672 [PMID: 5081694]

3 **Buckley RJ**, Smith S, Herschorn S, Comisarow RH, Barkin M. Echinococcal disease of the kidney presenting as a renal filling defect. *J Urol* 1985; **133**: 660-661 [PMID: 3981719]

4 **Gharbi HA**, Hassine W, Brauner MW, Dupuch K. Ultrasound examination of the hydatic liver. *Radiology* 1981; **139**: 459-463 [PMID: 7220891 DOI: 10.1148/radiology]

5 **Zmerli S**, Ayed M, Horchani A, Chami I, El Ouakdi M, Ben Slama MR. Hydatid cyst of the kidney: diagnosis and treatment. *World J Surg* 2001; **25**: 68-74 [PMID: 11213158]

6 **Pedrosa I**, Saíz A, Arrazola J, Ferreirós J, Pedrosa CS. Hydatid disease: radiologic and pathologic features and complications. *Radiographics* 2000; **20**: 795-817 [PMID: 10835129 DOI: 10.1148/radiographics.20.3.g00ma06795]

7 **Turgut AT**, Altin L, Topçu S, Kiliçoğlu B, Aliinok T, Kaptanoğlu E, Karademir A, Koşar U. Unusual imaging characteristics of complicated hydatid disease. *Eur J Radiol* 2007; **63**: 84-93 [PMID: 17275238 DOI: 10.1016/j.ejrad.2007.01.001]

8 **Horchani A**, Nouira Y, Kbaier I, Attyaoui F, Zribi AS. Hydatid cyst of the kidney. A report of 147 controlled cases. *Eur Urol* 2000; **38**: 461-467 [PMID: 11025387]

9 **Nouira K**, Nouira Y, Belhiba H, Mekni A, Menif E, Horchani A. A misleading renal tumour. *Tunis Med* 2007; **85**: 535-536 [PMID: 17644913]

10 **Sonmez FC**, Esen HH, Tavlı L, Kılınç M. Well-Differentiated Mucinous cystadenocarcinoma of the renal pelvis. *Eur J Gen Med* 2014; Suppl 1: 63-65 [DOI: 10.15197/sabad.1.11.36]

11 **Saxena S**, Gupta R, Nigam DK, Tahiliani ND, Saxena KN. Hydatid cyst of kidney presenting as hydatiduria. *J Assoc Physicians India* 1990; **38**: 359-356 [PMID: 2201677]

12 **Mongha R**, Narayan S, Kundu AK. Primary hydatid cyst of kidney and ureter with gross hydatiduria: A case report and evaluation of radiological features. *Indian J Urol* 2008; **24**: 116-117 [PMID: 19468374 DOI: 10.4103/0970-1591.38617]

P- Reviewer: Nishio K, Schoenhagen P **S- Editor**: Ji FF
L- Editor: A **E- Editor**: Liu SQ

Published by **Baishideng Publishing Group Inc**
8226 Regency Drive, Pleasanton, CA 94588, USA
Telephone: +1-925-223-8242
Fax: +1-925-223-8243
E-mail: bpgoffice@wjgnet.com
Help Desk: http://www.wjgnet.com/esps/helpdesk.aspx
http://www.wjgnet.com